Research Report

Further Investigation of Bearing and Tearout of Steel Bolted Connections

FINAL REPORT

AISC RESEARCH REPORT NO. 04
MAY 2024

Project Title:	**Further Investigation of Bearing and Tearout of Steel Bolted Connections**
Primary Investigator(s):	**Mark D. Denavit, Javad Esmaeelpour, and Pratik Poudel**
Research Organization(s):	**University of Tennessee, Knoxville**

DISCLAIMER

The material contained herein has been developed by researchers based on their research findings and is for general information only. The information in it should not be used without first securing competent advice with respect to its suitability for any given application. The publication of the information is not intended as a representation or warranty on the part of the American Institute of Steel Construction (AISC) or of any other person named herein, that the information is suitable for any general or particular use or of freedom from infringement of any patent or patents. Anyone making use of the information assumes all liability arising from such use.

PREFACE

The American Institute of Steel Construction (AISC), headquartered in Chicago, is a non-partisan, not-for-profit technical institute and trade association established in 1921 to serve the structural steel design community and construction industry in the United States. As part of its technical activities, AISC actively funds and supports research related to structural steel design and construction. AISC members primarily come from the structural steel construction community, including producers, fabricators, and engineers.

Many AISC members are engineers, so much of our research supports the engineering community, including maintaining and updating our technical publications such as Design Guides, The Steel Construction Manual, and our Specifications and Provisions. We distribute our specifications free for their use. The primary goal of those specifications is the reliability of structures and, through that, the safety of the public.

AISC does not use the results of research for profit, nor do we sell reports of the research or derivatives from it. Our work is performed in the interest of public safety. As such, we fund projects to, in part, support the development of next-generation steel systems for enhanced performance, safety, sustainability, and economy.

It is reasonably common for AISC research projects to receive additional direct, indirect, or in-kind support from external organizations such as federal or state agencies or member companies . As such, the partial or complete contents of this Report may also reside in the public domain of these external funding agencies.

FURTHER INVESTIGATION OF BEARING AND TEAROUT OF STEEL BOLTED CONNECTIONS

Final Report
submitted to the
American Institute of Steel Construction

by

Mark D. Denavit, Javad Esmaeelpour, and Pratik Poudel
Department of Civil and Environmental Engineering
University of Tennessee, Knoxville

May 2024

Abstract

Current design requirements for the limit state of tearout were developed primarily based on experimental results of a limited range of configurations that do not necessarily represent the wide range of configurations to which the limit state applies. This experimental study examines configurations that have not been tested previously, including edge skewed to the direction of force, corner beyond the hole, interior bolts, and eccentrically loaded bolt groups. The findings provide a wealth of data on the behavior of connections with small edge distances and strength for the limit state of tearout. The data support a range of new design recommendations, including improved definition of tearout length when the edge is skewed to the direction of force, new strength equation when there is a corner beyond the hole, and validation of a modified version of the instantaneous center of rotation method for eccentrically loaded bolt groups that appropriately considers tearout. These results will enable more efficient and accurate design of steel bolted connections with small edge distances.

The work was conducted at the University of Tennessee, Knoxville by Prof. Mark Denavit in collaboration with graduate students Javad Esmaeelpour and Pratik Poudel. The research team can be contacted by email (mdenavit@utk.edu), phone (865-974-7714), or mail (325 John D. Tickle Building, 851 Neyland Drive, Knoxville TN 37996-2313).

Chapter 1: Introduction

The limit state of tearout, together with bearing and bolt shear rupture, defines the effective strength of a bolt in a group. Tearout strength can vary from bolt to bolt within a group due to variations in the clear distance, defined as the distance in the direction of force between the edge of the hole and the edge of adjacent hole or edge of the material. Provisions for tearout have been included in the AISC *Specification* for decades (even though the term tearout was introduced in the 2005 edition of the AISC *Specification*), however, the provisions have evolved over time with experimental and numerical research. Yet the research that forms the background of the provisions was predominantly conducted on single bolt connections where the load is perpendicular to the edge of the connected material, despite tearout applying to many other cases in design.

The nominal strength for the limit state of tearout for a bolt in a standard, oversize, or short-slotted hole is defined in the 2022 edition of the AISC *Specification* (AISC 2022) by Equations J3-6c and J3-6d, shown here as Equations 1 and 2.

$$R_n = 1.2 l_c t F_u \tag{1}$$

$$R_n = 1.5 l_c t F_u \tag{2}$$

where, R_n is the nominal strength of a bolt, l_c is the clear distance, in the direction of force, between the edge of the hole and the edge of the adjacent hole or edge of the material, t is the thickness of the connected material, and F_u is the specified minimum tensile strength of the connected material.

The nominal strength for the limit state of bearing for a bolt in a normal, oversize, or short-slotted hole is defined by AISC *Specification* Equations J3-6a and J3-6b, shown here as Equations 3 and 4.

$$R_n = 2.4 d t F_u \tag{3}$$

$$R_n = 3.0 d t F_u \tag{4}$$

where, d is the nominal bolt diameter.

Equations 1 and 3 are used when deformation at the bolt hole at service load is a design consideration. Equations 2 and 4 are used when deformation at the bolt hole under service load is not a design consideration. The ratio between Equations 3 and 4 is same as between Equations 1 and 2. For bolts with a large edge distance, the full bearing strength (i.e., Equation 4) is often not achieved until relatively large deformations occur. Bearing strength when deformation at the bolt hole at service load is a design consideration corresponds not to a maximum strength, but rather the load at 1/4 in. deformation (Kim and Yura 1999). However, research has shown little difference between the maximum tearout strength and the load at 1/4 in. deformation (Franceschetti and Denavit 2021).

Researchers have also proposed alternative equations that can provide better predictions of tearout strength than those in the AISC *Specification*. One alternative equation, proposed by Kamtekar (2012), uses length l_{v1}, in lieu of the clear distance, l_c. Length l_{v1} is the distance between the edge of the bolt hole and the edge of the adjacent hole or edge of the material, measured in the direction of the applied force, along lines that are tangent to the bolt. For an exterior bolt with edge perpendicular to the direction of the applied force such as shown in Figure 1a, l_{v1} is given by Equation 5.

$$l_{v1} = L_e - \frac{\sqrt{d_h^2 - d^2}}{2} \tag{5}$$

where, d_h is the diameter of the bolt hole.

For an interior bolt with an adjacent bolt in the direction of the applied force such as shown in Figure 1b, l_{v1} is given by Equation 6.

$$l_{v1} = s - \sqrt{d_h^2 - d^2} \tag{6}$$

where, s is the center-to-center spacing between the holes.

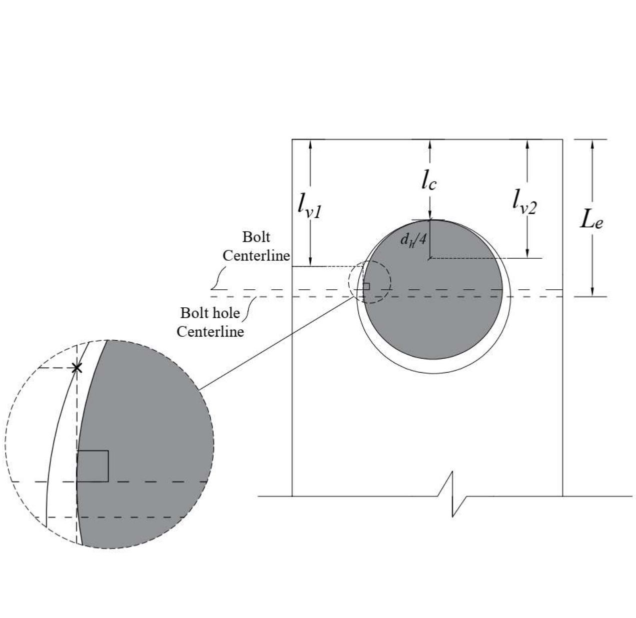

(a) edge bolt (b) interior bolt

Figure 1. Definition of different lengths used in tearout strength calculation.

Another alternative equation, proposed by Clements and Teh (2013), uses length l_{v2}, in lieu of the clear distance. Length l_{v2} is the average of the clear distance, l_c, and the edge distance, L_e. For an exterior bolt with edge perpendicular to the direction of the applied force (Figure 1a), l_{v2} is given by Equation 7.

$$l_{v2} = L_e - \frac{d_h}{4} \tag{7}$$

For an interior bolt with an adjacent bolt in the direction of the applied force (Figure 1b), l_{v2} is given by Equation 8.

$$l_{v2} = s - \frac{d_h}{2} \tag{8}$$

Franceschetti and Denavit (2021) compared the two alternative equations to the current provisions and experimental results. They found that Equations 9 and 10, using alternative lengths l_{v1} and l_{v2}, are better than Equation 2 using l_c in predicting tearout strength. Specifically, the current design equations do not result in consistent test-to-predicted ratios across edge distances and tend to underpredict the strengths at smaller edge distances. A factor of 1.2 is used in Equations 9 and 10 regardless of whether deformation at bolt holes at service loads is a design consideration given that there is little difference between the maximum tearout strength and the load at 1/4 in. deformation.

$$R_n = 1.2 l_{v1} t F_u \tag{9}$$

$$R_n = 1.2 l_{v2} t F_u \tag{10}$$

The experiments from which these observations were made covered a range of plate thicknesses, plate material strengths, and bolt diameters, but they all had a single bolt with the direction of force perpendicular to the edge of the connected material. While this case is common, the limit state of tearout is applicable to other conditions as well, including when the direction of force is skewed to the edge of material and interior bolts. The lack of experimental validation for these cases means their strength is uncertain. While alternative tearout lengths have been shown to improve accuracy, it is unclear how l_{v1} and l_{v2} should be defined when the direction of force is skewed to the edge of the connected material. Also, the strength provisions, even with the alternative tearout lengths may overestimate the strength when the direction of force is towards the corner of the material.

Beyond the strength of individual bolts, other questions related to deformation compatibility within a bolt group exist. Specifically, it is uncertain whether the full bearing strength of the interior bolts can be obtained concurrently with the full tearout strength of the edge bolts, given that these strengths may occur at different levels of deformation. Some unconservative error has been observed experimentally for multiple-bolt specimens at the ultimate load level (Franceschetti and Denavit 2021).

Additional uncertainty arises when a bolt group is subjected to eccentric load. The strength of eccentrically loaded bolt groups is commonly computed using the instantaneous center of rotation (IC) method. The IC method, developed by Crawford and Kulak (1971), assumes rigid body movement of the connected material allowing individual bolt deformations to be computed based on their location with respect to the IC.

In the IC method, forces in the bolts are computed from the deformations and an assumed load-deformation relationship given by Equation 11 and based on experimental testing of a 3/4 in. diameter A325 bolt.

$$R = R_{ult}\left(1 - e^{-10\Delta}\right)^{0.55} \tag{11}$$

where, R is the load in the bolt at a deformation Δ, R_{ult} is maximum load in the bolt, and Δ is the deformation of the bolt.

The deformation in the bolts is assumed to be proportional to their distance from the IC and the bolt farthest from the IC is assumed to have a deformation of Δ_{max} = 0.34 in. The load in each bolt is computed from Equation 11 and is assumed to act perpendicular to a line between the bolt and the IC. The IC is determined as that which results in static equilibrium, typically using an iterative approach. In practice, the IC method is applied using tabulated solutions. The AISC *Manual* includes tables of a coefficient C for various bolt groups and loading configurations. The coefficient C is defined such that the strength of a bolt group is C times the strength of an individual bolt.

The IC method has primarily been validated against cases where the strength of each bolt can be assumed to be equal. Shear rupture controlled the strength of the bolts in the connections that were tested by Crawford and Kulak (1971). Researchers from McGill University (Badawi 1983; Wing and Harris 1983) investigated eccentrically loaded bolt groups failing in bearing. Kulak (1975) and Soliman et al. (2021) investigated eccentrically loaded bolted connections with slip-critical bolts. These tests all had sufficient edge distance for tearout to not control.

When an eccentrically loaded bolt group has smaller edge distances, tearout can control the strength of some of the bolts. This is problematic because the tabulated solutions assume the bolts are all the same strength, which they would not be if some are controlled by tearout. Also, the tabulated solutions do not specify the direction of force in the bolts, which is needed to determine tearout strength. Given these limitations, many engineers use the "poison bolt method" for eccentrically loaded bolt groups that are susceptible to tearout. They compute the lowest strength that any of the bolts could have by identifying the smallest clear distance, l_c, for any direction of loading. Then they assume that the lowest possible bolt strength is the strength of all the bolts. The poison bolt method is safe but can be overly conservative.

Denavit et al. (2021) proposed a modified version of the IC method that accounts for tearout. The modified IC method follows the same general procedure and iterative scheme as the standard IC method but considers the limit state of tearout when determining load in each bolt. The force on each bolt is assumed to act perpendicular to a line connecting the IC and the bolts, just as in the standard IC method. Then, based on this direction of force, the clear distance as defined in the AISC *Specification* is computed for each bolt based on the geometry of the connected material. With the clear distance, R_{ult} is computed as the minimum strength for the limit states of bolt shear rupture, bearing, and tearout and used in Equation 11 to compute the force in each bolt. The evaluation of clear distance is performed for each bolt in each iteration as the IC is determined. The modified IC method is more complex and computationally intensive than the standard IC method. It also requires detailed information about the geometry of the connected material and is thus less suitable for tabulated solutions.

Denavit et al. (2021) also conducted experiments on ten single plate shear connections, a common application of eccentrically loaded bolt groups. They identified that smaller edge distance did not necessarily reduce the strength of the connection. However, the tests did not include bolt groups subject to higher eccentricity where the impact of tearout is expected to be greater and the accuracy of the modified IC method could be more thoroughly validated.

Al-Amery (2022) conducted experiments on eccentrically loaded bolt groups with smaller edge distances. However, aspects of this work warrant further consideration. Photographs of the test specimens suggest that they did not fail in tearout. Moreover, the material properties of the plate were not measured. As such, these experiments provide limited information on the limit state of tearout. Al-Amery also proposed a method for calculating the strength of eccentrically loaded bolt groups that is based on the IC method, but accounts for the "residual strength" of bolts not failing in tearout. Their proposed method is based on the premise that only one or a few bolts fail in tearout and that the remaining bolts have residual strength that enables them to bear load beyond the tearout failure of the edge bolts. In this method, the strength of the connection is computed using the IC method first assuming the strength of an individual bolt is limited by tearout. Then the residual strength is computed using the IC method for the remaining bolts assuming that the strength of an individual bolt is equal to the difference between the shear strength or bearing strength and the tearout strength. The total strength is taken as the sum of the tearout strength and residual strength.

Despite the prior experimental investigations by Denavit et al. (2021) and Al-Amery (2022), the behavior of eccentrically loaded bolted connections susceptible to tearout remains uncertain. Furthermore, uncertainty in the design of such connections forces engineers to make potentially overly conservative assumptions. While various methods to compute the strength of eccentrically loaded bolt groups susceptible to tearout have been proposed, targeted experimental validation is necessary to prove their efficacy.

Objectives and Scope

This work builds upon previous work by Denavit et al. (2021) to gain further insight on the limit state of tearout and how best it should be incorporated into design standards. Several series of experimental tests were performed, including four series of tests of one- and two-bolt connections loaded concentrically and two series of tests of eccentrically loaded bolt groups.

The objective of this work is to evaluate tearout strength in cases that have not previously been investigated experimentally. This study includes specimens that have connected material with a skewed edge, a plate corner that lies beyond the bolt, and a single interior bolt. Additionally, to permit detailed evaluation of deformation compatibility, three different sets of specimens were tested for three different conditions: one with only the edge bolt installed, one with only the interior bolt installed, and one with both bolts installed. Moreover, this study also incorporates tests on eccentrically loaded connections with small edge distances performed at two different eccentricities. The results of these unique experiments were analyzed to form recommendations for design.

Chapter 2: Concentrically Loaded Experiments

This chapter describes physical experiments of concentrically loaded one- and two-bolt structural steel connections.

Materials and Methods

Fifty-one bolted connections specimens were tested in this study. In each specimen, a test plate was sandwiched between two pull plates as shown in Figure 2. The three plies were connected with one or two bolts. The connection was loaded in tension in a uniaxial test machine (Figure 3). The specimens were designed to fail in either bearing or tearout of the test plate. New pull plates and test bolts were used for each specimen to eliminate any potential influence of wear on these parts.

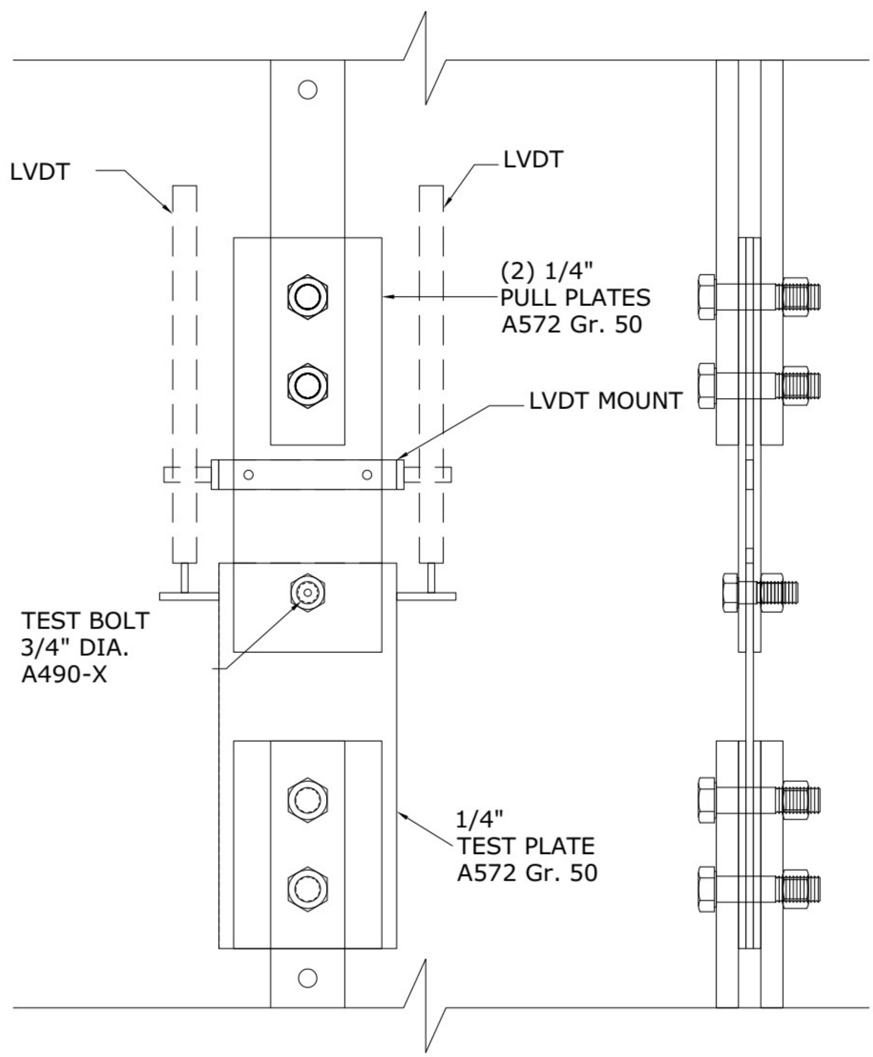

Figure 2. Schematic of typical specimen (specimen 1 shown)

Figure 3. Test setup (specimen 1 shown)

The specimens were separated into four groups. The first group consisted of twelve specimens designed to investigate the effect of skew between the edge of the connected material and direction of force. The test plates of these specimens were fabricated as shown in Figure 4a. Skew angles, θ, of 45, 30, 15, and zero degrees were investigated. Each skew angle was tested with three edge distances, L_e, defined as the distance from the edge to the center of the hole measured perpendicular to the edge. Details of the specimens, including measured edge distance, are listed in Table 1.

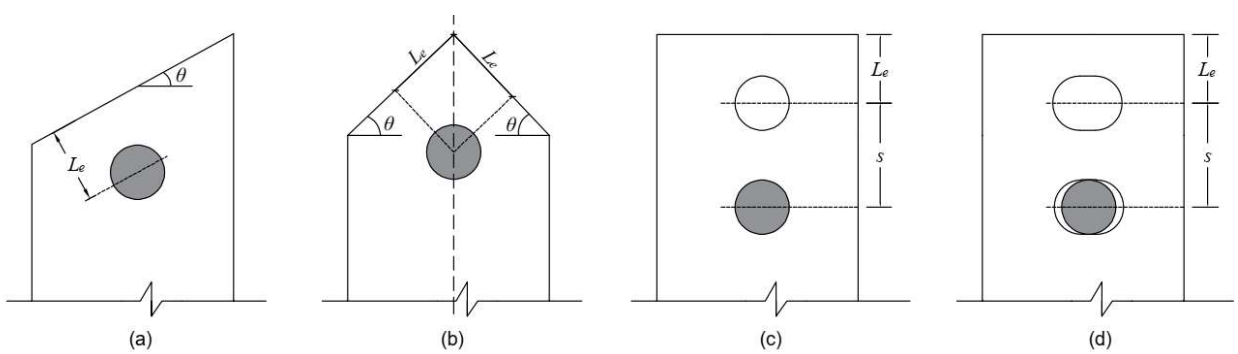

Figure 4. Test plate for investigation of tearout strength for a) skewed plate edge, b) plate corner beyond the bolt, c) for interior bolts, d) interior bolts with slotted hole.

Table 1. Test Matrix – Skewed Edge Specimens

Index	Hole Type	L_e (in.)	θ (deg)
1	STD	1.0225	0
2	STD	1.0294	15
3	STD	0.9945	30
4	STD	0.9770	45
5	STD	1.2570	0
6	STD	1.2814	15
7	STD	1.2090	30
8	STD	1.2390	45
9	STD	1.5123	0
10	STD	1.5208	15
11	STD	1.5359	30
12	STD	1.5068	45

The second group consisted of five specimens designed to investigate the strength of bolts when the direction of force is towards a corner of the connected material. The test plates of all specimens in this group had right-angle corners and the edge distance, L_e, was the same for both edges as illustrated in Figure 4b. However, this edge distance varied across the specimens within the group. Details of the specimens, including measured edge distance, are listed in Table 2.

Table 2. Test Matrix – Corner Specimens

Index	Hole Type	L_e (in.)
13	STD	0.9759
14	STD	1.2450
15	STD	1.5085
16	STD	1.7690
17	STD	2.0390

The third group consisted of fifteen specimens that had two bolt holes but only the interior bolt was installed as illustrated by grey shading in Figure 4c and Figure 4d. This group was divided into three subgroups, those with standard holes (STD, d_h = 13/16 in.) in the test plate, those with oversize holes (OVS, d_h = 15/16 in.) in the test plate, and those short-slotted holes transverse to the direction of load (SSLT, width in the direction of loading = 13/16 in., length in the direction perpendicular to loading = 1 in.) in the test plate. Standard holes were used in the pull plates for all specimens. The edge distance, L_e, for these specimens was 1 in. and the center-to-center spacing between the holes, s, varied from 2 to 3 in. Details of the specimens, including measured edge distance and spacing, are listed in Table 3.

The fourth group of specimens were designed to investigate the deformation compatibility of connections controlled by both bearing and tearout. This group consisted of nineteen specimens, which can be classified into three subcategories based on their bolt configurations. The first type includes three specimens with a single bolt at the edge, each having the same center-to-center spacing between holes but varying edge distances. The second type consists of four specimens with a single bolt in the interior hole, sharing the same edge distance but differing center-to-center distances. The remaining specimens had bolts in both holes. Each two-bolt specimen is paired with the results of two singly bolted specimens (one interior and one edge specimen) allowing for a comparative analysis of the load carrying performance of each bolt. Details of the specimens, including measured edge distance and spacing, are listed in Table 4.

Table 3. Text Matrix – Interior Bolt Specimens

Index	Hole Type	L_e (in.)	*s* (in.)
18	STD	1.0005	1.9975
19	STD	0.9978	2.2425
20	STD	0.9993	2.4960
21	STD	1.0008	2.7500
22	STD	1.0006	2.9960
23	OVS	1.0045	2.0050
24	OVS	1.0043	2.2570
25	OVS	1.0001	2.4985
26	OVS	0.9020	2.7470
27	OVS	1.0009	2.9980
28	SSLT	1.0013	1.9905
29	SSLT	1.1180	2.2550
30	SSLT	0.9945	2.4880
31	SSLT	1.0058	2.7495
32	SSLT	1.0013	3.0015

Table 4. Test Matrix – Deformation Compatibility Specimens

Index	Bolts Installed	Hole Type	L_e (in.)	*s* (in.)
33	Edge Bolt Only	STD	1.0040	2.0005
34	Edge Bolt Only	STD	1.5033	2.0000
35	Edge Bolt Only	STD	2.0065	1.9975
36	Interior Bolt Only	STD	1.0053	2.0025
37	Interior Bolt Only	STD	1.0005	2.9970
38	Interior Bolt Only	STD	1.0015	3.9980
39	Interior Bolt Only	STD	1.0035	5.9975
40	Both Bolts	STD	1.0063	1.9980
41	Both Bolts	STD	1.0058	2.9990
42	Both Bolts	STD	1.0030	3.9960
43	Both Bolts	STD	1.0053	6.0040
44	Both Bolts	STD	1.5033	1.9975
45	Both Bolts	STD	1.5040	2.9985
46	Both Bolts	STD	1.5083	3.9975
47	Both Bolts	STD	1.5023	5.9980
48	Both Bolts	STD	2.0050	1.9990
49	Both Bolts	STD	2.0035	3.0000
50	Both Bolts	STD	2.0043	3.9965
51	Both Bolts	STD	2.0028	5.9990

The test plates were 0.242 in. thick (measured thickness from coupons) and were all fabricated from the same heat of steel. All the plate material used in this study was specified as ASTM A572 Gr. 50, but also met other standards. The measured yield strength of the test plates was F_y = 60.4 ksi and the measured tensile strength of the test plates was F_u = 76.9 ksi, based on the average of four tensile coupon tests that were performed in accordance with ASTM E8 (ASTM 2022). The elongation was 22.7% based on an 8 in. gage length.

Different fabrication techniques were used based on the width of the specimen. The skewed edge, corner, and interior bolt specimens had water jet cut edges. The deformation compatibility specimens had milled edges. The standard and oversize holes were drilled. The slotted holes were milled.

All bolts used to connect the test and pull plates (i.e., test bolts) were 3/4 in. diameter A490. The threads of these bolts were excluded from the shear planes. The bolts were installed finger tight. The measured diameter of these bolts was 0.748 in.

Applied load and connection deformation were recorded during testing. Connection deformation was taken as the average of two deformation measurements made with linear variable differential transformers (LVDTs) that were attached to the specimens as shown in Figure 2. The vertical distance between attachment points of the LVDTs ranged from 6 to 11 in. The contribution of tensile deformations of the pull plates in the measurement was shown to be negligible in previous similar experiments (Franceschetti and Denavit 2021). The maximum force resisted by the connection, $R_{exp,u}$, and the force at 1/4 in. connection deformation, $R_{exp,d}$, were quantified in post-processing.

Upon installation in the uniaxial test machine, the specimens were subjected to displacement-controlled loading at a rate of 0.1 in./min. The tests were halted when a notable reduction in force was detected. For the deformation compatibility specimens, loading was carried out until a connection deformation of at least 2 in. was attained to fully examine the load-deformation response.

Results and Discussion

Skewed Edge Specimens

The load-deformation response for specimens 1 through 12 are presented in Figure 5. The specimens exhibited an initial linear response followed by a gradual reduction in stiffness, eventually leading to a peak load. All specimens exhibited a sharp drop in load following the peak. The failure mechanism for these specimens was tearout. As shown in Figure 6, bolt hole deformation was not perfectly vertical (i.e., the direction of force). Rather the direction of bolt hole deformations was tilted slightly towards the edge. Cracks propagated in a direction between perpendicular to the edge of the plate and parallel to the direction of the force.

Strength results, including the maximum load, $R_{exp,u}$, the load at 1/4 in. deformation, $R_{exp,d}$, and the ratio between the two are listed in Table 5. An increase in either the skew angle or nominal edge distance resulted in an increase in strength.

The various lengths used in the tearout strength equations (i.e., l_c, l_{v1}, and l_{v2}) are listed in Table 6. The clear distance, l_c, was determined in accordance with the AISC *Specification* as the distance in the direction of force between the edge of hole and the edge of the material. Two values of distance l_{v1} are listed in Table 6. The distance l_{v1} is defined similar to the clear distance, but along lines tangent to the bolt. With a skewed edge, the two lines tangent to the bolt have different lengths: $l_{v1,avg}$ is the average of the two lengths, $l_{v1,min}$ is the minimum of the two lengths. The distance l_{v2} is not clearly defined for cases with a skewed edge. Noting that l_{v2} is intended to be a simple measure, it is taken as l_c plus one-quarter of the diameter of the hole for these specimens.

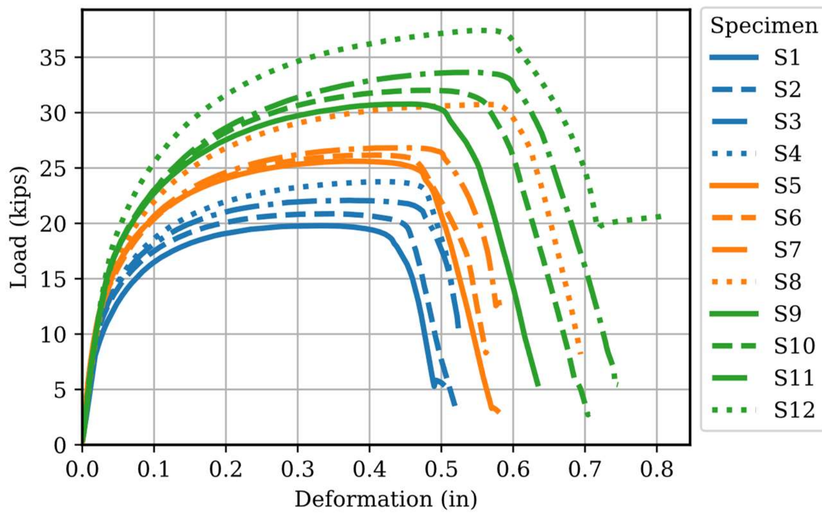

Figure 5. Load-deformation response for specimens 1 through 12.

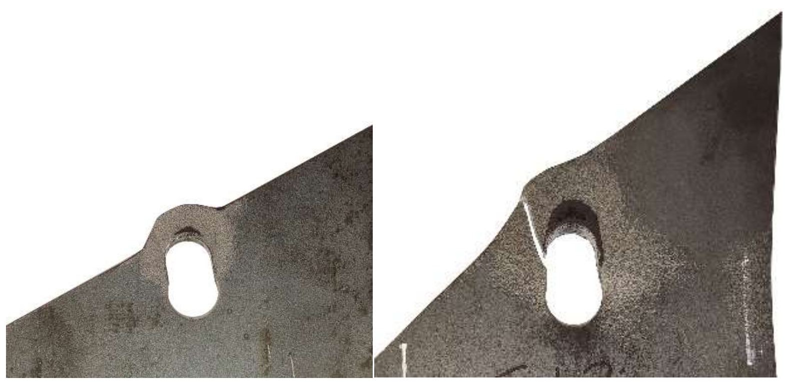

Figure 6. Specimen 3 (left) and 12 (right) after testing.

Table 5. Strength Results – Skewed Edge Specimens

Index	$R_{exp,d}$ (kips)	$R_{exp,u}$ (kips)	$R_{exp,u}/R_{exp,d}$
1	19.58	19.80	1.011
2	20.59	20.88	1.014
3	21.62	22.08	1.021
4	22.75	23.77	1.045
5	24.87	25.62	1.030
6	25.13	26.18	1.042
7	25.59	26.83	1.048
8	28.11	30.74	1.094
9	28.85	30.80	1.068
10	29.66	32.02	1.080
11	30.20	33.65	1.114
12	33.35	37.43	1.122

Table 6. Tearout Lengths – Skewed Edge Specimens

Index	l_c (in.)	$l_{v1,avg}$ (in.)	$l_{v1,min}$ (in.)	l_{v2} (in.)
1	0.607	0.885	0.885	0.815
2	0.662	0.968	0.863	0.864
3	0.745	1.053	0.826	0.947
4	0.977	1.282	0.890	1.179
5	0.854	1.161	1.161	1.055
6	0.922	1.227	1.122	1.124
7	0.993	1.303	1.076	1.195
8	1.348	1.652	1.260	1.550
9	1.108	1.411	1.411	1.310
10	1.170	1.474	1.369	1.372
11	1.370	1.676	1.450	1.572
12	1.728	2.036	1.644	1.929

A comparison between experimental strength results and computed strength results at the deformation limit load is presented in Table 7. Four different strength calculation approaches are shown. The first uses the clear distance, l_c, and Equation 12. The second uses the average value of the distance l_{v1} and Equation 13. The third uses the minimum value of the distance l_{v1} and Equation 13. The fourth uses the distance l_{v2} and Equation 14.

$$R_n = \min\left(1.2 l_c t F_u, 2.4 d t F_u\right) \tag{12}$$

$$R_n = \min\left(1.2 l_{v1} t F_u, 2.4 d t F_u\right) \tag{13}$$

$$R_n = \min\left(1.2 l_{v2} t F_u, 2.4 d t F_u\right) \tag{14}$$

A comparison between experimental strength results and computed strength results at the ultimate limit load is presented in Table 8. As in Table 7, four different strength calculation approaches are shown. The four different approaches in Table 8 use the same lengths as in Table 7, but with Equations 15, 16, and 17 instead of Equations 12, 13, and 14, respectively.

$$R_n = \min\left(1.5 l_c t F_u, 3.0 d t F_u\right) \tag{15}$$

$$R_n = \min\left(1.2 l_{v1} t F_u, 3.0 d t F_u\right) \tag{16}$$

$$R_n = \min\left(1.2 l_{v2} t F_u, 3.0 d t F_u\right) \tag{17}$$

Strength comparisons are also shown graphically in Figure 7.

Table 7. Deformation Limit Strength Comparison – Skewed Edge Specimens

Index	Eq. 12 (I_c)		Eq. 13 ($I_{v1,avg}$)		Eq. 13 ($I_{v1,min}$)		Eq. 14 (I_{v2})	
	R_n (kips)	$R_{exp,d}/R_n$	R_n (kips)	$R_{exp,d}/R_n$	R_n (kips)	$R_{exp,d}/R_n$	R_n (kips)	$R_{exp,d}/R_n$
1	13.56	1.444	19.76	0.991	19.76	0.991	18.19	1.076
2	14.78	1.393	21.63	0.952	19.28	1.068	19.29	1.067
3	16.63	1.300	23.51	0.920	18.45	1.172	21.14	1.023
4	21.82	1.043	28.63	0.795	19.87	1.145	26.34	0.864
5	19.06	1.305	25.94	0.959	25.94	0.959	23.57	1.055
6	20.59	1.220	27.41	0.917	25.06	1.003	25.11	1.001
7	22.18	1.154	29.09	0.880	24.03	1.065	26.68	0.959
8	30.10	0.934	33.41	0.841	28.15	0.999	33.41	0.841
9	24.73	1.166	31.52	0.915	31.52	0.915	29.25	0.986
10	26.12	1.136	32.91	0.901	30.56	0.970	30.64	0.968
11	30.59	0.987	33.41	0.904	32.38	0.933	33.41	0.904
12	33.41	0.998	33.41	0.998	33.41	0.998	33.41	0.998
Average		1.173		0.914		1.018		0.979
St. Dev.		0.165		0.058		0.080		0.076

Table 8. Ultimate Limit Strength Comparison – Skewed Edge Specimens

Index	Eq. 15 (I_c)		Eq. 16 ($I_{v1,avg}$)		Eq. 16 ($I_{v1,min}$)		Eq. 17 (I_{v2})	
	R_n (kips)	$R_{exp,u}/R_n$	R_n (kips)	$R_{exp,u}/R_n$	R_n (kips)	$R_{exp,u}/R_n$	R_n (kips)	$R_{exp,u}/R_n$
1	16.94	1.169	19.76	1.002	19.76	1.002	18.19	1.088
2	18.47	1.130	21.63	0.965	19.28	1.083	19.29	1.082
3	20.79	1.062	23.51	0.939	18.45	1.196	21.14	1.045
4	27.28	0.871	28.63	0.830	19.87	1.196	26.34	0.902
5	23.83	1.075	25.94	0.988	25.94	0.988	23.57	1.087
6	25.74	1.017	27.41	0.955	25.06	1.045	25.11	1.043
7	27.72	0.968	29.09	0.922	24.03	1.116	26.68	1.006
8	37.62	0.817	36.90	0.833	28.15	1.092	34.61	0.888
9	30.92	0.996	31.52	0.977	31.52	0.977	29.25	1.053
10	32.65	0.981	32.91	0.973	30.56	1.048	30.64	1.045
11	38.23	0.880	37.43	0.899	32.38	1.039	35.10	0.959
12	41.76	0.896	41.76	0.896	36.72	1.019	41.76	0.896
Average		0.989		0.932		1.067		1.008
St. Dev.		0.109		0.057		0.073		0.077

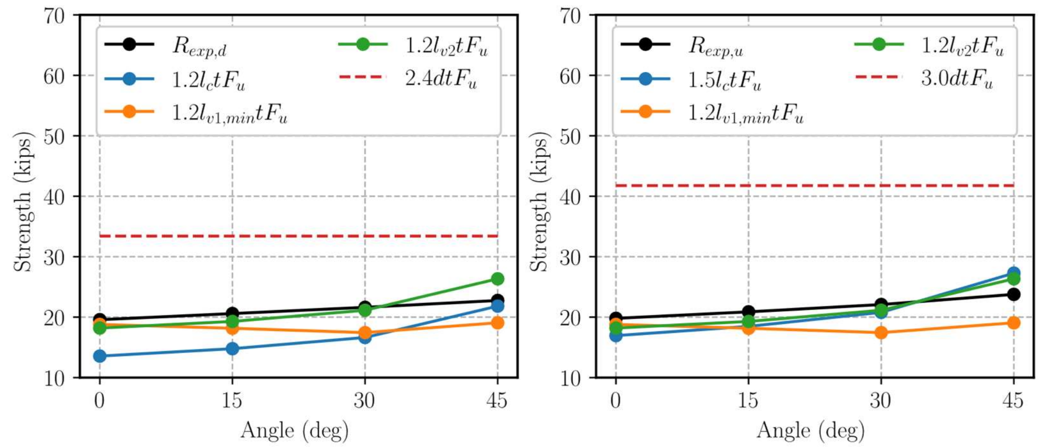

(a)

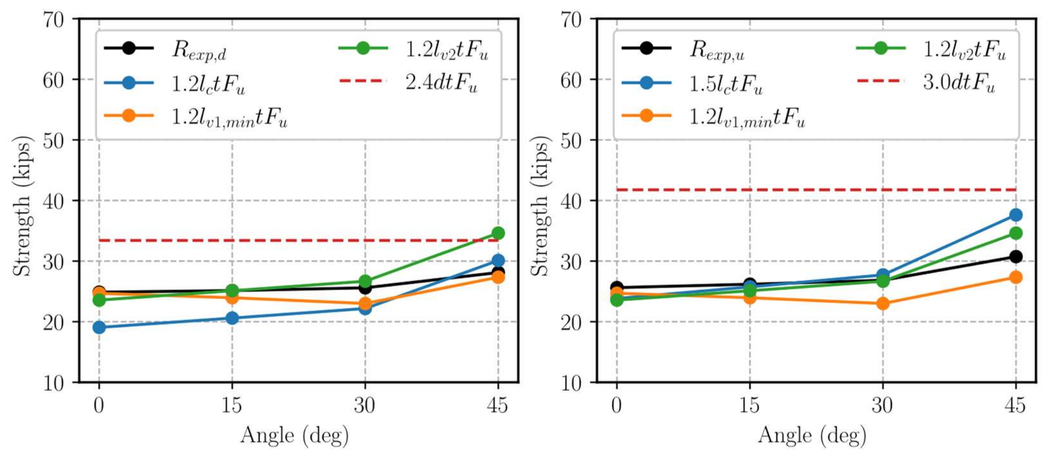

(b)

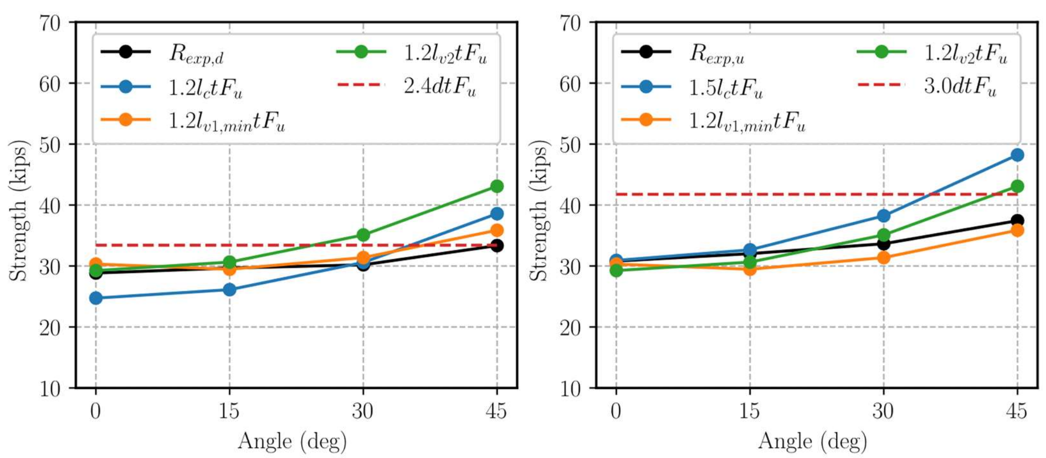

(c)

Figure 7. Comparison of plate strength (1/4 in. deformation level on the left and ultimate load level on the right) obtained from the experiment with tearout strength from equations using l_c, $l_{v1,\min}$, and l_{v2} and bearing limits for skewed edge sets with a) 1 in. edge distance, b) 1.25 in. edge distance, c) 1.5 in. edge distance.

The equations that use l_c show the greatest variation in test-to-predicted ratio (i.e., $R_{exp,d}/R_n$ and $R_{exp,u}/R_n$). Equation 12 is generally conservative for the estimation of the deformation limit load. However, the test-to-predicted ratio is seen to vary with both edge distance and skew angle. As observed in previous research (Franceschetti and Denavit 2021), tearout strength equations that use clear distance are conservative at smaller edge distances. As seen in Table 7, the conservatism vanishes at higher skew angles. On average, Equation 15 is accurate for the estimation of the ultimate load. However, the test-to-predicted ratio varies with skew angle and the test-to-predicted ratios as low as 0.817 are seen at the highest skew angle.

The equations that use $l_{v1,\mathrm{avg}}$ are generally unconservative with test-to-predicted ratios averaging less than 1. The equations that use l_{v2} are more accurate with average test-to-predicted ratios close to 1 and little variation in test-to-predicted ratio with edge distance. However, the variation with skew angle for the equations that use l_{v2} is similar to that for the equations using l_c. The equations that use $l_{v1,\mathrm{min}}$ are generally conservative and show little variation with edge distance and skew angle.

As noted previously, the direction of bolt hole deformation was tilted slightly away from the direction of force and towards the skewed edge (Figure 6). It was possible for these specimens to deform in a direction different from the direction of force because they were not restrained laterally. If lateral restraint were provided, as may be provided in a real connection by the other bolts in a group, the observed strengths may have been greater. Finite element simulation can be used to estimate the effect of such lateral restraint.

Corner Specimens

Specimens 13 through 17 had a corner beyond the hole in the direction of force. The load-deformation response for these specimens, shown in Figure 8, was similar to that of the skewed edge specimens. The observed failure mechanism of these plates, shown in Figure 9, was tearout but also included significant yielding between the bolt hole and the edge of the plate.

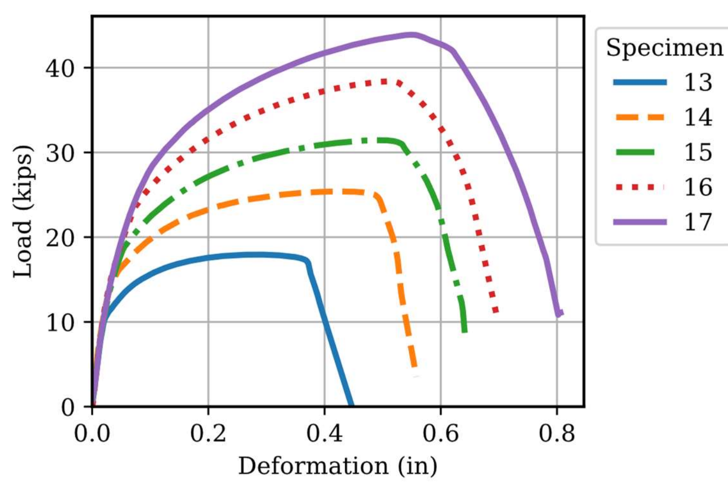

Figure 8. Load-deformation response for specimens 13 through 17.

Figure 9. Specimen 13 (left) and 17 (right) after testing.

Strength results are presented in Table 9. As observed previously, strength increases with increasing edge distance. The ratio $R_{exp,u}/R_{exp,d}$, also increases with increasing edge distance.

The various lengths used in the tearout strength equations (i.e., l_c, l_{v1}, and l_{v2}) are listed in Table 10. The clear distance, l_c, was determined in accordance with the AISC *Specification* as the distance in the direction of force between the edge of the hole and the edge of the material which, for these specimens, was the corner. The distance l_{v1}, being measured along lines tangent to the bolt, is less than l_c for these specimens. Typically, l_{v1} is greater than l_c. The distance l_{v2} is not clearly defined for cases with a corner beyond the hole. As with the skewed edge specimens, l_{v2} is taken as l_c plus one-quarter of the diameter of the hole for these specimens. In addition to the tearout lengths, Table 10 lists the distance l_{cc} defined as the least distance between the edge of the hole to the edge of material. It is measured along a line perpendicular to the edge, and not in the direction of force. The distance l_{cc} is used in a new strength equation described below.

Table 9. Strength Results – Corner Specimens

Index	$R_{exp,d}$ (kips)	$R_{exp,u}$ (kips)	$R_{exp,u}/R_{exp,d}$
13	17.887	17.948	1.003
14	24.206	25.399	1.049
15	28.591	31.457	1.100
16	33.587	38.397	1.143
17	37.287	43.893	1.177

Table 10. Tearout Lengths – Corner Specimens

Index	l_c (in.)	l_{v1} (in.)	l_{v2} (in.)	l_{cc} (in.)
13	0.976	0.854	1.178	0.572
14	1.358	1.237	1.559	0.842
15	1.732	1.613	1.933	1.107
16	2.098	1.977	2.300	1.366
17	2.481	2.360	2.682	1.636

A comparison of experimental strength results to computed strength results at the deformation limit load is presented in Table 11 and at the ultimate limit load in Table 12. Strength comparisons are also shown in Figure 10.

Table 11. Deformation Limit Strength Comparison – Corner Specimens

Index	Eq. 12 (l_c)		Eq. 13 (l_{v1})		Eq. 14 (l_{v2})		Eq. 20 (l_{cc})	
	R_n (kips)	$R_{exp,d}/R_n$	R_n (kips)	$R_{exp,d}/R_n$	R_n (kips)	$R_{exp,d}/R_n$	R_n (kips)	$R_{exp,d}/R_n$
13	21.81	0.820	19.08	0.938	26.31	0.680	14.91	1.200
14	30.32	0.798	27.62	0.877	33.41	0.725	21.94	1.103
15	33.41	0.856	33.41	0.856	33.41	0.856	28.84	0.991
16	33.41	1.005	33.41	1.005	33.41	1.005	33.41	1.005
17	33.41	1.116	33.41	1.116	33.41	1.116	33.41	1.116
Average		0.919		0.958		0.876		1.083
St. Dev.		0.137		0.106		0.185		0.086

Table 12. Ultimate Limit Strength Comparison – Corner Specimens

Index	Eq. 15 (l_c)		Eq. 16 (l_{v1})		Eq. 17 (l_{v2})		Eq. 21 (l_{cc})	
	R_n (kips)	$R_{exp,u}/R_n$	R_n (kips)	$R_{exp,u}/R_n$	R_n (kips)	$R_{exp,u}/R_n$	R_n (kips)	$R_{exp,u}/R_n$
13	27.26	0.658	19.08	0.941	26.31	0.682	14.91	1.204
14	37.90	0.670	27.62	0.920	34.82	0.729	21.94	1.158
15	41.76	0.753	36.03	0.873	41.76	0.753	28.84	1.091
16	41.76	0.919	41.76	0.919	41.76	0.919	35.58	1.079
17	41.76	1.051	41.76	1.051	41.76	1.051	41.76	1.051
Average		0.810		0.941		0.827		1.116
St. Dev.		0.170		0.066		0.154		0.063

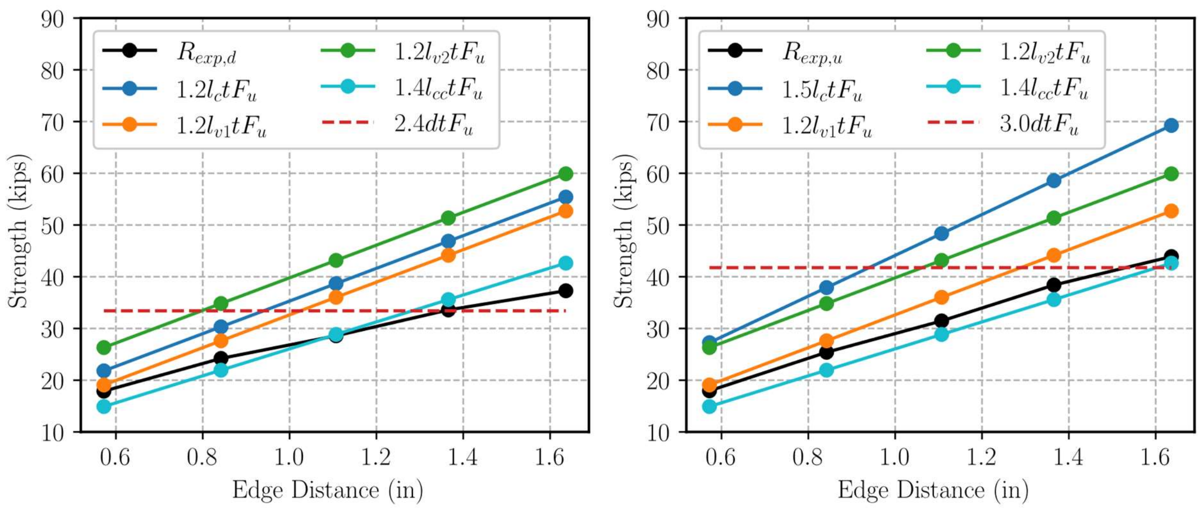

Figure 10. Comparison of plate strength (1/4 in. deformation level on the left and ultimate load level on the right) from the experiment with the tearout strength from equations using l_c, l_{cc}, l_{v1}, and l_{v2} tearout strength equations and bearing limits for corner sets.

Comparison of the experimental results with the calculated results obtained from the equations using l_c, l_{v1}, and l_{v2} reveals an overestimation of the strength for these specimens, with l_{v1} exhibiting the least error. To better estimate the plate strength, an alternative assessment of strength can be made using simple plastic analysis. Figure 11 shows a free-body diagram of a portion of the plate beyond the hole. The bolt is applying a force of R_n on the plate which is assumed to be resisted by tensile forces acting on two surfaces perpendicular to the edges. The width of the surfaces, i.e., the smallest distance between the edge of the plate to the edge of the hole, is defined as l_{cc}. The maximum tensile force acting on each surface is $l_{cc}tF_u$.

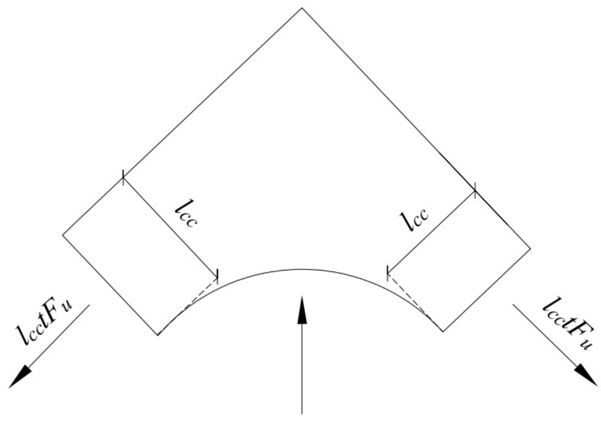

Figure 11- Analysis of the forces in the plate

Equation 18 is derived by setting the sum of the forces in the direction of R_n to zero.

$$R_n = \sqrt{2} l_{cc} t F_u \tag{18}$$

Equation 18 can be approximated as:

$$R_n = 1.4 l_{cc} t F_u \tag{19}$$

Combining Equation 19 with the bearing limit state yields Equation 20 for when deformation at the bolt hole at service load is a design consideration and Equation 21 for when deformation at the bolt hole at service load is not a design consideration.

$$R_n = \min\left(1.4 l_{cc} t F_u, 2.4 d t F_u\right) \tag{20}$$

$$R_n = \min\left(1.4 l_{cc} t F_u, 3.0 d t F_u\right) \tag{21}$$

The comparison to the experimental results presented in Table 11 and Table 12 reveals that the proposed Equation 19 is modestly conservative and thus better than the existing or alternative tearout equations which are unconservative.

Interior Bolt Specimens

Specimens 18 through 32 had two holes in the test plate, but only a single bolt was installed. The objective of these tests was to evaluate the strength of an interior bolt independent from a group. As with the other specimens, the load-deformation relationship was initially linear, followed by a gradual decrease in stiffness until the maximum load was reached, followed by a drop in the load. Figure 12 shows the load deformation results for specimens 28 through 32, those with slotted holes. Photographs of three specimens after testing are shown in Figure 13.

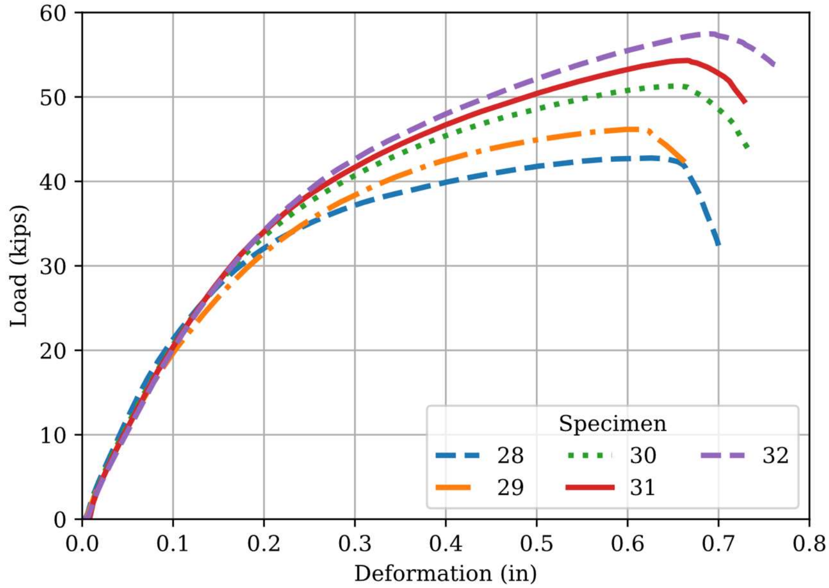

Figure 12. Load-deformation response for specimens 28 through 32.

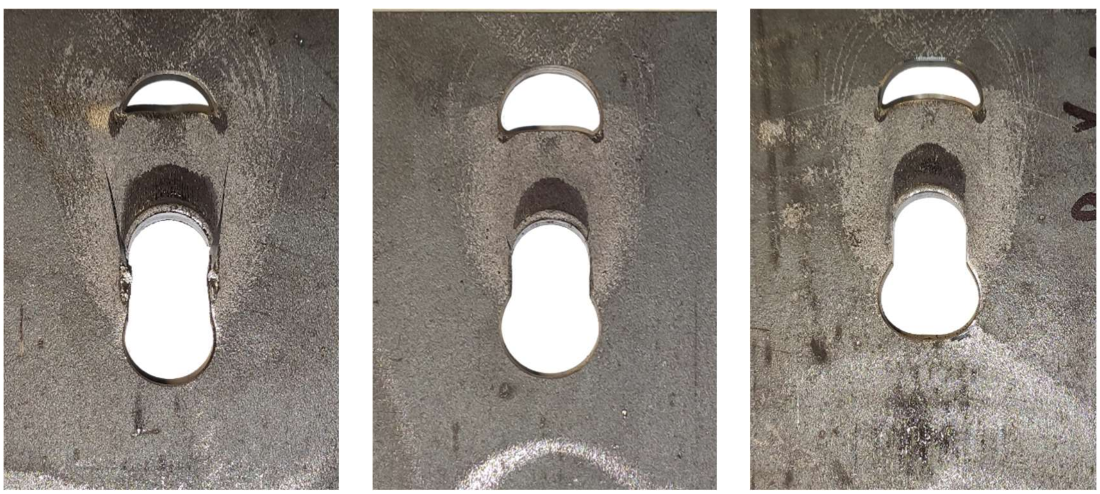

Figure 13- Specimen 18 (left), 23 (middle), and 28 (right) after testing.

Strength results are presented in Table 13. For a given bolt spacing, the specimens with standard holes exhibit slightly higher strength compared to those with oversize and slotted holes as shown in Figure 14. While both strength and the ratio $R_{exp,u}/R_{exp,d}$ increase with increasing bolt spacing for all of the specimens, the rate of the increase diminishes as the distance from the edge becomes larger for the specimens with standard holes.

The various lengths used in the tearout strength equations (i.e., l_c, l_{v1}, and l_{v2}) are listed in Table 14. The clear distance, l_c, was determined in accordance with the AISC *Specification* as the distance in the direction of force between the edge of hole and the edge of adjacent hole (i.e., $l_c = s - d_h$). The distance l_{v1} was calculated using Equation 6 for specimens with standard and oversize holes. For specimens with slotted holes, the distance l_{v1} was measured from a CAD drawing of the specimen drawn using measured dimensions. The distance l_{v2} was calculated using Equation 8. For slotted holes, the dimension d_h in Equation 8 was taken as the measured width of the slot.

Table 13. Strength Results – Interior Bolt Specimens

Index	$R_{exp,d}$ (kips)	$R_{exp,u}$ (kips)	$R_{exp,u}/R_{exp,d}$
18	38.54	45.64	1.184
19	40.13	50.49	1.258
20	43.13	57.79	1.340
21	41.39	58.85	1.422
22	41.11	58.38	1.420
23	34.16	40.06	1.173
24	39.19	47.41	1.210
25	39.28	51.32	1.306
26	39.37	54.68	1.389
27	40.05	56.50	1.411
28	35.03	42.78	1.221
29	35.43	46.18	1.303
30	37.58	51.30	1.365
31	38.44	54.32	1.413
32	39.02	57.48	1.473

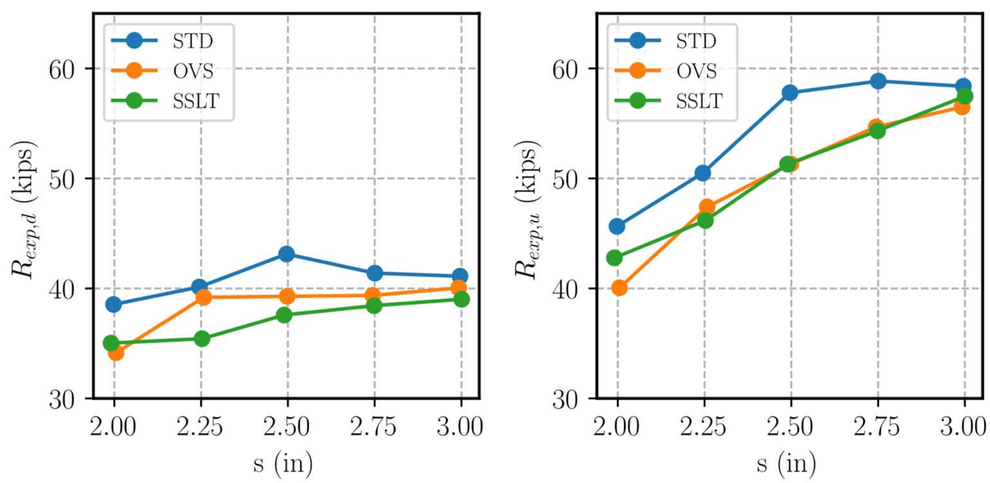

Figure 14. Comparison of plate strength (1/4 in. deformation level on the left and ultimate load level on the right) obtained from the experiment for single interior bolt sets with STD, OVS, and SSLT.

A comparison of experimental strength results to computed strength results at the deformation limit load is presented in Table 15 and at the ultimate limit load in Table 16. Strength comparisons are also shown in Figure 15.

The experimental strengths are greater than calculated strengths for all specimens and all equations evaluated. Where the calculated strengths are based on tearout and the strength from the various equations are different (i.e., smaller spacing), the equations using l_c are the most conservative. The equations using l_{v1} and l_{v2}, which tend to be greater than l_c, result in bearing controlling more often, especially when deformation at the bolt hole at service load is a design consideration. However, as described in the following section, the strength from these tests may overestimate the contribution of a single interior bolt in a group.

Table 14. Tearout Lengths – Interior Bolt Specimens

Index	l_c (in.)	l_{v1} (in.)	l_{v2} (in.)
18	1.193	1.699	1.595
19	1.442	1.949	1.845
20	1.691	2.196	2.094
21	1.947	2.454	2.349
22	2.194	2.705	2.595
23	1.074	1.450	1.539
24	1.325	1.700	1.792
25	1.565	1.940	2.032
26	1.816	2.197	2.279
27	2.066	2.456	2.526
28	1.192	1.416	1.591
29	1.445	1.669	1.848
30	1.692	1.916	2.091
31	1.939	2.163	2.343
32	2.191	2.417	2.596

Table 15. Deformation Limit Strength Comparison – Interior Bolt Specimens

Index	Eq. 12 (l_c)		Eq. 13 (l_{v1})		Eq. 14 (l_{v2})	
	R_n (kips)	$R_{exp,d}/R_n$	R_n (kips)	$R_{exp,d}/R_n$	R_n (kips)	$R_{exp,d}/R_n$
18	26.63	1.447	33.41	1.154	33.41	1.154
19	32.19	1.247	33.41	1.201	33.41	1.201
20	33.41	1.291	33.41	1.291	33.41	1.291
21	33.41	1.239	33.41	1.239	33.41	1.239
22	33.41	1.231	33.41	1.231	33.41	1.231
23	23.97	1.425	32.39	1.055	33.41	1.022
24	29.58	1.325	33.41	1.173	33.41	1.173
25	33.41	1.176	33.41	1.176	33.41	1.176
26	33.41	1.178	33.41	1.178	33.41	1.178
27	33.41	1.199	33.41	1.199	33.41	1.199
28	26.62	1.316	31.63	1.107	33.41	1.048
29	32.27	1.098	33.41	1.061	33.41	1.061
30	33.41	1.125	33.41	1.125	33.41	1.125
31	33.41	1.150	33.41	1.150	33.41	1.150
32	33.41	1.168	33.41	1.168	33.41	1.168
Average		1.241		1.163		1.161
St. Dev.		0.103		0.069		0.073

Table 16. Ultimate Limit Strength Comparison – Interior Bolt Specimens

Index	Eq. 15 (l_c)		Eq. 16 (l_{v1})		Eq. 17 (l_{v2})	
	R_n (kips)	$R_{exp,u}/R_n$	R_n (kips)	$R_{exp,u}/R_n$	R_n (kips)	$R_{exp,u}/R_n$
18	33.29	1.371	37.95	1.203	35.62	1.281
19	40.24	1.255	41.76	1.209	41.19	1.226
20	41.76	1.384	41.76	1.384	41.76	1.384
21	41.76	1.409	41.76	1.409	41.76	1.409
22	41.76	1.398	41.76	1.398	41.76	1.398
23	29.97	1.337	32.39	1.237	34.38	1.165
24	36.97	1.282	37.97	1.249	40.01	1.185
25	41.76	1.229	41.76	1.229	41.76	1.229
26	41.76	1.309	41.76	1.309	41.76	1.309
27	41.76	1.353	41.76	1.353	41.76	1.353
28	33.27	1.286	31.63	1.353	35.53	1.204
29	40.34	1.145	37.28	1.239	41.26	1.119
30	41.76	1.228	41.76	1.228	41.76	1.228
31	41.76	1.301	41.76	1.301	41.76	1.301
32	41.76	1.376	41.76	1.376	41.76	1.376
Average		1.311		1.274		1.278
St. Dev.		0.075		0.097		0.092

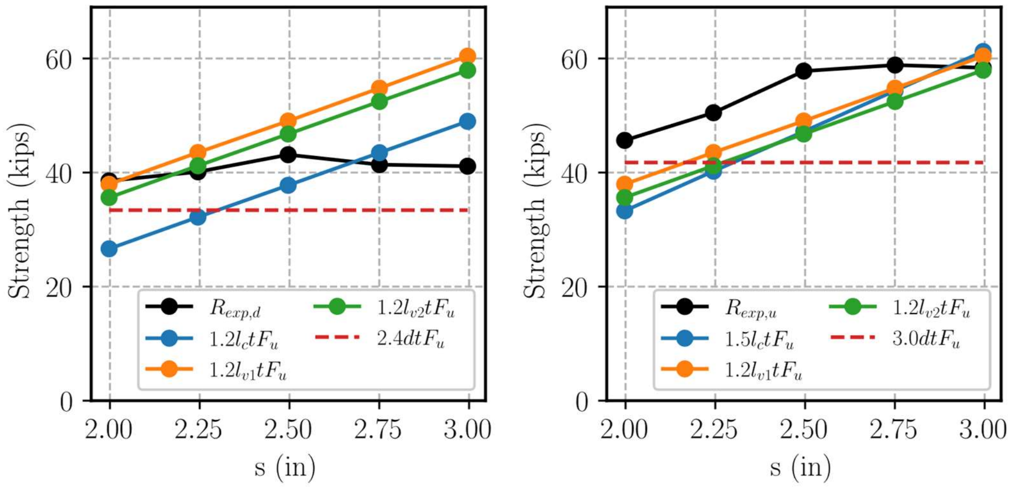

(a)

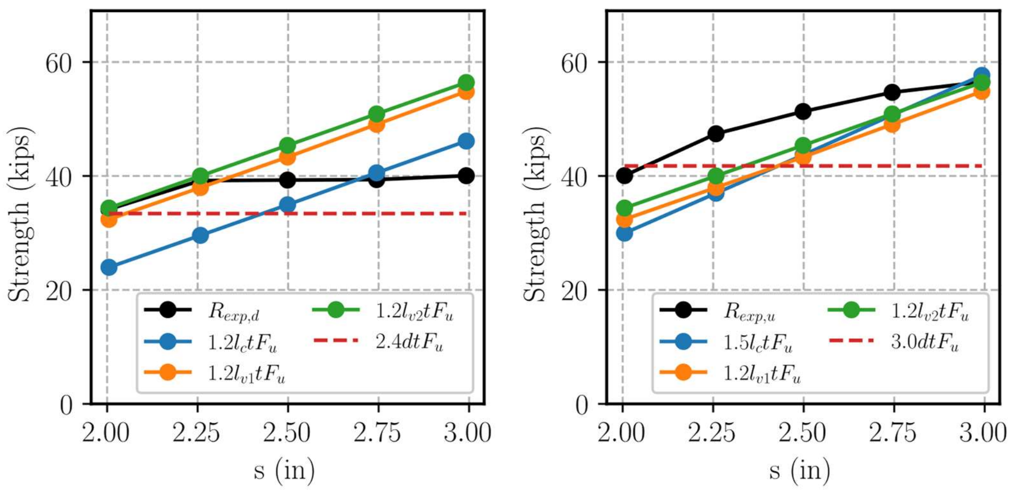

(b)

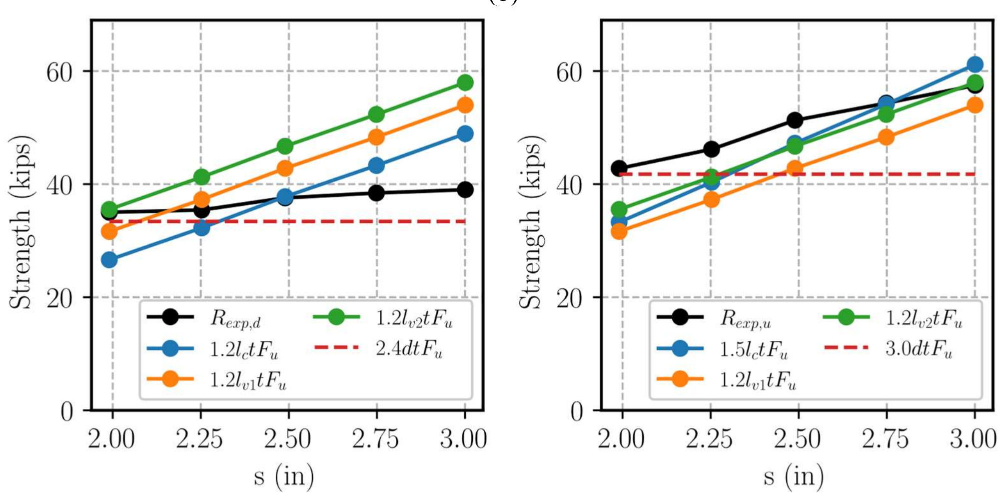

(c)

Figure 15. Comparison of plate strength (1/4 in. deformation level on the left and ultimate load level on the right) obtained from the experiment with tearout strength from equations using l_c, l_{v1}, and l_{v2} and bearing limits for single interior bolt sets with a) STD, b) OVS, c) SSLT.

Deformation Compatibility

Specimens 33 through 51 were designed to assess the validity of the deformation compatibility assumptions implicit in the AISC *Specification*. These specimens all had two bolt holes in the test plate. Some specimens were tested with just the edge bolt installed, some were tested with just the interior bolt installed, and some were tested with both bolts installed. The load-deformation was similar to that of the other specimens with the exception that these specimens were loaded well past the peak strength to more fully evaluate the load-deformation relationship. Photographs of two specimens after testing are shown in Figure 16.

Figure 16. Specimen 46 (left) and 51 (right) after testing.

Strength results are presented in Table 17. The strength results are also plotted in Figure 17. This figure compares the measured strength of specimens 40 through 51 (i.e., the specimens with both bolts installed) to the sum of the measured strengths from the corresponding specimens with a single bolt installed. The corresponding specimens were based on the edge distance and spacing. For example, specimen 40 had an edge distance of L_e = 1 in. and a spacing of s = 2 in.; thus, the corresponding specimens were 33 with L_e = 1 in. and 36 with s = 2 in. Figure 17 shows that the combined ultimate strength of the single-bolt specimens is consistently higher than the ultimate strength of the two-bolt specimens. A similar trend is observed for the deformation load level, except for some specimens that have a higher internal spacing.

The various lengths used in the tearout strength equations (i.e., l_c, l_{v1}, and l_{v2}) are listed in Table 18. The distances were calculated as described previously, however, two of each distance are presented in Table 18 for the specimens with two bolts, one for each bolt. A comparison of experimental strength results to computed strength results at the deformation limit load is presented in Table 19 and at the ultimate limit load in Table 20.

Table 17. Strength Results – Deformation Compatibility Specimens

Index	$R_{exp,d}$ (kips)	$R_{exp,u}$ (kips)	$R_{exp,u}/R_{exp,d}$
33	19.91	20.04	1.006
34	28.94	30.86	1.066
35	35.00	41.28	1.179
36	38.87	45.97	1.183
37	42.26	60.13	1.423
38	43.69	67.49	1.545
39	43.56	72.24	1.658
40	48.78	54.29	1.113
41	53.73	63.61	1.184
42	61.90	71.26	1.151
43	61.92	74.35	1.201
44	58.23	64.04	1.100
45	62.77	72.61	1.157
46	67.98	82.91	1.220
47	74.68	91.19	1.221
48	64.41	73.71	1.144
49	71.57	84.74	1.184
50	79.55	96.22	1.210
51	82.68	101.68	1.230

Table 18. Tearout Lengths – Deformation Compatibility Specimens

Index	l_c (in.)		l_{v1} (in.)		l_{v2} (in.)	
	Edge	Interior	Edge	Interior	Edge	Interior
33	0.602	---	0.856	---	0.803	---
34	1.101	---	1.353	---	1.302	---
35	1.604	---	1.858	---	1.805	---
36	---	1.199	---	1.706	---	1.602
37	---	2.193	---	2.701	---	2.595
38	---	3.193	---	3.702	---	3.595
39	---	5.193	---	5.700	---	5.595
40	0.604	1.194	0.858	1.701	0.805	1.596
41	0.604	2.195	0.857	2.702	0.805	2.597
42	0.602	3.194	0.858	3.709	0.803	3.595
43	0.603	5.200	0.857	5.710	0.804	5.601
44	1.102	1.194	1.356	1.702	1.303	1.596
45	1.102	2.195	1.356	2.702	1.303	2.597
46	1.106	3.193	1.360	3.701	1.307	3.595
47	1.100	5.194	1.354	5.701	1.301	5.596
48	1.603	1.195	1.857	1.702	1.804	1.597
49	1.601	2.195	1.855	2.704	1.802	2.597
50	1.603	3.193	1.857	3.700	1.803	3.595
51	1.601	5.195	1.855	5.703	1.802	5.597

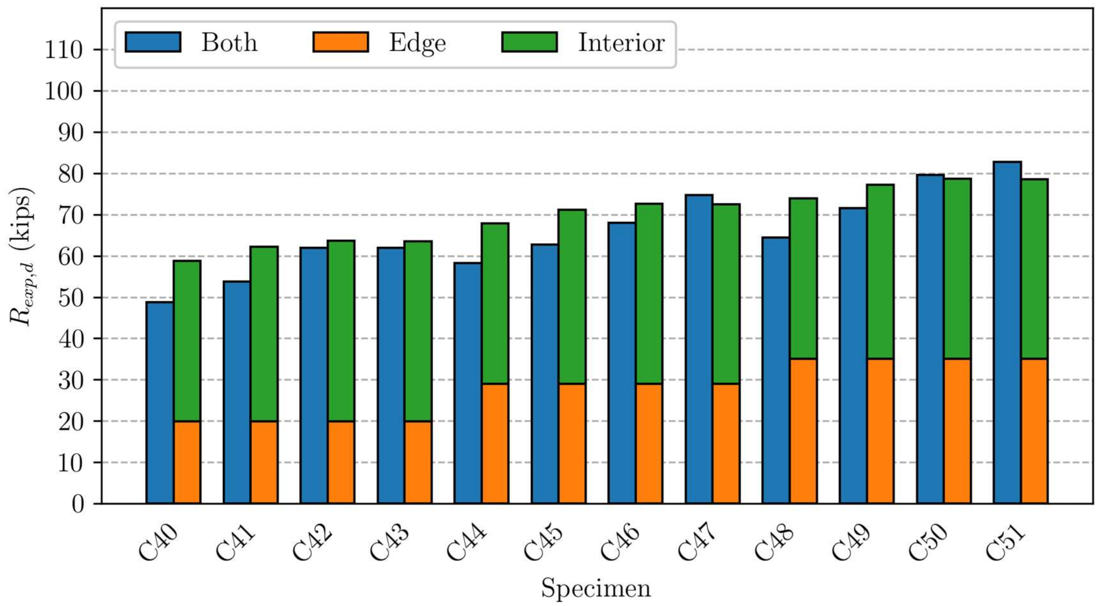

(a)

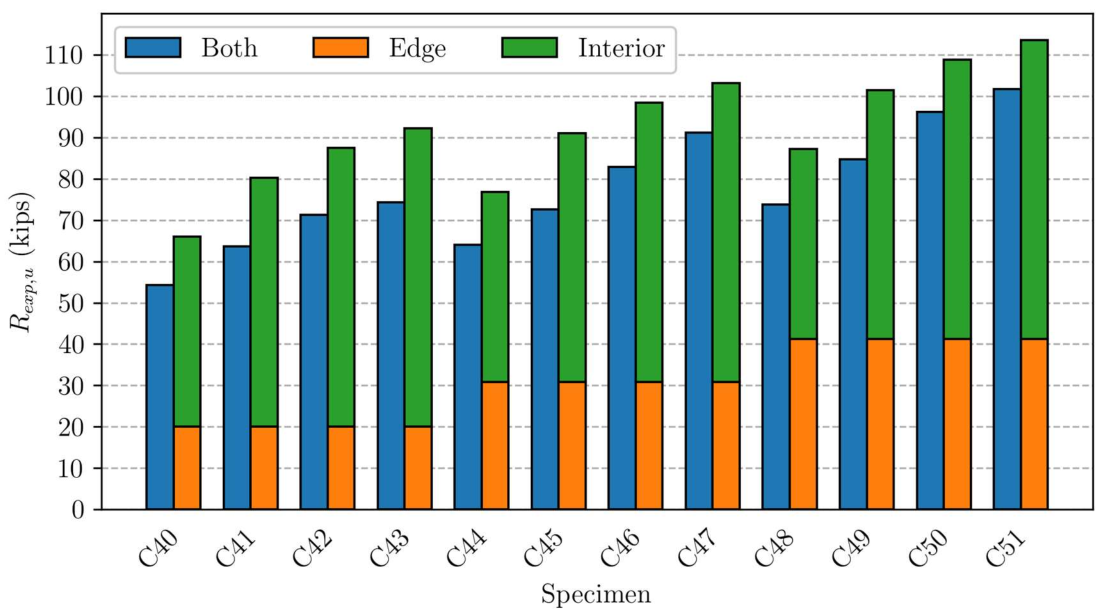

(b)

Figure 17. Comparison of plate strength for specimens with individual hole bolted against specimens with both holes bolted for the same plate configuration at (a) 1/4 in. deformation level and (b) ultimate load level.

Table 19. Deformation Limit Strength Comparison – Deformation Compatibility Specimens

Index	Eq. 12 (I_c)		Eq. 13 (I_{v1})		Eq. 14 (I_{v2})	
	R_n (kips)	$R_{exp,d}/R_n$	R_n (kips)	$R_{exp,d}/R_n$	R_n (kips)	$R_{exp,d}/R_n$
33	13.44	1.481	19.11	1.041	17.94	1.110
34	24.58	1.178	30.22	0.958	29.08	0.995
35	33.41	1.048	33.41	1.048	33.41	1.048
36	26.78	1.452	33.41	1.164	33.41	1.164
37	33.41	1.265	33.41	1.265	33.41	1.265
38	33.41	1.308	33.41	1.308	33.41	1.308
39	33.41	1.304	33.41	1.304	33.41	1.304
40	40.14	1.215	52.58	0.928	51.39	0.949
41	46.89	1.146	52.56	1.022	51.38	1.046
42	46.85	1.321	52.58	1.177	51.33	1.206
43	46.87	1.321	52.55	1.178	51.37	1.205
44	51.26	1.136	63.69	0.914	62.50	0.932
45	58.02	1.082	63.70	0.985	62.51	1.004
46	58.11	1.170	63.78	1.066	62.60	1.086
47	57.97	1.288	63.65	1.173	62.46	1.196
48	60.08	1.072	66.82	0.964	66.82	0.964
49	66.82	1.071	66.82	1.071	66.82	1.071
50	66.82	1.191	66.82	1.191	66.82	1.191
51	66.82	1.237	66.82	1.237	66.82	1.237
Average		1.226		1.105		1.120
St. Dev.		0.123		0.127		0.121

Table 20. Ultimate Limit Strength Comparison – Deformation Compatibility Specimens

Index	Eq. 15 (I_c)		Eq. 16 (I_{v1})		Eq. 17 (I_{v2})	
	R_n (kips)	$R_{exp,u}/R_n$	R_n (kips)	$R_{exp,u}/R_n$	R_n (kips)	$R_{exp,u}/R_n$
33	16.80	1.192	19.11	1.048	17.94	1.117
34	30.72	1.005	30.22	1.021	29.08	1.061
35	41.76	0.988	41.49	0.995	40.31	1.024
36	33.47	1.374	38.10	1.206	35.76	1.285
37	41.76	1.440	41.76	1.440	41.76	1.440
38	41.76	1.616	41.76	1.616	41.76	1.616
39	41.76	1.730	41.76	1.730	41.76	1.730
40	50.18	1.082	57.15	0.950	53.62	1.012
41	58.61	1.085	60.91	1.044	59.73	1.065
42	58.57	1.217	60.93	1.170	59.68	1.194
43	58.59	1.269	60.90	1.221	59.72	1.245
44	64.08	0.999	68.29	0.938	64.73	0.989
45	72.52	1.001	72.05	1.008	70.86	1.025
46	72.63	1.142	72.13	1.149	70.95	1.169
47	72.47	1.258	72.00	1.267	70.82	1.288
48	75.10	0.981	79.48	0.927	75.94	0.971
49	83.52	1.015	83.18	1.019	82.01	1.033
50	83.52	1.152	83.24	1.156	82.03	1.173
51	83.52	1.217	83.18	1.222	81.99	1.240
Average		1.198		1.165		1.194
St. Dev.		0.214		0.223		0.210

The equations are generally conservative with average test-to-predicted ratios greater than 1 at both the ultimate and deformation limit levels. However, the strength of the specimens with two bolts installed and a spacing of 2 in. is overestimated by the strength equations using l_{v1} and l_{v2}. The maximum error is approximately 9%. Notably, the strength of the specimen with only the interior bolt installed and a spacing of 2 in. (i.e., specimen 36) is not overestimated by the strength equations. The strength equations using l_c do not overestimate the strength. It is unclear whether this is because the strength equations using l_c are more accurate or simply more conservative.

While the error when s = 2 in. is relatively small, it was consistent across several specimens with varying edge distance and warrants further investigation. Finite element simulation may be particularly helpful as the force in each bolt can be quantified to better understand the behavior and the cause of the overestimation. The tests with only one bolt installed were intended to be a proxy of the force in each bolt, but the behavior of the interior bolt in the group appears to be different than the behavior of the same bolt when alone.

The strength of specimens with a small edge distance and large spacing, such as specimen 43, is underpredicted by the strength equations. This result indicates that the deformation compatibility effects that motivated this series of specimens does not have a clear deleterious effect on the evaluation of strength. Deformation compatibility is further explored by examining the load-deformation response of the connections.

Plots of load vs. deformation for specimens 40 and 42 are shown in Figure 18. The two corresponding specimens with only one bolt installed are also shown on this figure, as is the sum of the responses from the two corresponding specimens with only one bolt installed. The vertical dashed lines indicate the deformation at the maximum load in the response. Four horizontal dashed lines show key strength results for each specimen. The computed strengths are based on equations when deformation at the bolt hole at service loads is not a design consideration.

Figure 18 shows that the specimens achieve their peak load at different levels of deformation. The edge bolt reaches a peak at about 1/4 in. deformation while the interior bolt reaches a peak at about 1/2 in. deformation for specimen 40 and 1 in. deformation for specimen 42. The combined group strength reaches a peak at a relatively low deformation, approximately when the strength of the edge bolt starts to decrease. Based on this observation, an accurate estimation of the strength of a bolt group would be obtained by using the load in the interior bolts at a relatively low level of deformation, and not their peak load, as the strength of the interior bolts. The mostly conservative results shown in Table 19 and Table 20 may be due to conservative bearing strength equations. However, this evaluation is made challenging by the apparent differences in behavior between interior bolts in a group and interior bolts alone. These differences are also seen in the load-deformation response by comparing the specimen with both bolts installed to the sum of the responses from the two tests with only a single bolt installed. Finite element simulations are recommended to further explore these deformation compatibility effects and develop stronger conclusions.

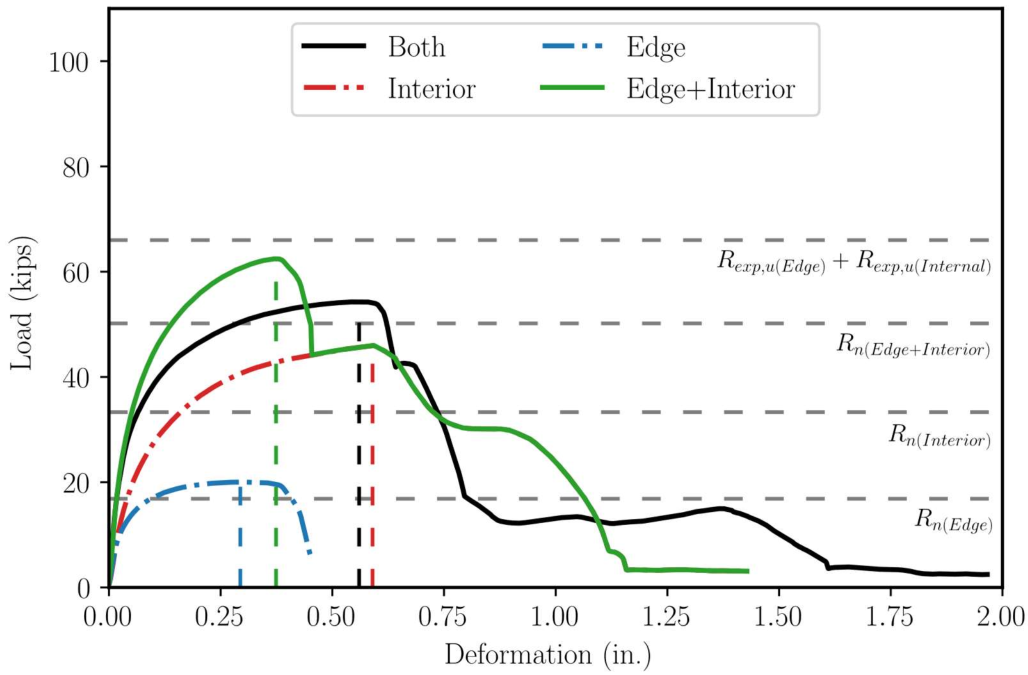

(a) Specimen 40

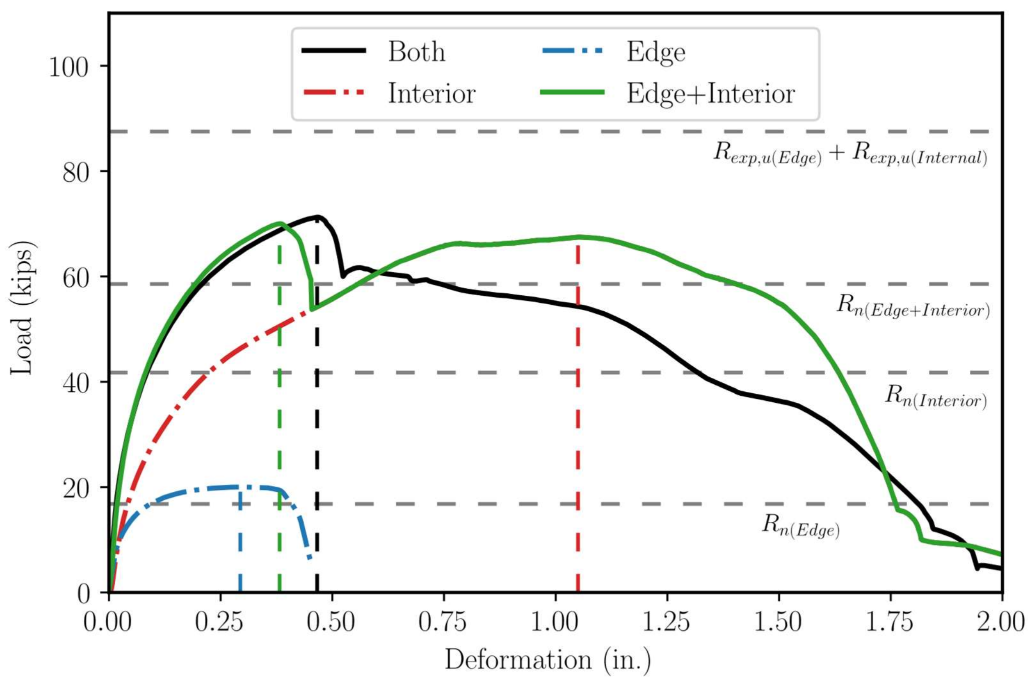

(b) Specimen 42

Figure 18.Combined load-deformation plots.

Chapter 3: Eccentrically Loaded Bolt Group Experiments (Lower Eccentricity)

The experimental evaluation of eccentrically loaded bolt groups is divided into two configurations. This chapter describes testing of two-bolt connections with lower eccentricity.

Materials and Methods

To investigate the behavior of eccentrically loaded bolt groups, 16 specimens as shown in Figure 19 were tested. Each specimen included two eccentrically loaded bolt groups each with two bolts (i.e., the connections between the test plate and the rocker plates). The specimens were designed to fail through bearing or tearout in the test plate.

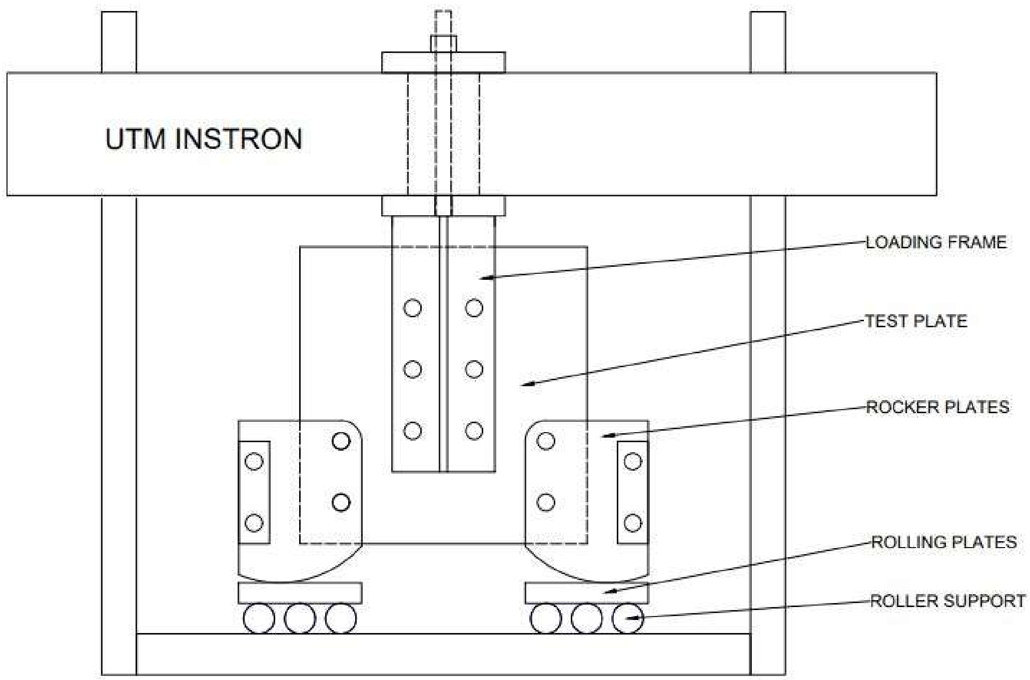

Figure 19: Schematic view of test configuration.

The test specimens included both standard hole and short slotted hole specimens with a variety of edge distances as listed in Table 21. Two specimens (3L and 8L) were also tested with loose bolts instead of finger tight bolts to investigate the effect of confinement provided by the bolts. The edge distance was varied between 0.75 in. and 2.5 in. for standard hole specimens, and between 1.125 in. and 2 in. for slotted hole specimens.

The test configuration depicted in Figure 19 included a loading frame attached to the crosshead of an Instron universal testing machine (UTM). The loading frame assembly consisted of T-shaped and L-shaped parts, as shown in Figure 20. The T-shaped part was connected to the UTM crosshead with a threaded rod. The flange of the L-shaped part was connected to the flange of the

T-shaped part by two vertical bolts, leaving a 1/4 in. gap for the test plate. Six bolts passed through the stem of the T- and L-shaped parts and the test plate.

Table 21. Test Matrix with Nominal Dimensions

Index	L_{eh} (in.)	L_{ev} (in.)	Bolt Tightness	Hole Type
1	0.75	0.75	Finger Tight	Standard
1.1	0.75	1	Finger Tight	Standard
1.2	0.75	1.5	Finger Tight	Standard
2A	1	1	Finger Tight	Standard
2B	1	1	Finger Tight	Standard
3	1.25	1.25	Finger Tight	Standard
3L	1.25	1.25	Loose	Standard
4A	1.5	1.5	Finger Tight	Standard
4B	1.5	1.5	Finger Tight	Standard
5	2	2	Finger Tight	Standard
6	2.5	2.5	Finger Tight	Standard
7	1.125	1.125	Finger Tight	Short Slots
8	1.25	1.25	Finger Tight	Short Slots
8L	1.25	1.25	Loose	Short Slots
9	1.5	1.5	Finger Tight	Short Slots
10	2	2	Finger Tight	Short Slots

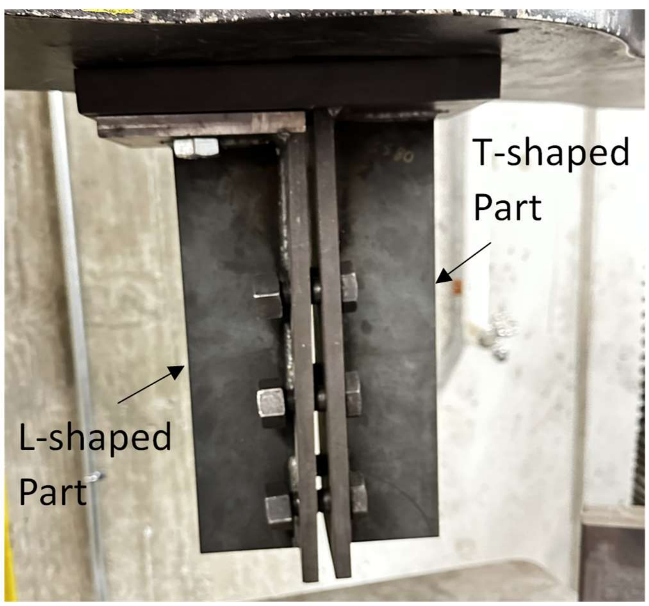

Figure 20: Loading frame assembly without test plate installed.

The test plate was connected to rocker plates on both ends by two 3/4 in. diameter bolts at 3 in. spacing. The rocker plate sat on the top of a rolling plate situated atop cylindrical rods to emulate roller supports and ensure that the reaction on the specimen was always vertical. The test bolts were at an eccentricity of 3 inches. The circular curve at the bottom of the rocker plate was designed so that the eccentricity of the connection remained a constant 3 in. as the rocker plate rotated. The center of the curve was located 3 in. from the centroid of the bolt group as shown in

Figure 21. Note, however, variation from the 3 in. eccentricity occurred as the rocker displaced horizontally due to greater bolt hole deformation in the bottom bolt compared to the top.

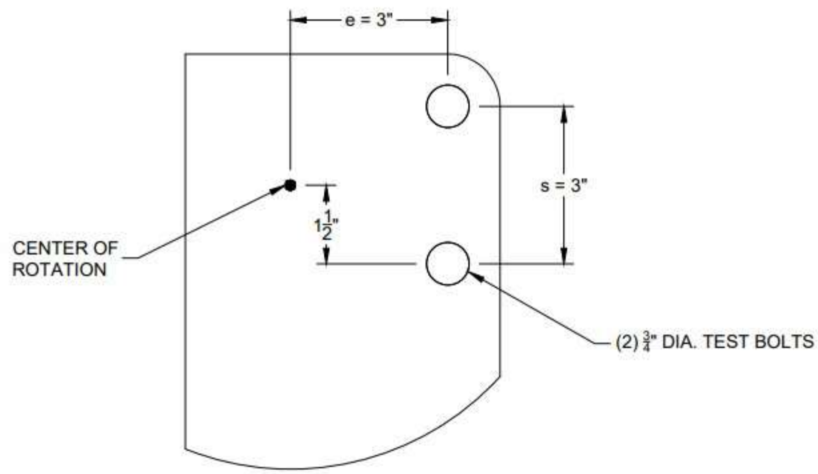

Figure 21. Location of the center of rotation in rocker plate.

The test plates were nominally 1/4 in. thick and made of ASTM A572 Gr 50 steel. The test plate specimens were fabricated by water jet cutting. The measured thickness was 0.2481 in. The yield strength of the plate material was 66.77 ksi and the tensile strength was 75.48 ksi based on the average of four tensile coupon tests conducted in accordance with ASTM E8 (ASTM 2022). The results of the coupon tests are summarized in Table 22. One of the coupons was tested with Optotrak markers installed so that the full range of stress-strain response could be measured. The measured response is shown in Figure 22 The gage of the Optotrak markers was 6 in. which was different than the gage used to determine the elongation listed in Table 22. A smaller gage length was used for the Optotrak data to ensure clear sight lines.

Table 22. Coupon Test Results

Sample Number	**Thickness (in.)**	**F_y (ksi)**	**F_u (ksi)**	**Elongation [a]**
1	0.24770	67.85	75.65	21.88%
2	0.24800	66.13	75.45	20.31%
3	0.24850	66.34	75.35	18.75%
4	0.24799	67.04	75.97	19.53%
Average	0.24805	66.84	75.61	20.12%

[a] Gage length = 8in.

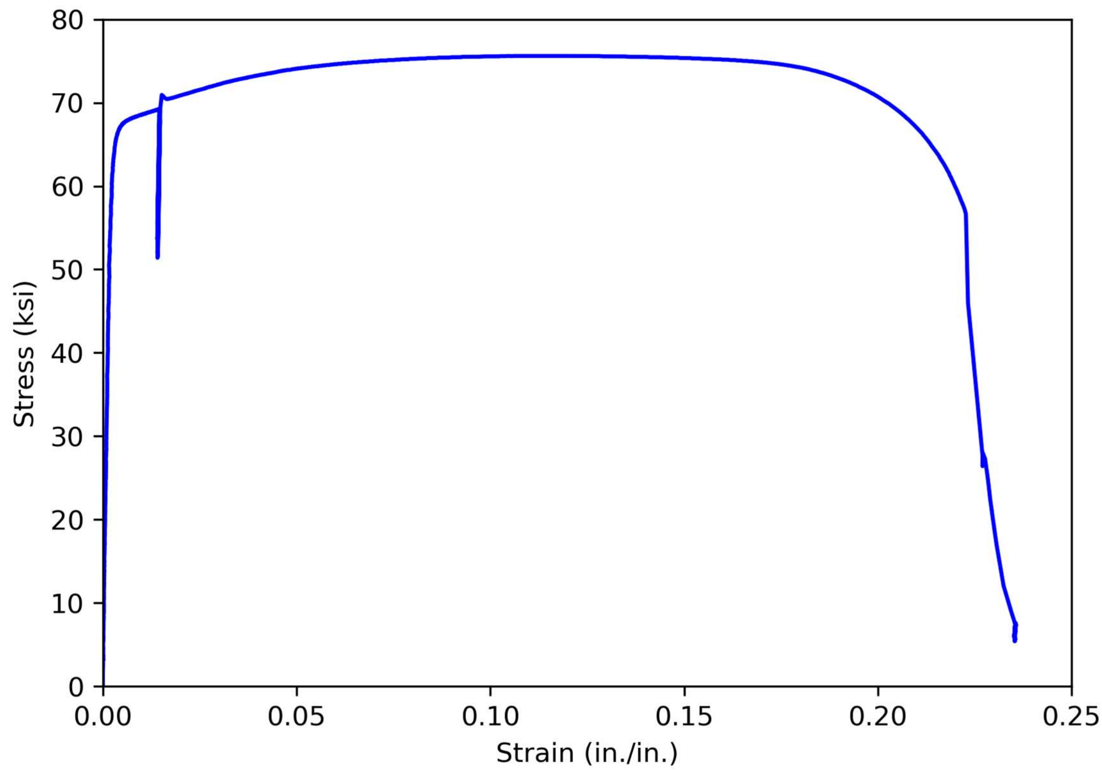

Figure 22: Stress-strain curve of test plate material.

The edge distance was defined as the distance from the center of the hole to the edge of plate as shown in Figure 23. Measured dimensions for each test specimen are listed in Table 23. The listed dimensions are the average dimensions of test specimens on both sides of the test plate. The diameter of the bolt hole, width and length of the slot, and distance from the edge of bolt hole to the edge of plate were measured. The measured edge distances L_{ev} and L_{eh} were calculated as the measured distance from the edge of the hole to the edge of the plate plus half the measured width of the hole.

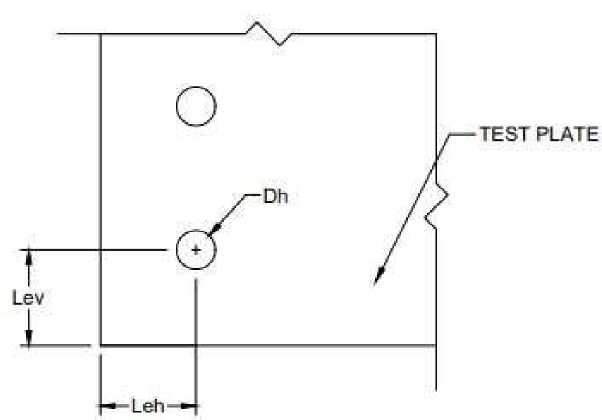

Figure 23. Dimension Definitions

Table 23. Measured Dimensions of Specimens

Specimen	Hole Type	Hole Diameter, d_h, or Width of Slot (in.)	Length of Slot (in.)	Edge Distance (in.)	
				L_{eh}	L_{ev}
1	Standard	0.811	-	0.754	0.754
1.1	Standard	0.810	-	0.752	1.004
1.2	Standard	0.810	-	0.755	1.504
2A	Standard	0.807	-	1.000	1.005
2B	Standard	0.811	-	1.006	1.004
3	Standard	0.811	-	1.242	1.258
3L	Standard	0.809	-	1.240	1.255
4A	Standard	0.805	-	1.505	1.498
4B	Standard	0.810	-	1.504	1.503
5	Standard	0.808	-	2.006	2.008
6	Standard	0.807	-	2.502	2.501
7	Slotted	0.802	1.116	1.113	1.127
8	Slotted	0.805	1.114	1.236	1.249
8L	Standard	0.812	1.123	1.235	1.254
9	Slotted	0.805	1.117	1.502	1.498
10	Slotted	0.807	1.111	1.998	2.000

The deformation of the specimens was measured using an Optotrak position measurement machine, which optically tracks the three-dimensional position of LED markers. Six LED markers were placed on the test plate and the rocker plates to assess the deformation and rotation of rocker plate relative to the test plate. The placement of the markers was as shown in Figure 24. The positions of the LED markers were measured at a frequency of 50 Hz. Load and crosshead displacement were measured internally by the UTM and synchronized to the Optotrak data in post-processing.

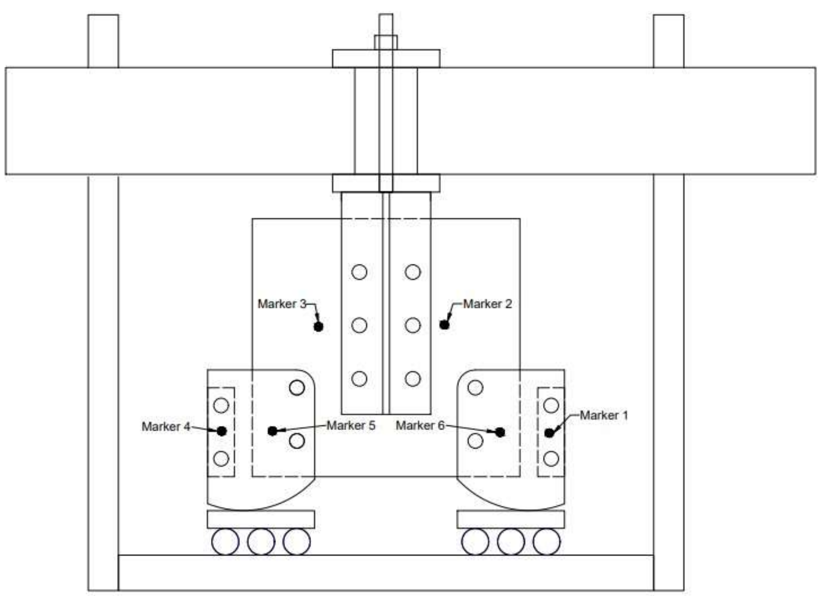

Figure 24: Positions of Markers in test configuration.

In post-processing, markers 4 and 5 were used for the left rocker plate, and markers 1 and 6 for the right rocker plate to compute vertical deformation and rotation. The average *y* coordinate of the markers on each plate determined their vertical position. Vertical deformation of the rocker was then obtained by subtracting the rocker plates' vertical position from that of the test plate. This vertical deformation was taken relative to the test plate. The rotation was calculated as the change in angle of the vector from one marker on the rocker plate to the other.

The applied load, measured using the UTM's internal load cell, was multiplied by the eccentricity to obtain the moment applied to each of the two connections. The test specimens were initially set to have an eccentricity of 3 in. As the test progressed, the eccentricity increased with the lateral movement of the plate. The *x* coordinate values of Marker 4 and 5, and Marker 1 and 6, were used to calculate the lateral displacement of the roller. The calculated movement was added to the initial eccentricity to get the instantaneous eccentricity.

For all specimens except 3L and 8L, all the bolts were finger-tightened before testing. The AISC *Specification* requires that bolts be installed at least snug tight. The use of finger tightened bolts in this work was done to reduce friction in the connection. Friction introduces variability between specimens, and reducing friction results in more predictable behavior, and provides a truer evaluation of bearing and tearout strength. The test bolts in specimens 3L and 8L were first finger-tightened then loosened by a quarter turn of the nut to evaluate the potential effects of friction, confinement, and gouging.

Displacement-controlled compressive load was applied at a displacement rate of the crosshead of 0.5 in, /min until a load of 100 lbs was achieved and a rate of 0.1 in./min thereafter. For most specimens, the test was stopped after it was clear that the maximum load had been achieved. For specimen 6, the test was stopped when the applied load neared the capacity of the UTM and the test plate neared contact with the rolling plates.

Results

Plots of load vs deformation and moment vs rotation for each of the specimens are presented in Figure 25 through Figure 40. The load in these figures is for each bolt group, note that the total load applied to the specimen was twice as much. The limits of the axes are held the same for these figures to aid visual comparison. At low loads, relatively large movements were observed as the bolts came into bearing. For clarity, these movements are excluded from Figure 25 through Figure 40 by shifting the curves along the x-axis. The shift was made such that a secant line connecting two points on the load deformation curve at 5% and 10% of the maximum load intersected the origin. The plots for the left and right bolt groups were shifted independently.

All specimens exhibited a similar pattern of behavior. As the bolts came into bearing, the load rose steadily. The load-deformation curve initially displayed a linear elastic region that progressively transitioned into an inelastic phase as the test plate yielded. The stiffness decreased until the peak load was reached and a gradual decline in load occurred thereafter. Once the specimens indicated a clear drop in load from the peak, the test was stopped, and the specimens were unloaded.

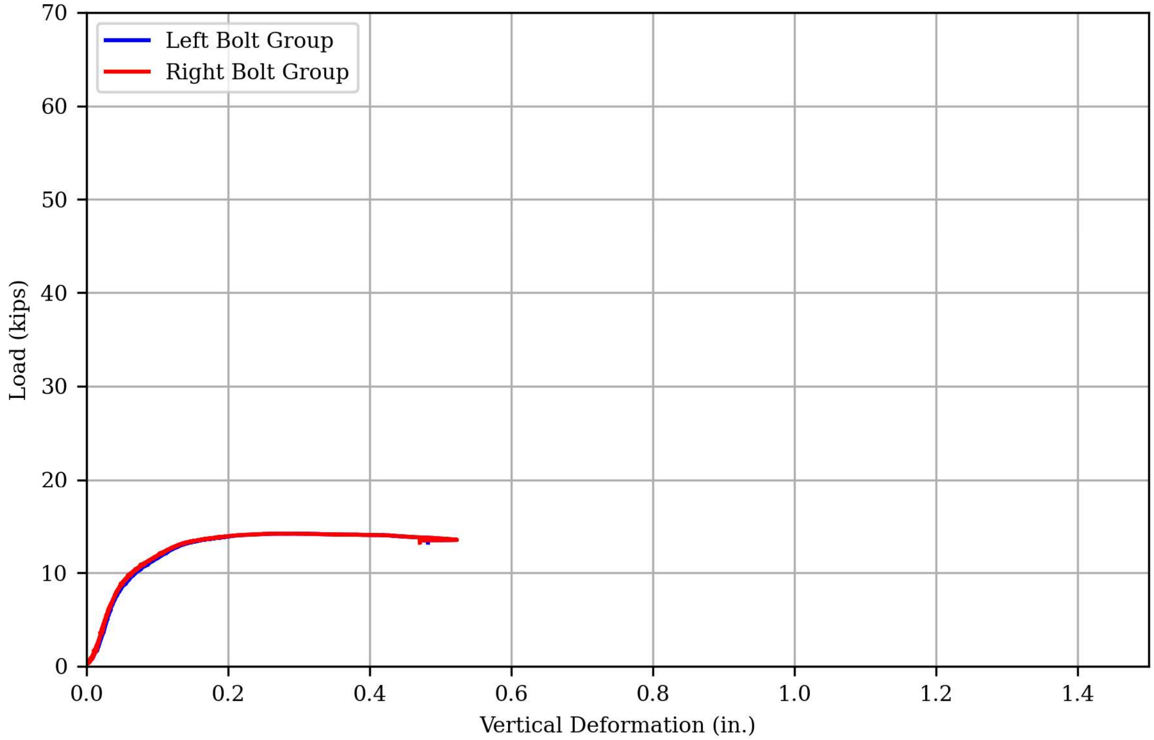

(a) Load vs Deformation

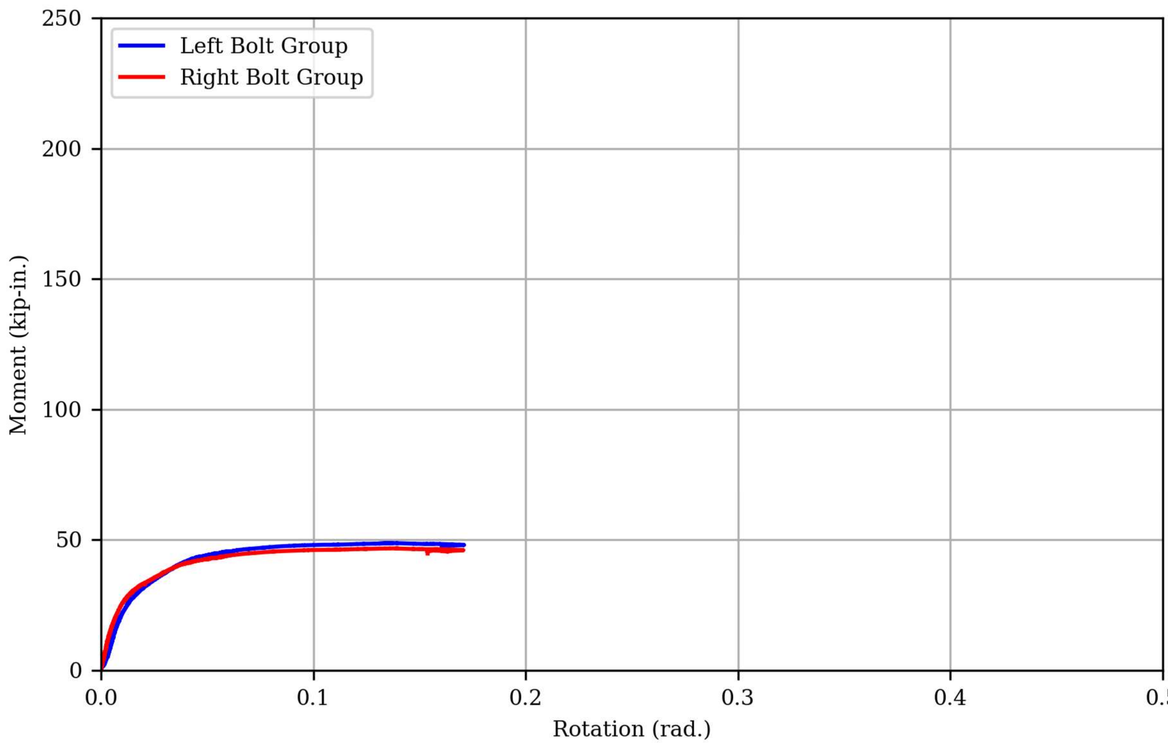

(b) Moment vs Rotation

Figure 25. Measured Response of Specimen 1.1

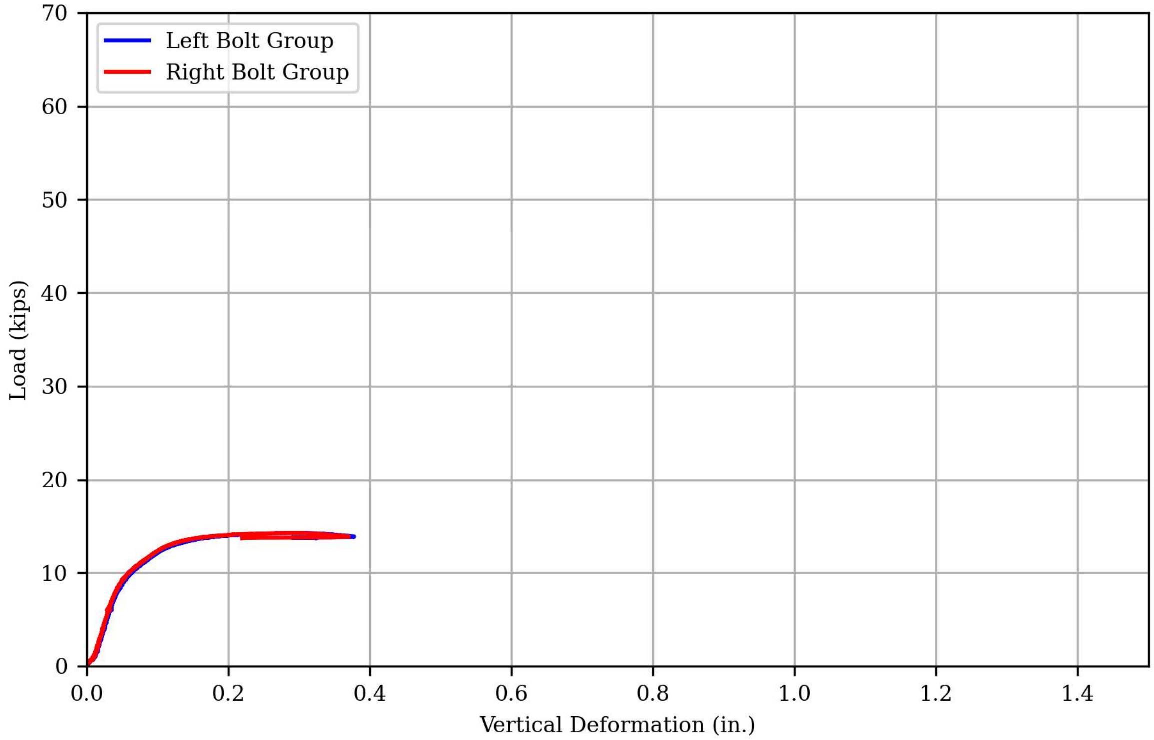

(a) Load vs Deformation

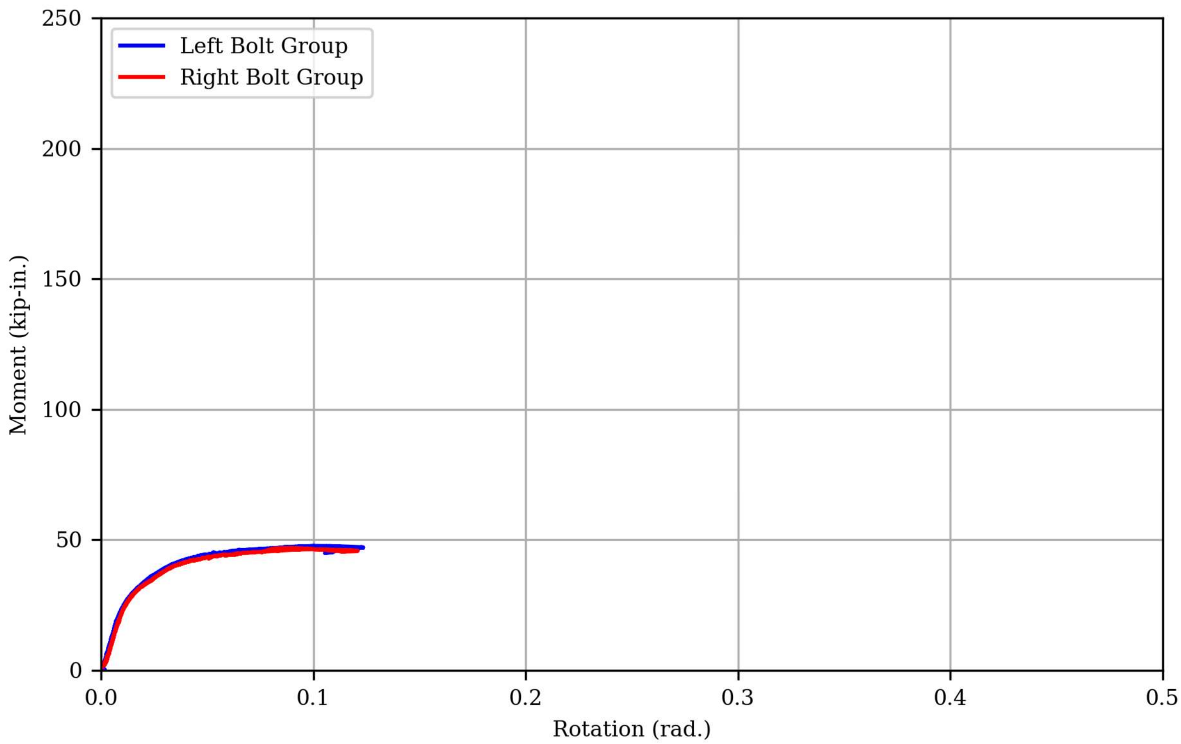

(b) Moment vs Rotation

Figure 26. Measured Response of Specimen 1.2

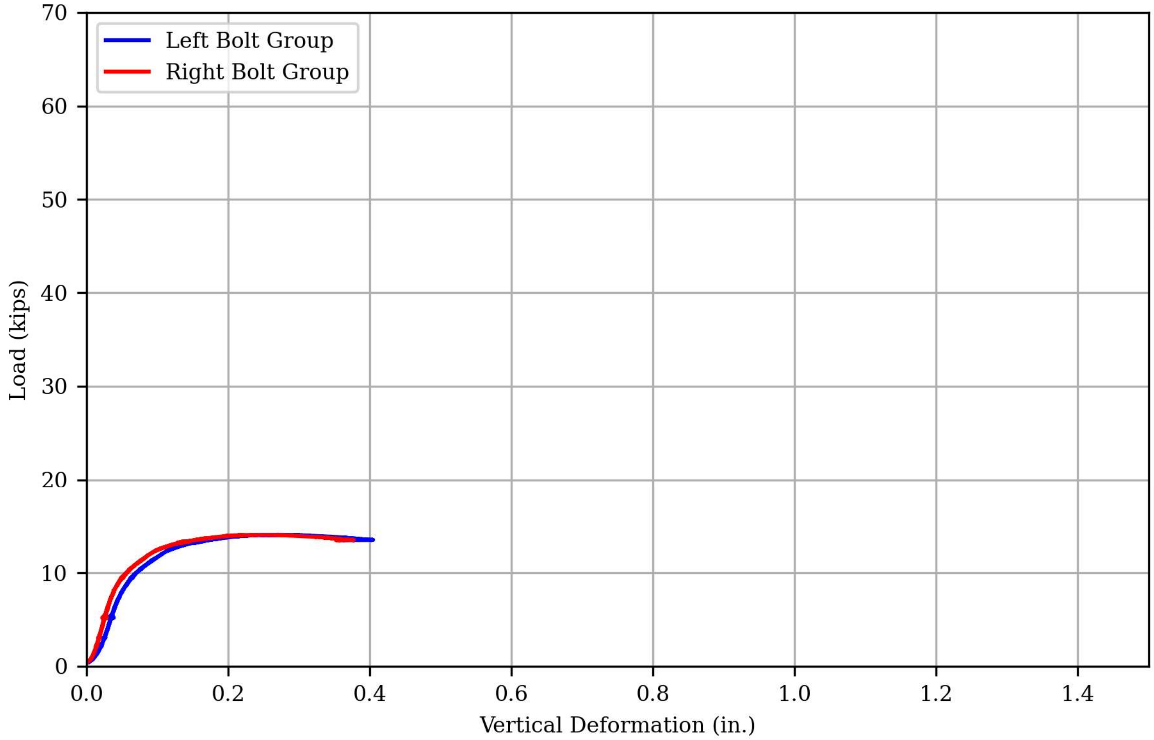

(a) Load vs deformation

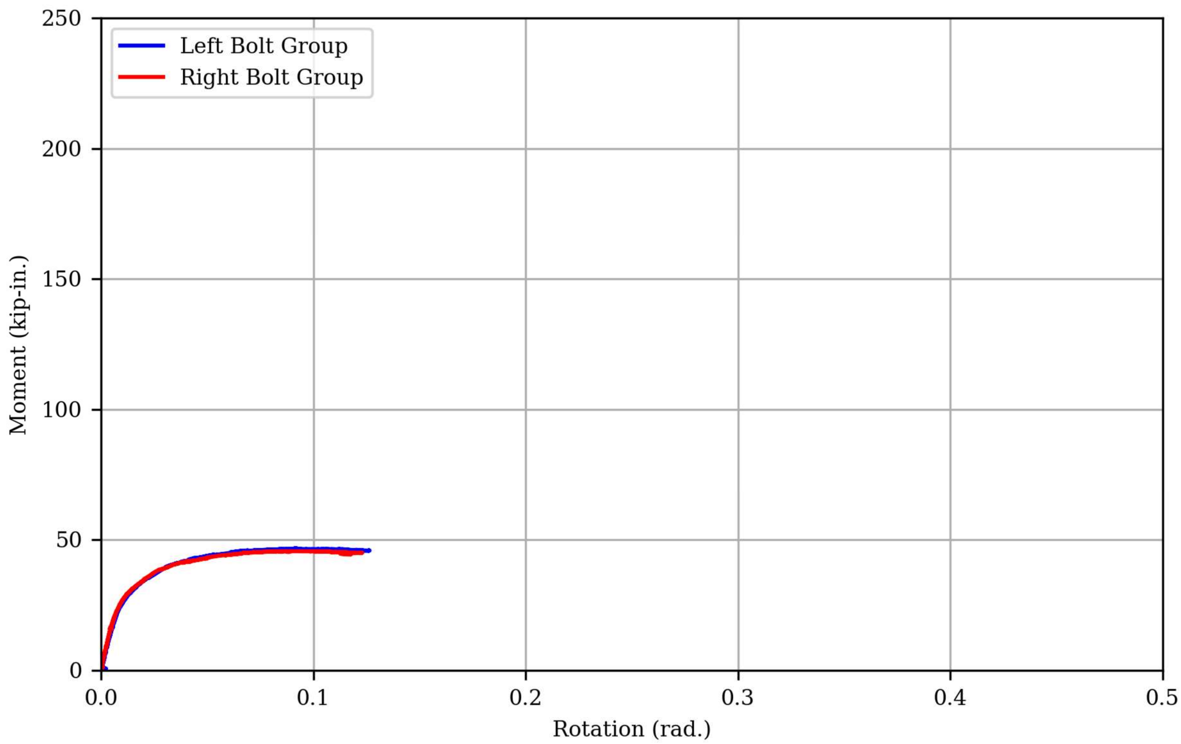

(b) Moment vs rotation

Figure 27. Measured response of specimen 1.3

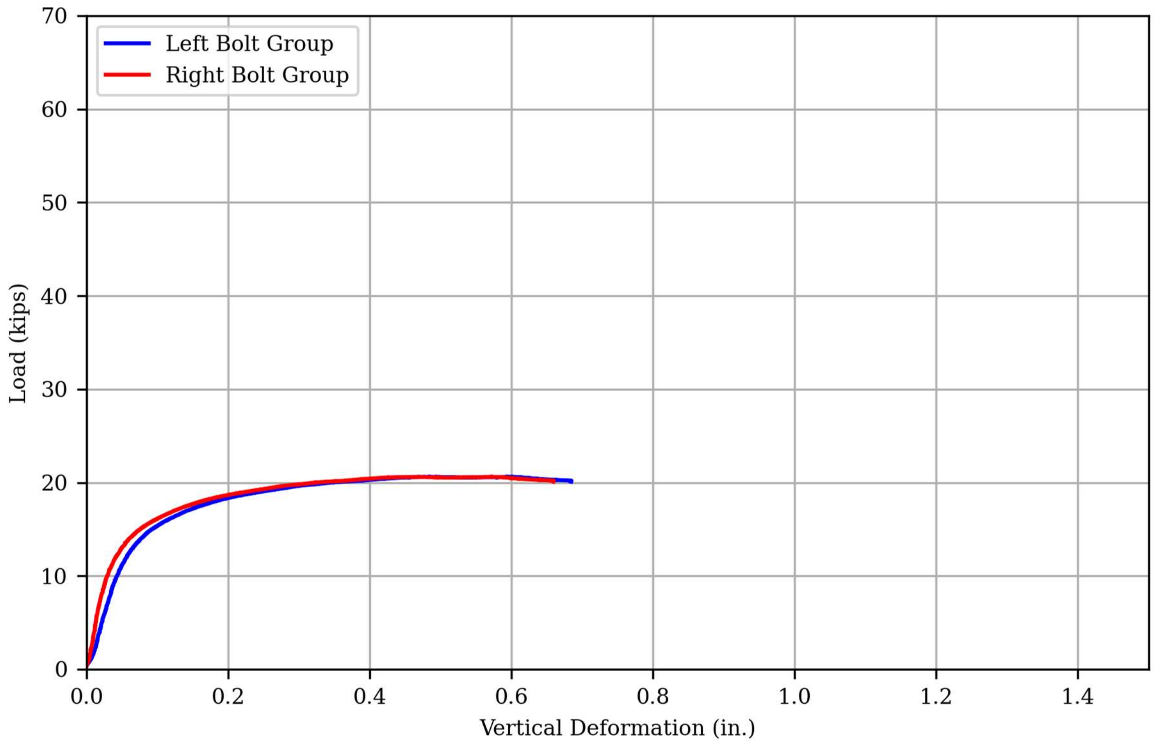

(a) Load vs Deformation

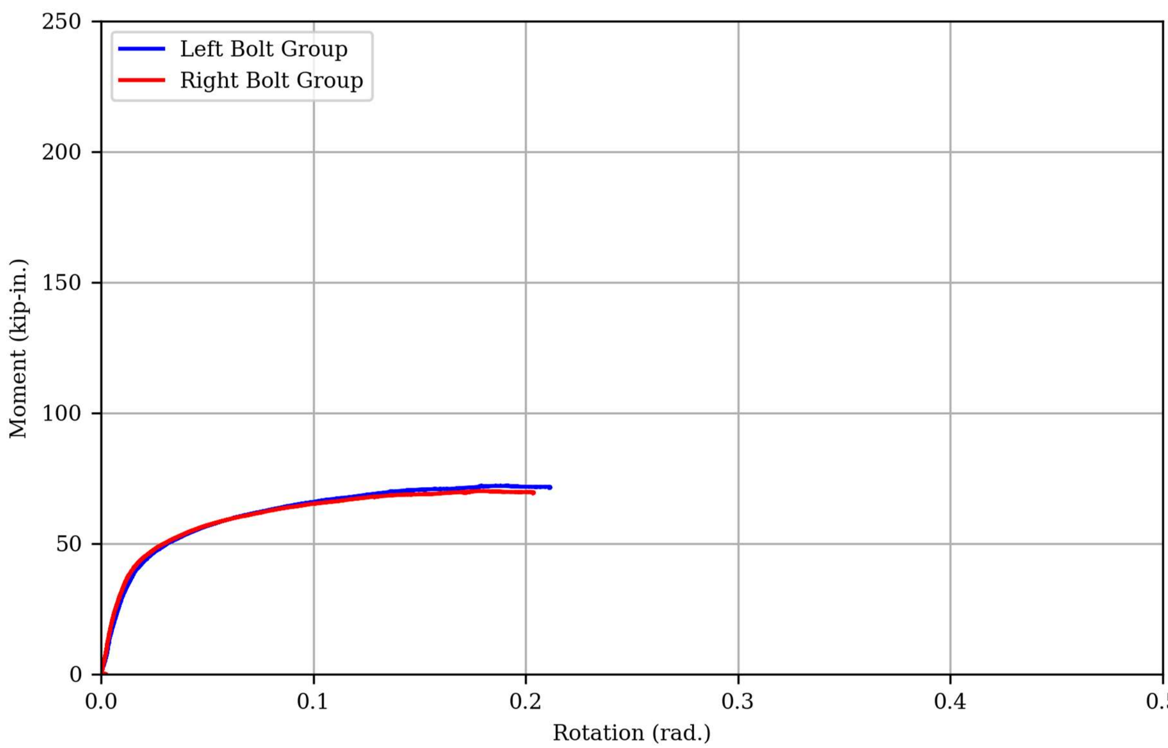

(b) Moment vs Rotation
Figure 28. Measured Response of Specimen 2A

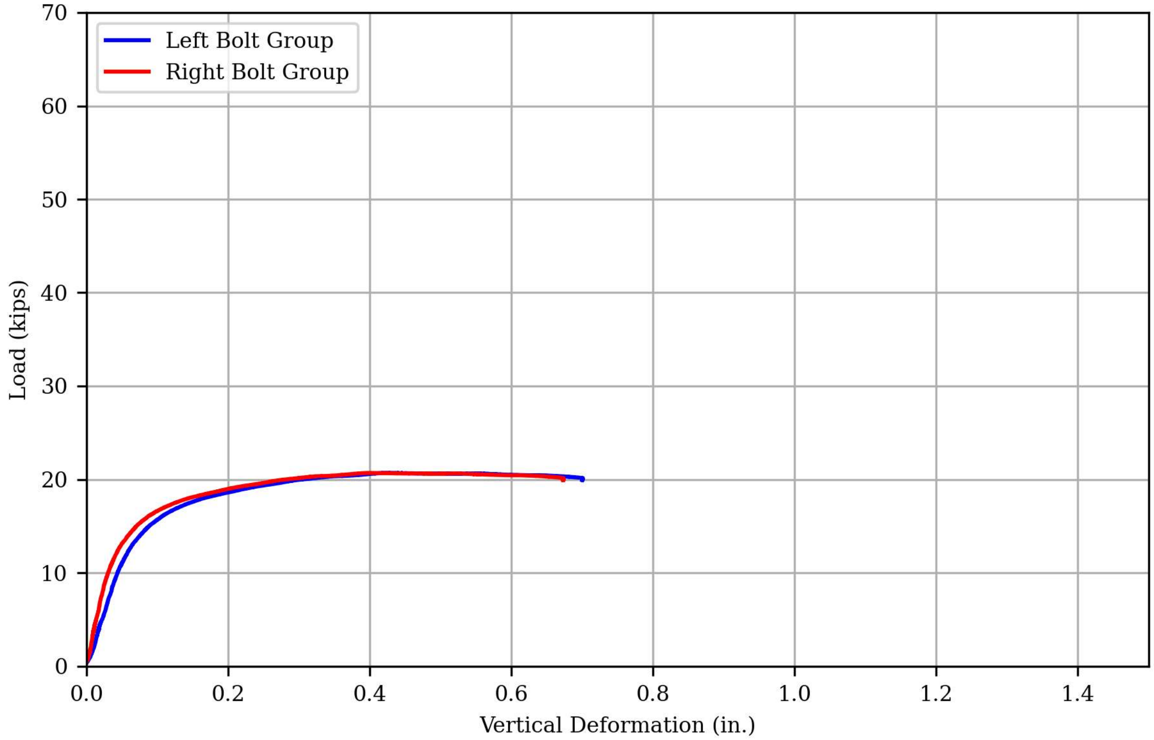

(a) Load vs deformation

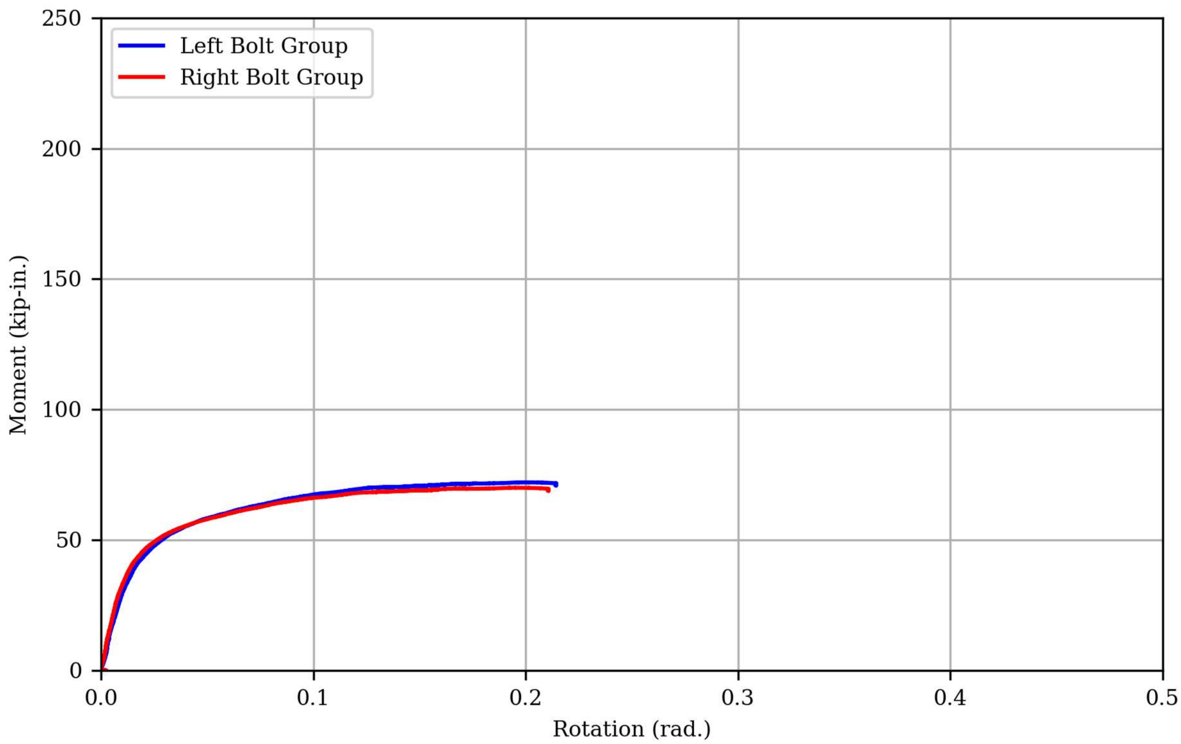

(b) Moment vs rotation

Figure 29. Measured response of specimen 2B

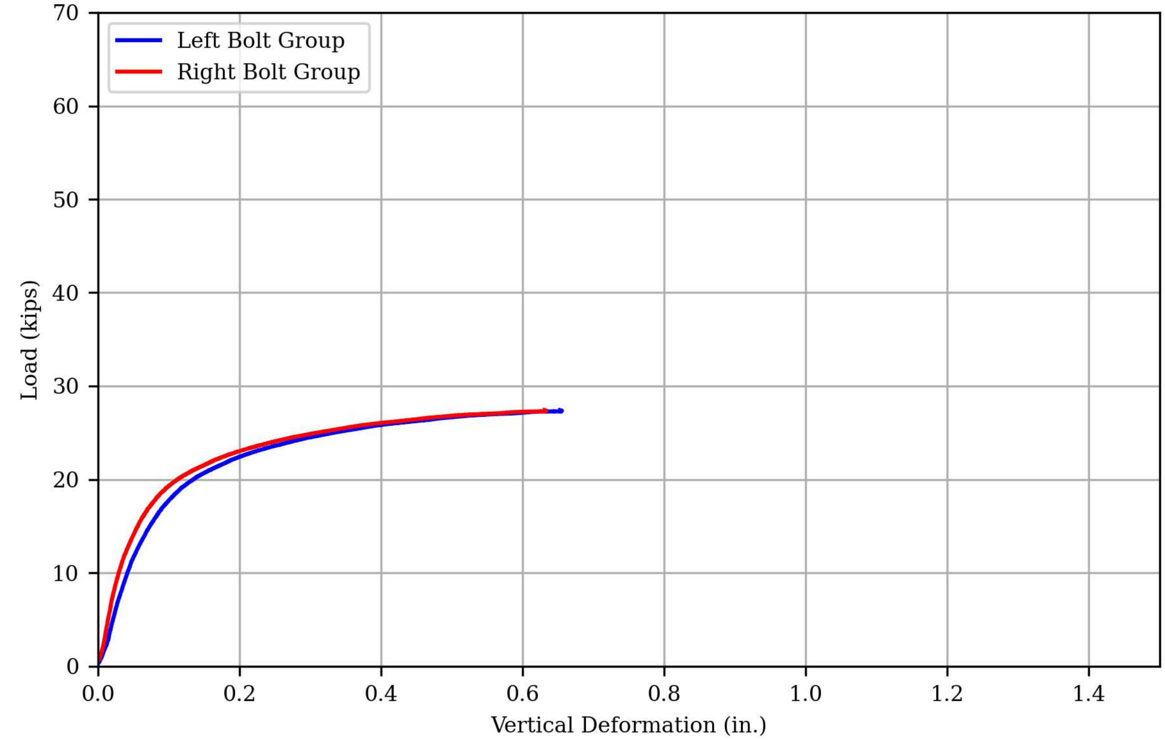

(a) Load vs Deformation

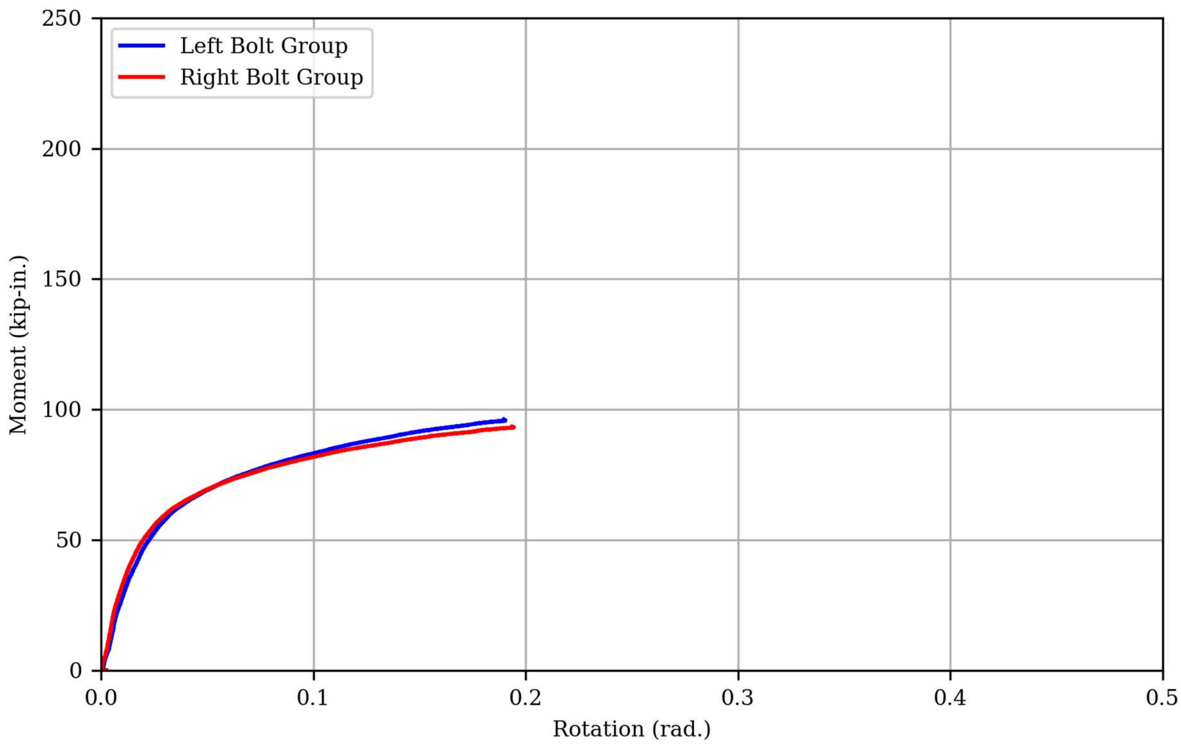

(b) Moment vs Rotation

Figure 30. Measured Response of Specimen 3

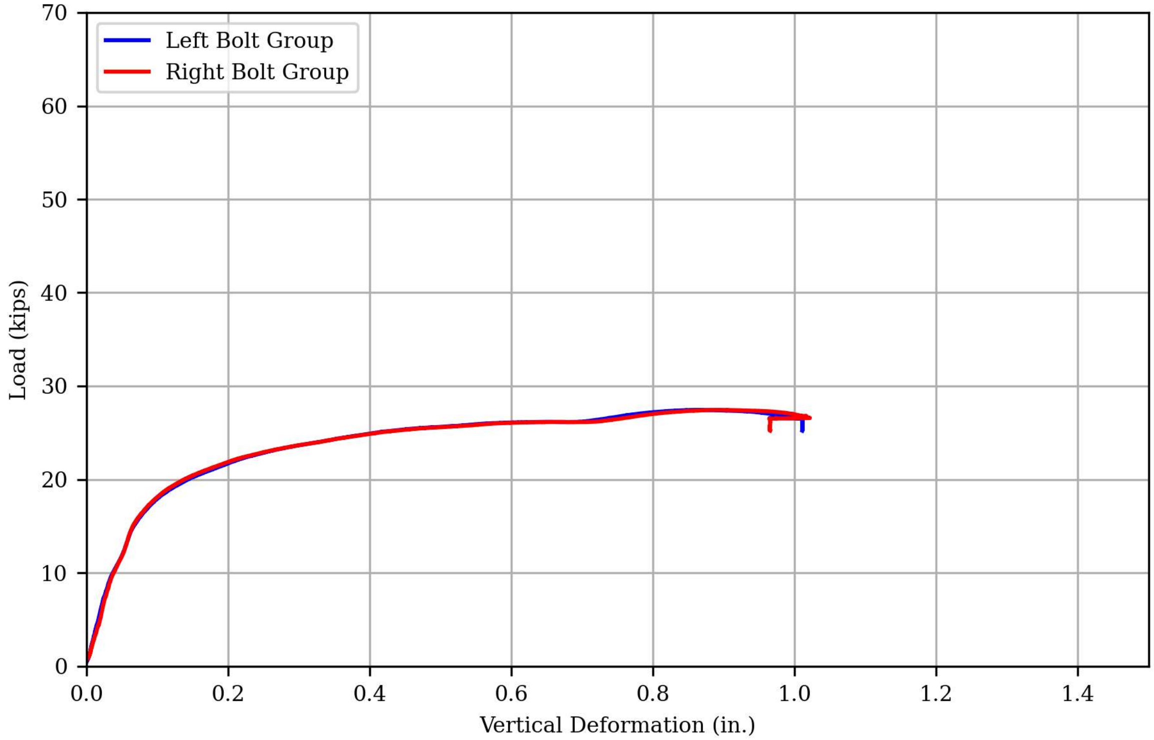

(a) Load vs deformation

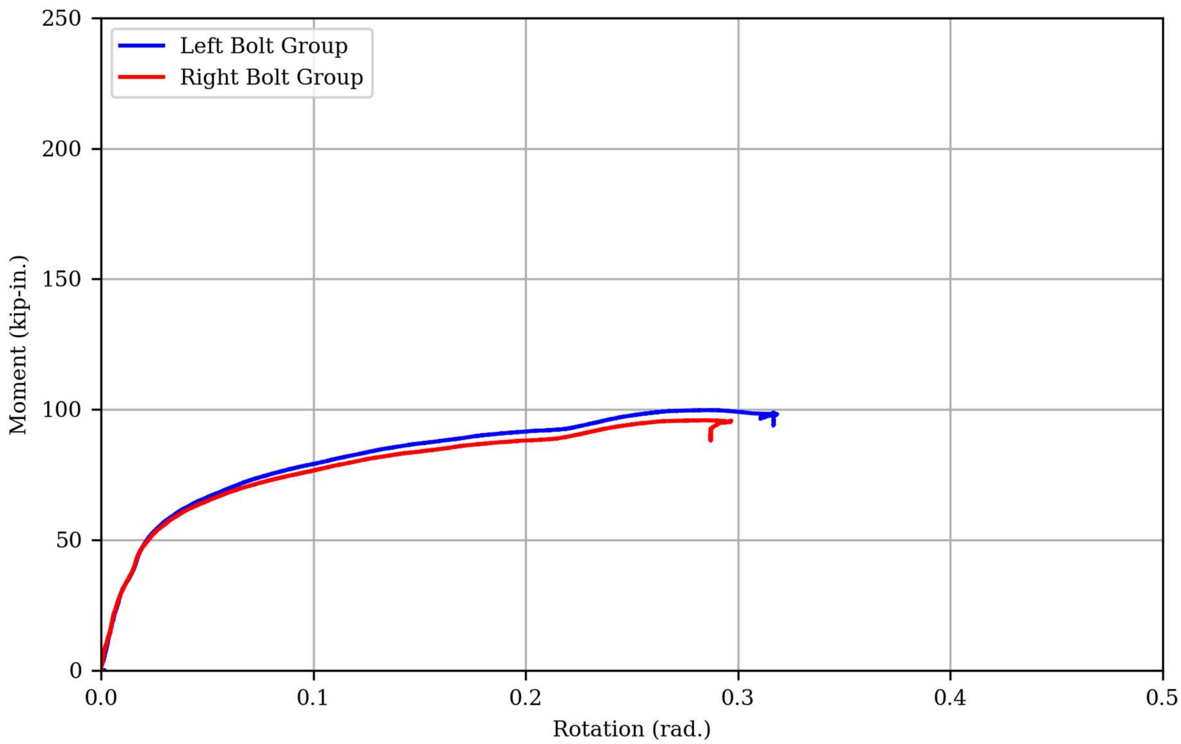

(b) Moment vs rotation

Figure 31. Measured response of specimen 3L

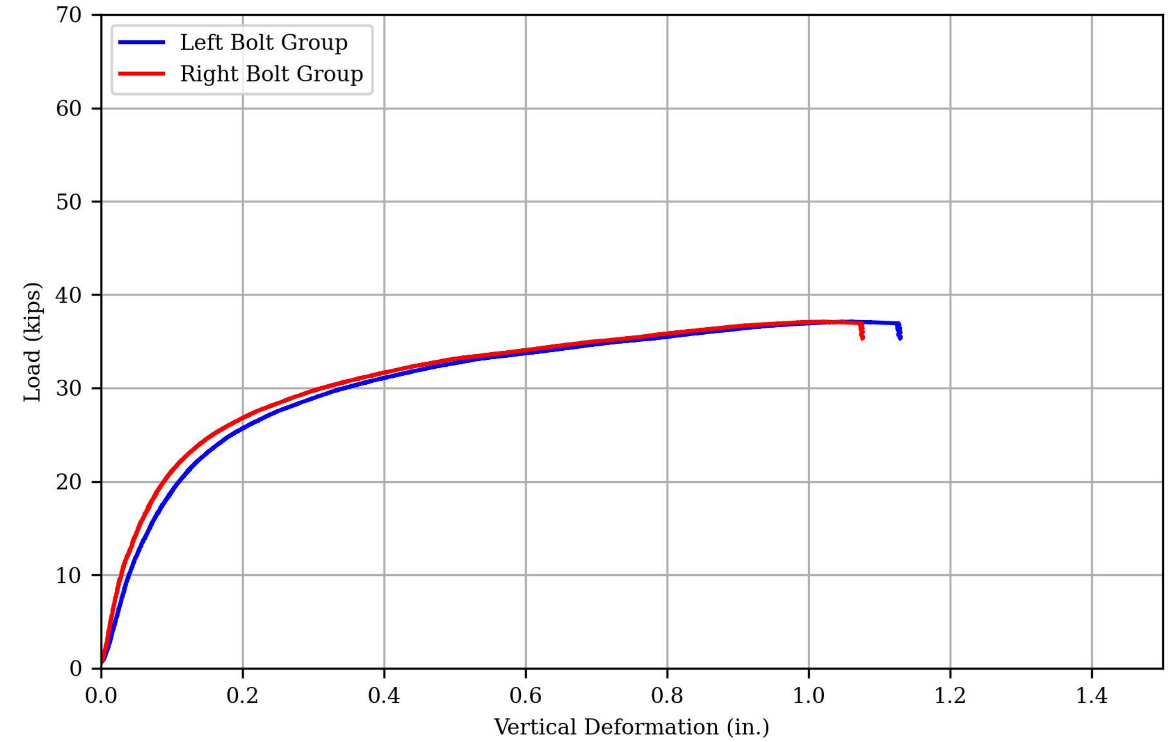

(a) Load vs Deformation

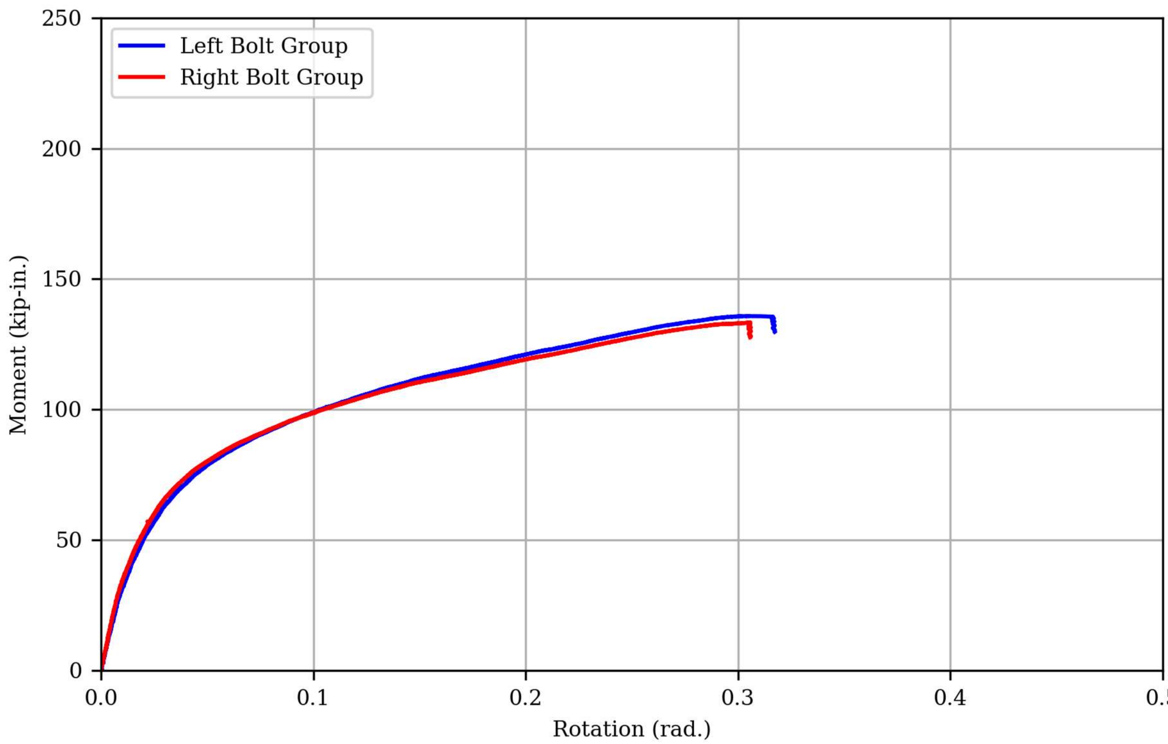

(b) Moment vs Rotation

Figure 32. Measured Response of Specimen 4A

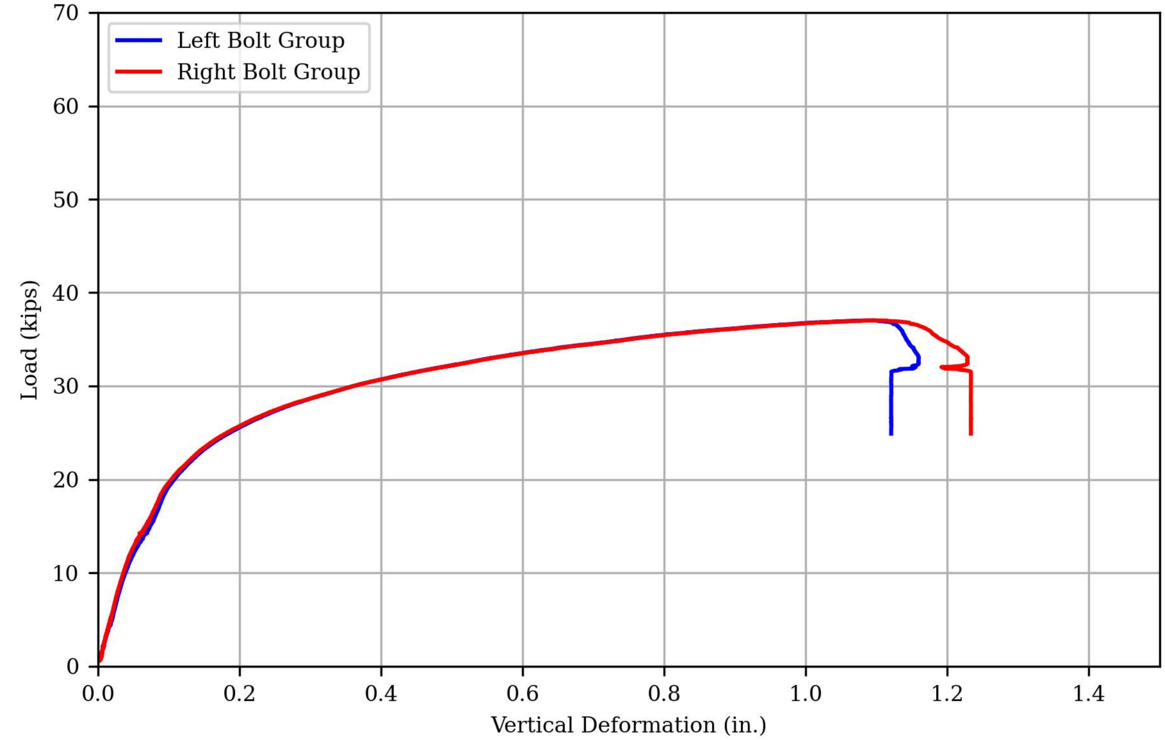

(a) Load vs deformation

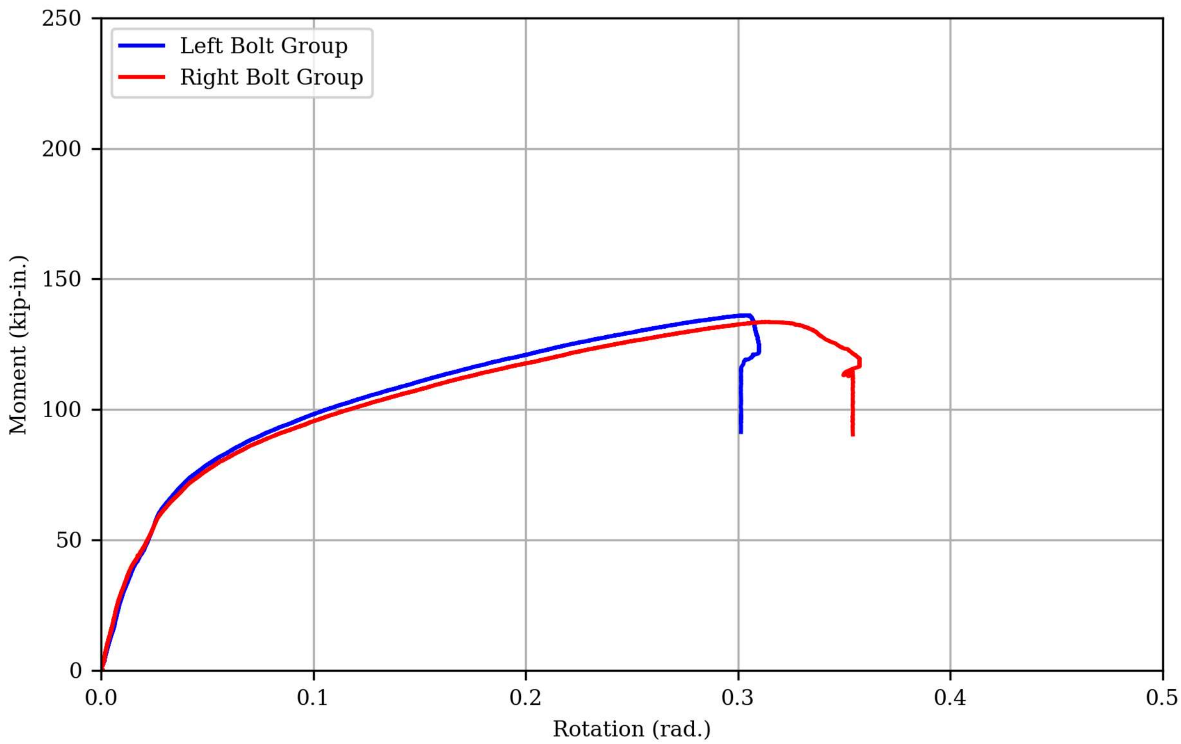

(b) Moment vs rotation

Figure 33. Measured response of specimen 4B

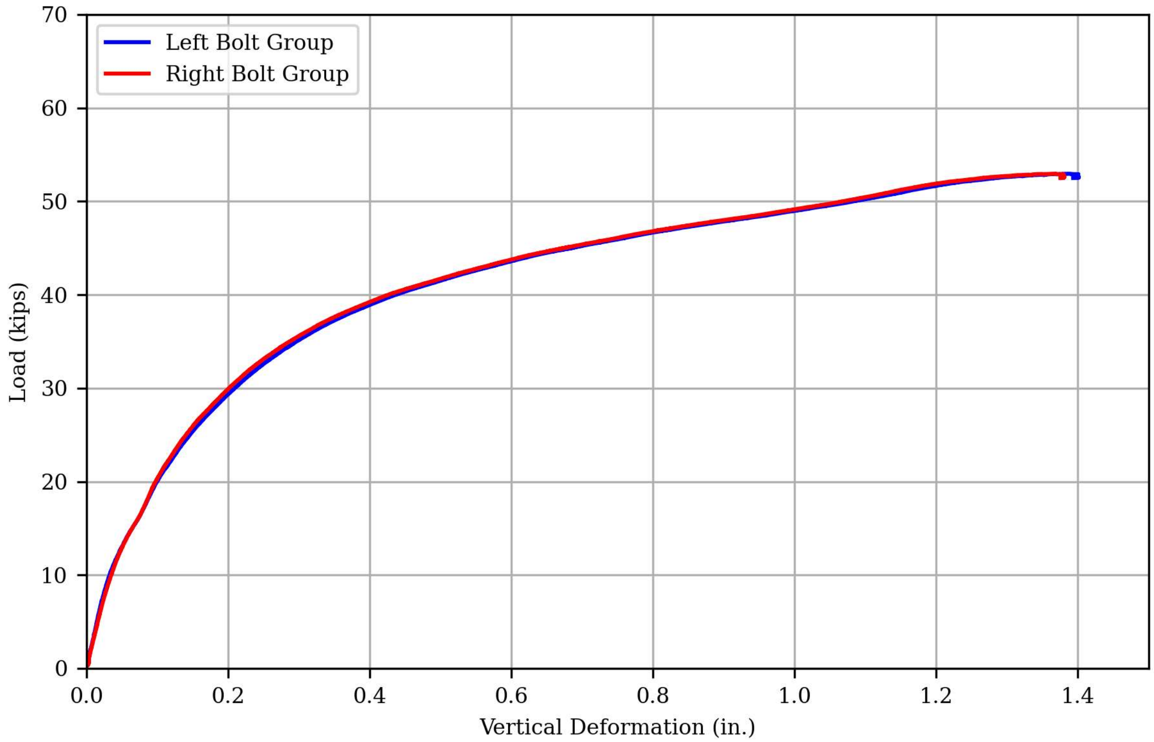

(a) Load vs Deformation

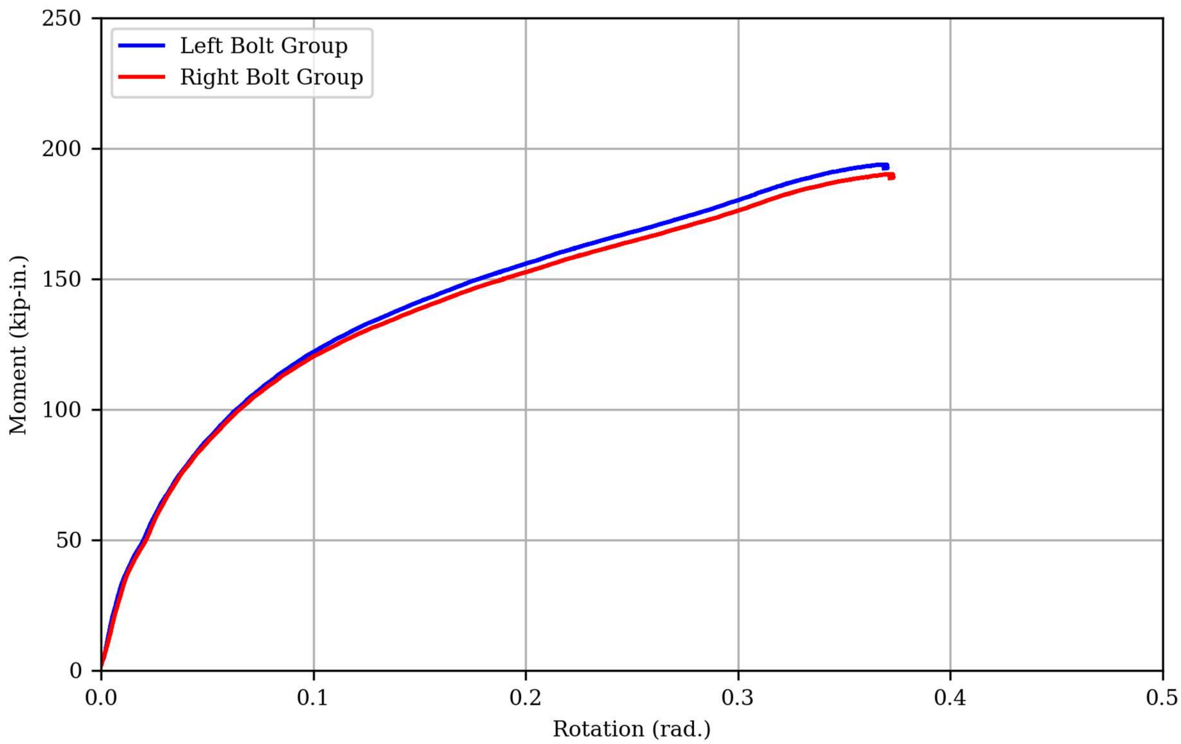

(b) Moment vs Rotation

Figure 34. Measured Response of Specimen 5

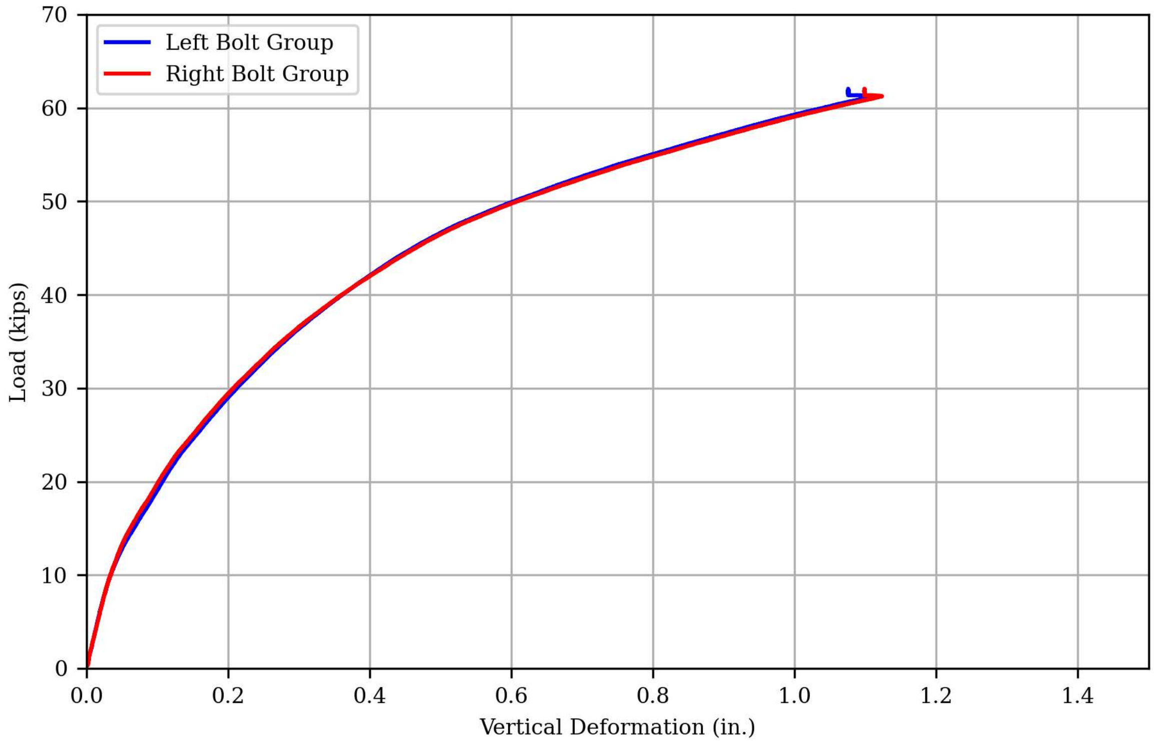

(a) Load vs deformation

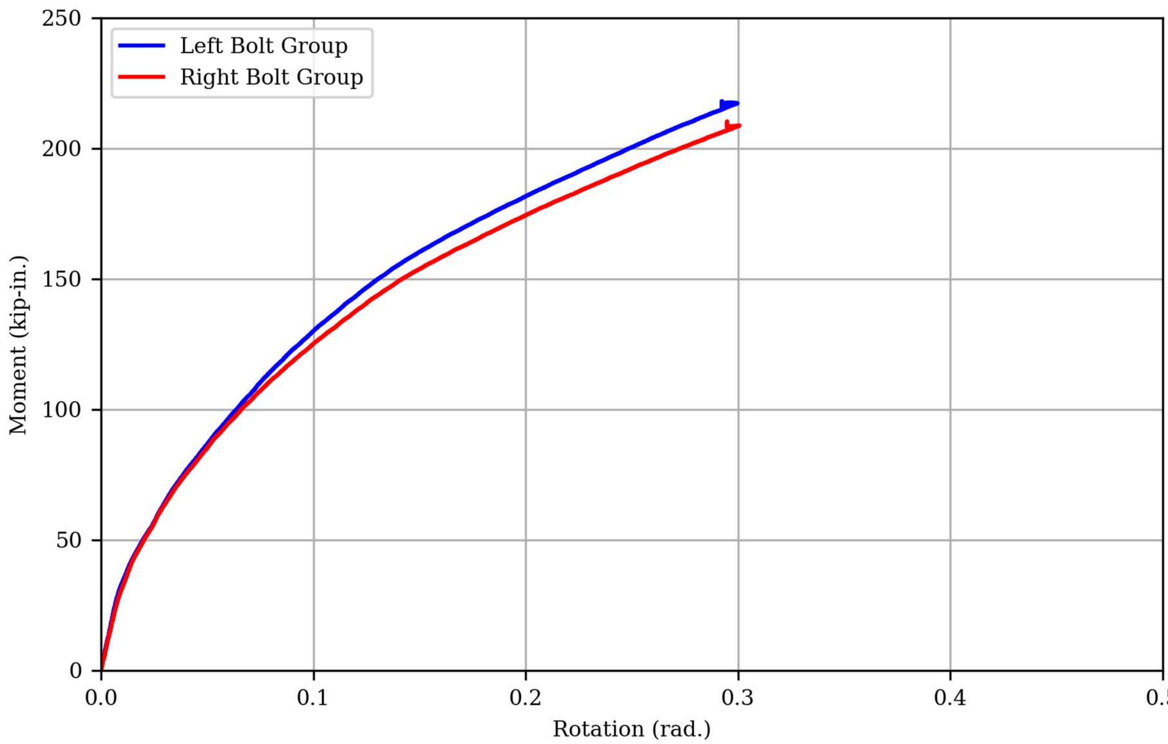

(b) Moment vs rotation

Figure 35. Measured response of specimen 6

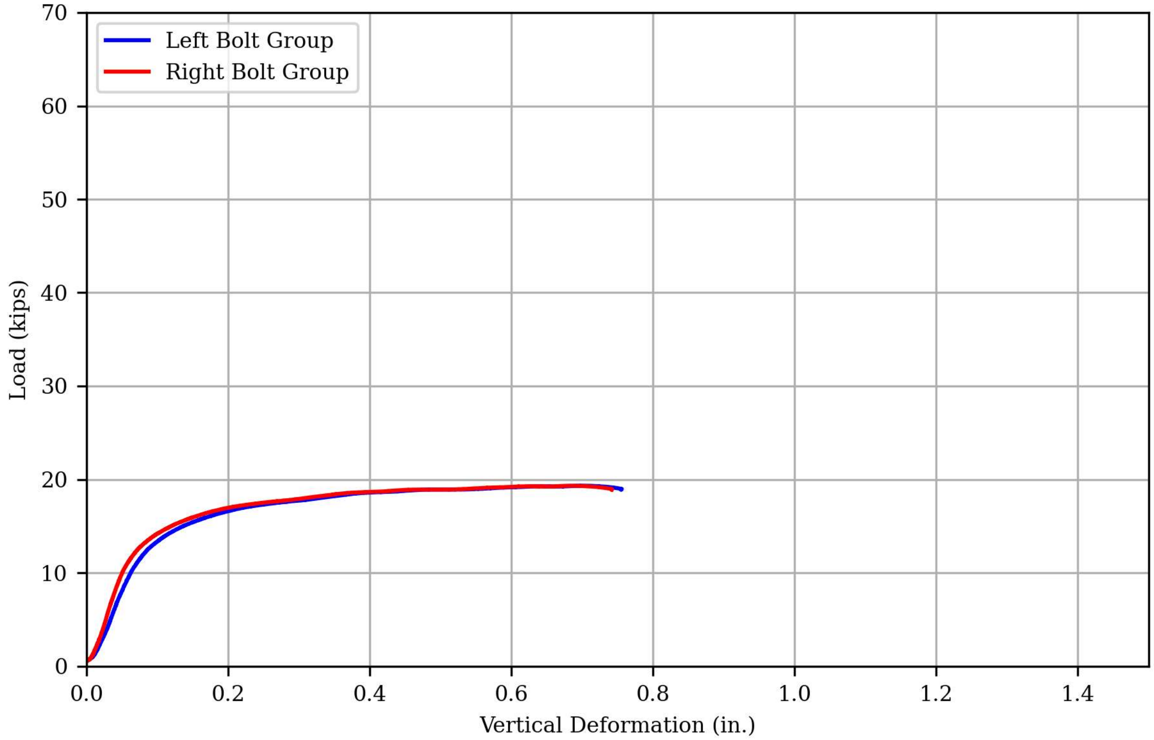

(a) Load vs Deformation

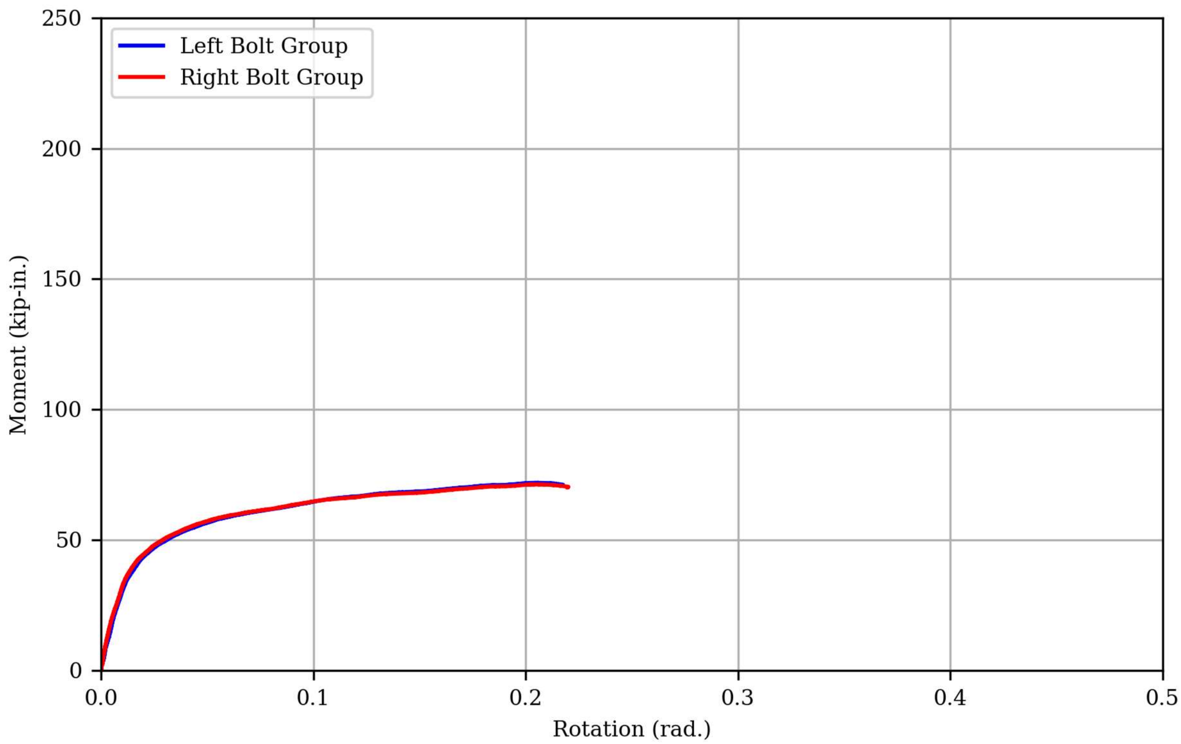

(b) Moment vs Rotation

Figure 36. Measured Response of Specimen 7

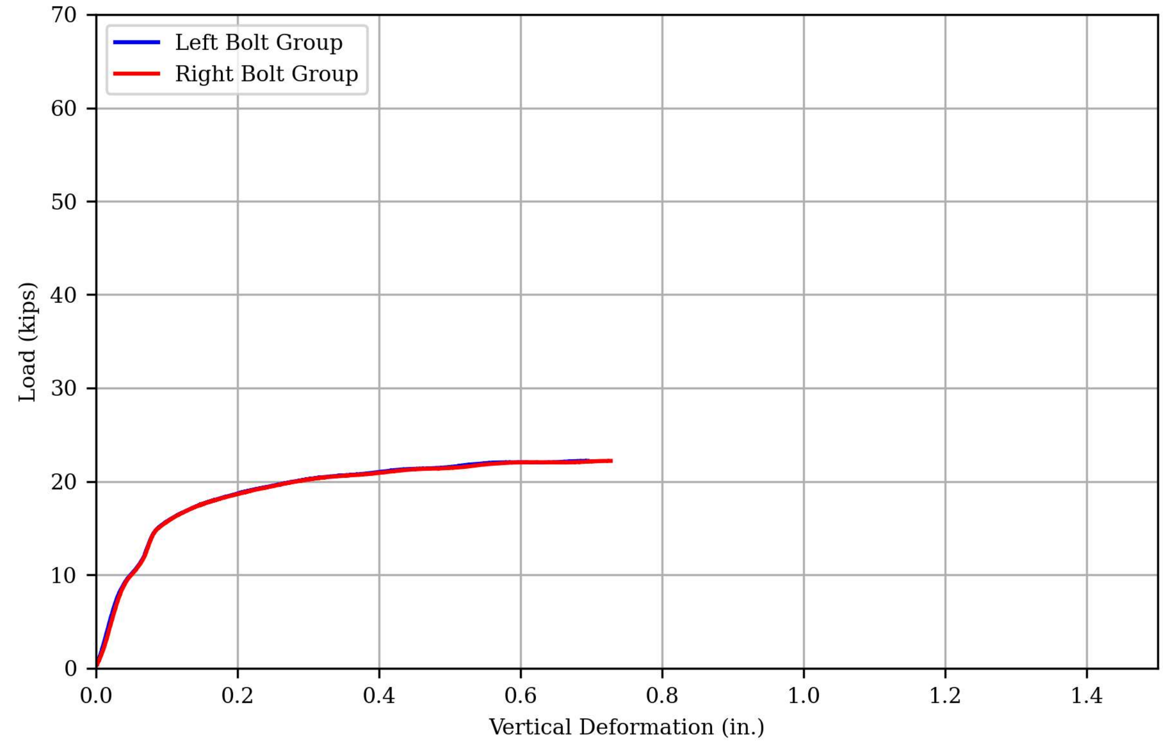

(a) Load vs deformation

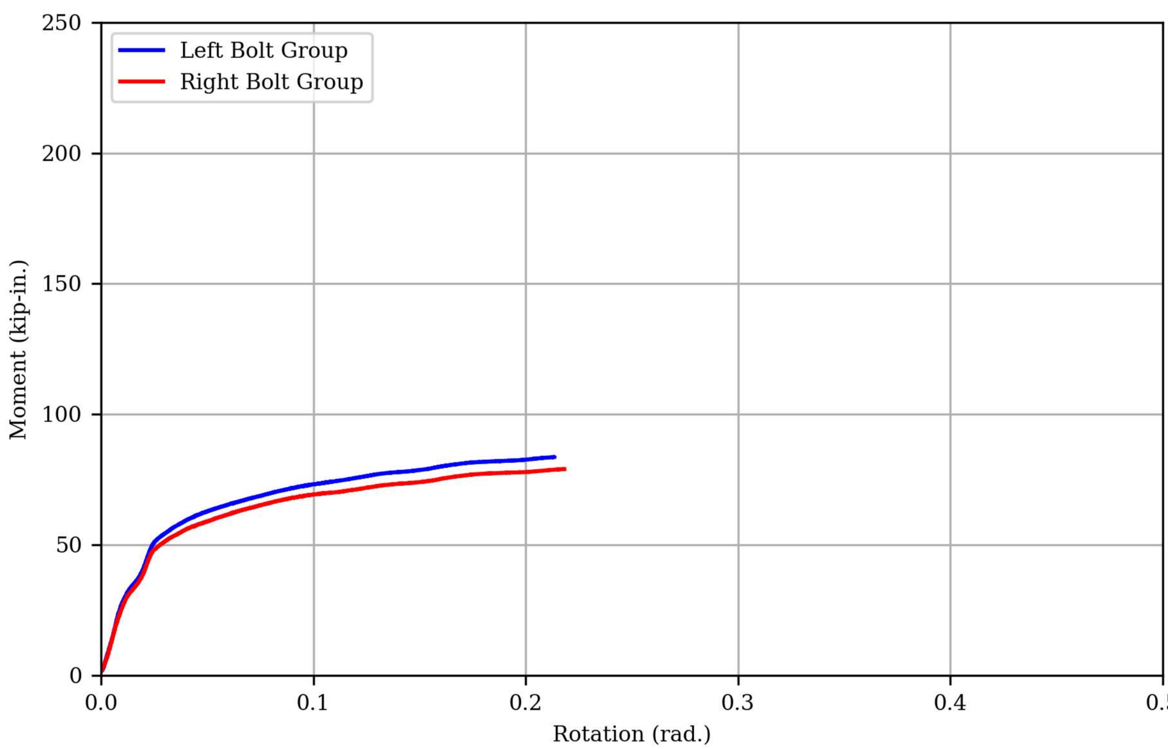

(b) Moment vs rotation

Figure 37. Measured response of specimen 8

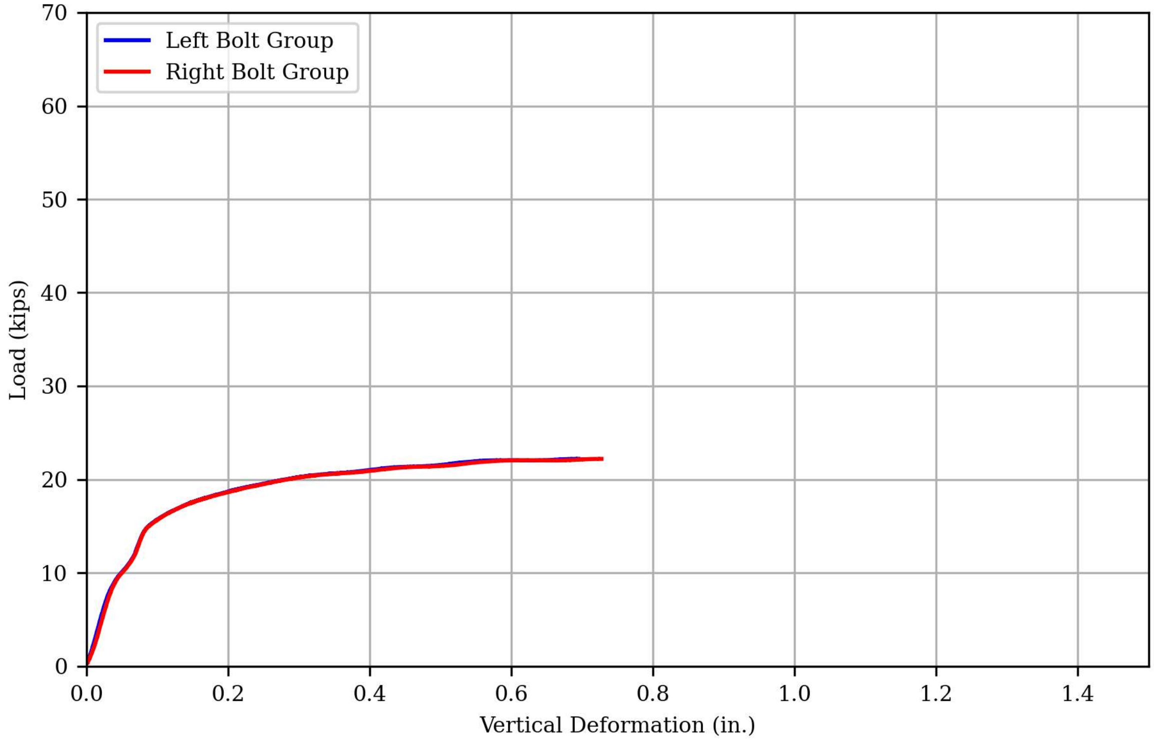

(a) Load vs Deformation

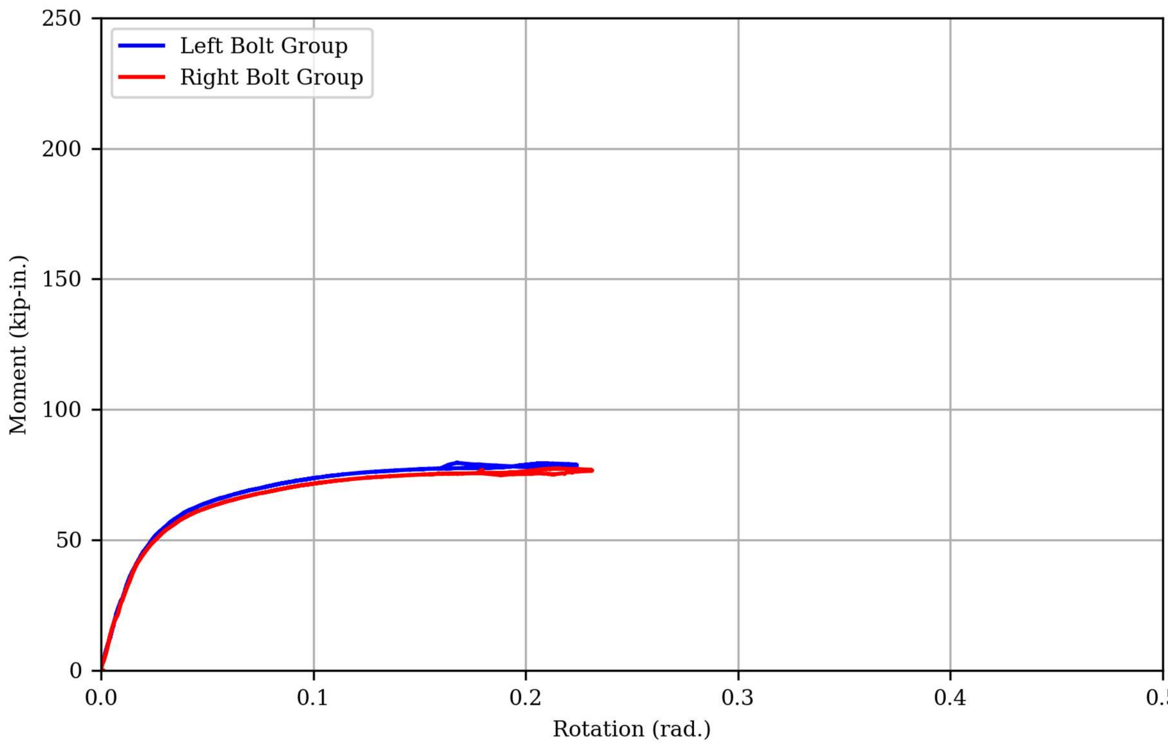

(b) Moment vs Rotation

Figure 38. Measured Response of Specimen 8L

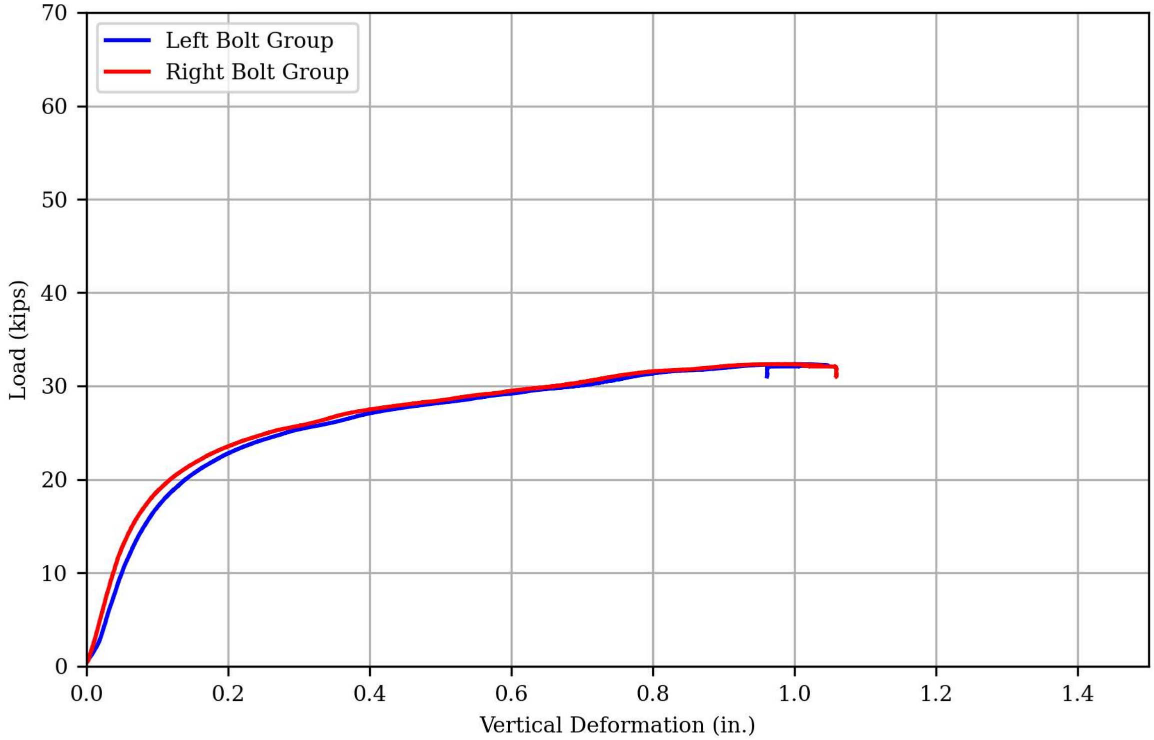

(a) Load vs Deformation

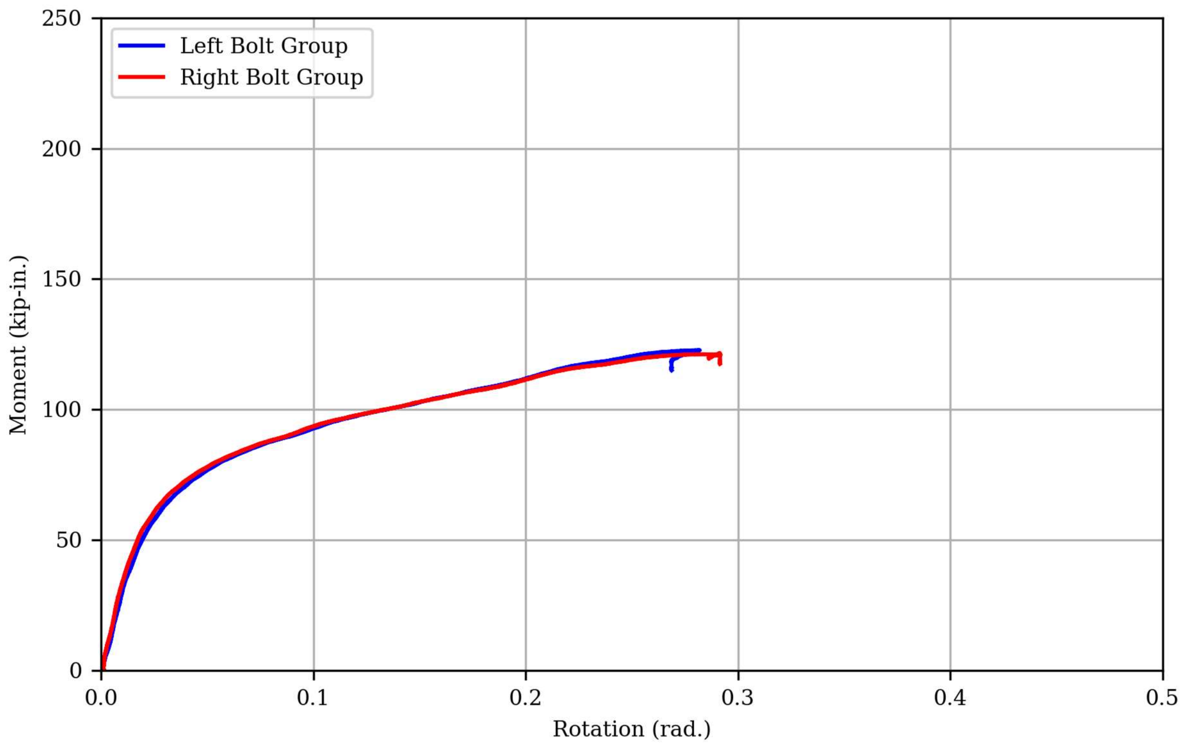

(b) Moment vs Rotation

Figure 39. Measured Response of Specimen 9

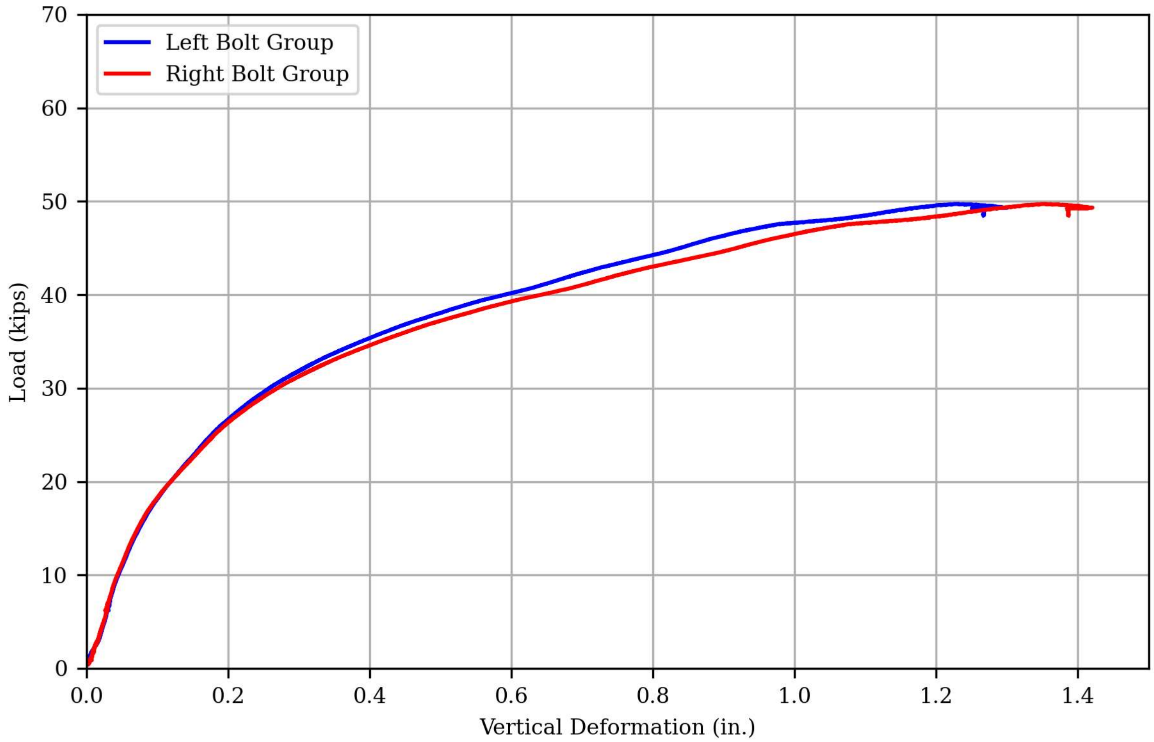

(a) Load vs Deformation

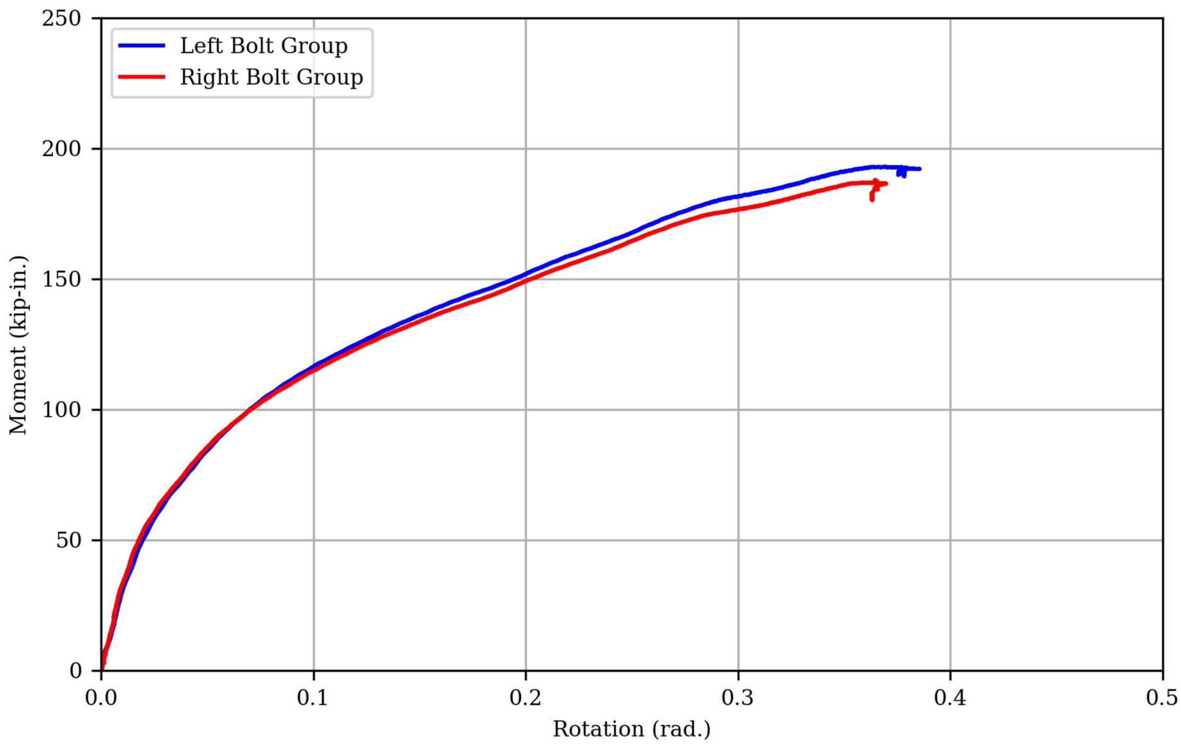

(b) Moment vs Rotation

Figure 40. Measured Response of Specimen 10

The strength for each specimen is listed in Table 24. In this table, the maximum load from the experiment ($R_{exp,u}$) and the load at the deformation limit ($R_{exp,d}$) are included. Note these values are for each bolt group, the total load on the specimen was twice as much. The deformation limit was defined as 0.083 rad of rotation which roughly corresponds to 1/4 in. deformation of the bottom bolt (assuming that the top bolt does not deform). Previous studies of bearing and tearout have used 1/4 in. of deformation as a practical limit to define bearing strength (Frank and Yura 1981). The angle of the deformation of the bottom bolts, α, is also listed in Table 24. This angle, defined from horizontal as shown in Figure 41, was measured using a protractor. The listed value of α is the average of the angles measured for the bottom bolts on either side of the test plate.

Table 24. Experimental Strengths, and Angle of Resultant Force.

Specimen	$R_{exp,u}$ (kips)	$R_{exp,d}$ (kips)	$R_{exp,u}/R_{exp,d}$	α (degrees)
1.1	14.16	14.16	1.00	8.5
1.2	14.24	14.21	1.00	9.5
1.3	14.04	14.01	1.00	9.0
2A	20.58	19.36	1.06	13.0
2B	20.66	19.67	1.05	13.3
3	27.39	24.33	1.13	22.5
3L	27.42	23.30	1.18	21.5
4A	37.05	29.01	1.28	23.5
4B	36.98	28.68	1.29	24.5
5	52.93	34.34	1.54	31.0
6	62.09	35.49	1.75	26.0
7	19.30	17.45	1.11	17.5
8	22.16	20.15	1.10	19.5
8L	21.01	19.51	1.08	17.5
9	32.30	25.38	1.27	27.0
10	49.70	34.14	1.46	31.5

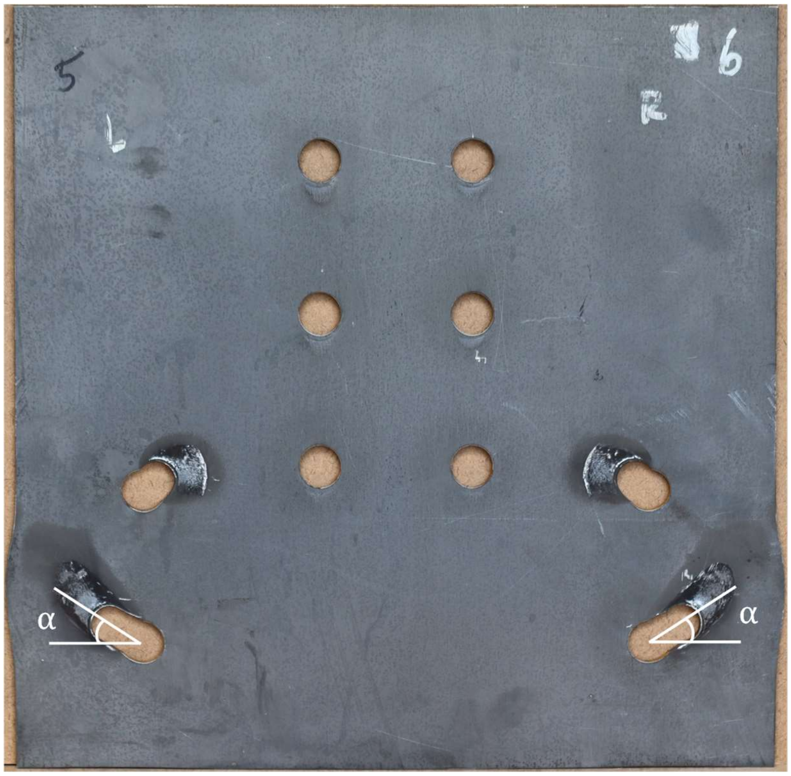

Figure 41: Measured angle of deformation of bottom bolt hole

Photographs of all the test specimens after testing are shown in Figure 42. All the specimens deformed in a similar manner. The test plate deformed at both upper and lower bolt hole locations, but with more pronounced deformation at the lower bolt hole locations. Flaking of mill scale was also observed. The flaking was observed primarily near the lower bolt hole where the plate underwent greater deformation.

Specimens 3L, 4A, 4B, 5, 9, and 10, had fractures at the bottom bolt holes. Minor cracks were observed in specimens 4A, 5, 9, and 10, while more significant cracks extending from the bolt hole to the plate edge were noted in 3L and 4B. Specimen 5 had cracks at both bottom holes. The other specimens had cracks at only one of the bottom holes.

(a) Specimen 1.1

(b) Specimen 1.2

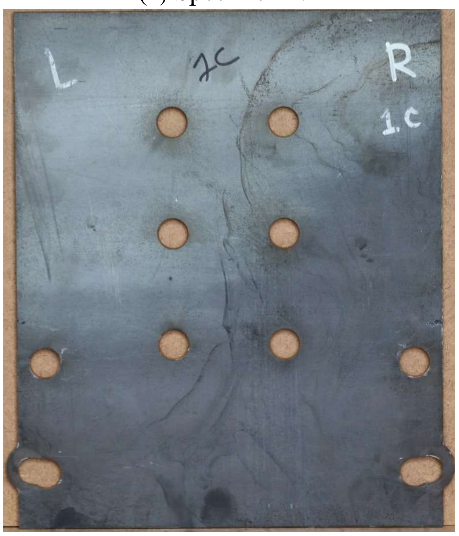

(c) Specimen 1.2

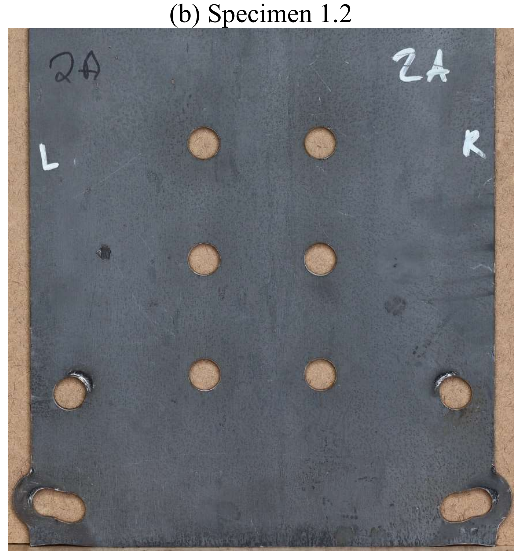

(d) Specimen 2A

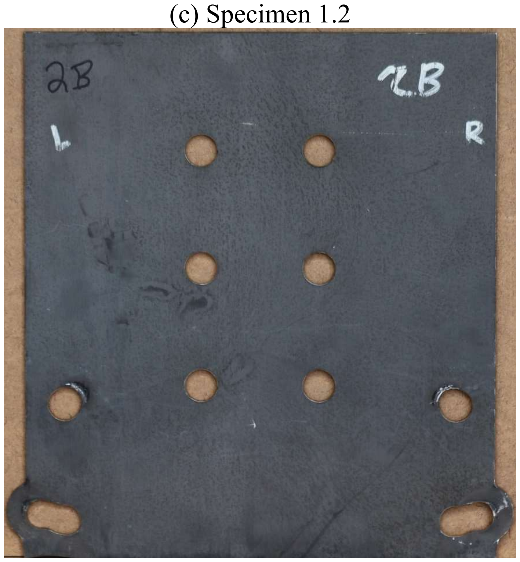

(e) Specimen 2B

(f) Specimen 3

Figure 42: Photos of all specimens after testing.

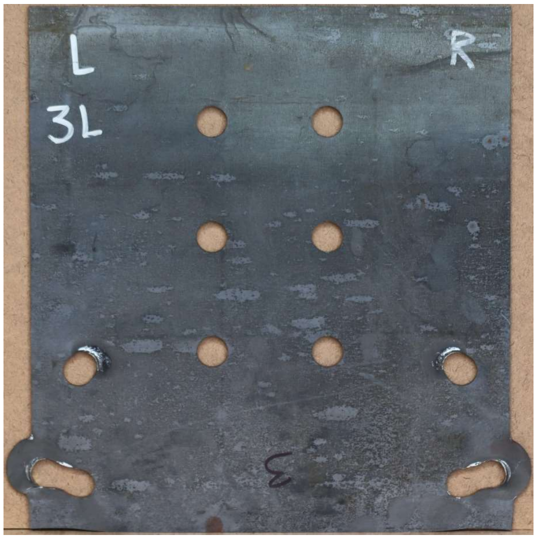

(g) Specimen 3L

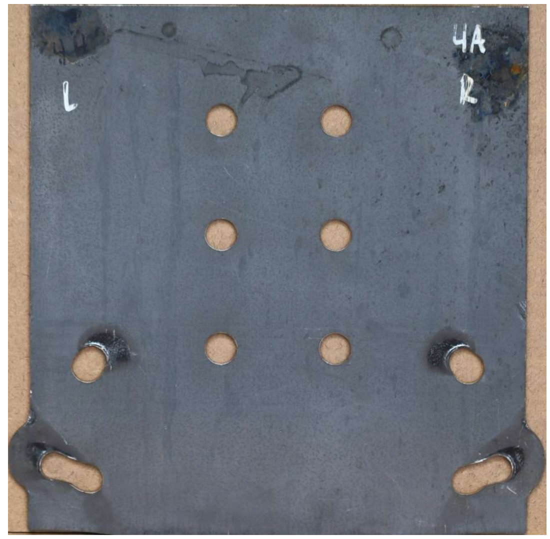

(h) Specimen 4A

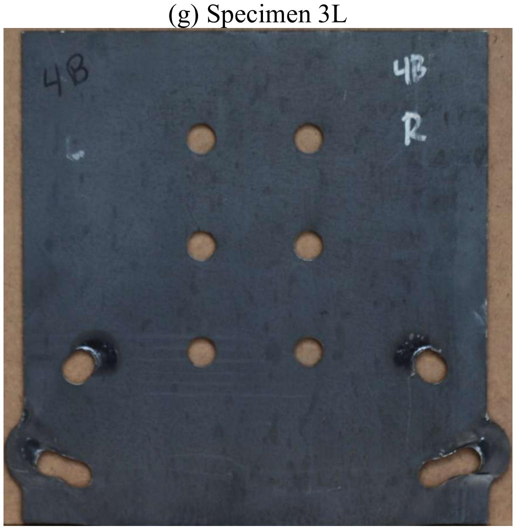

(i) Specimen 4B

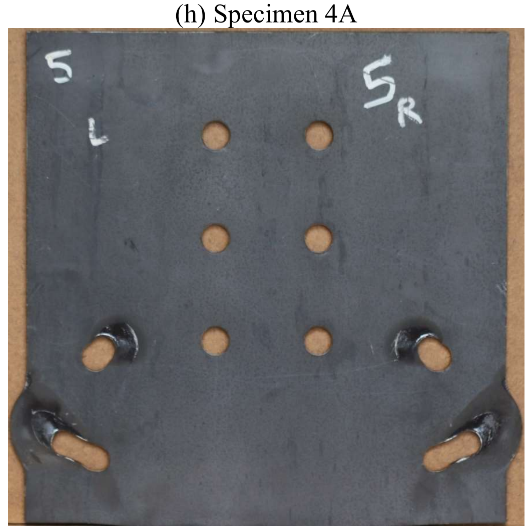

(j) Specimen 5

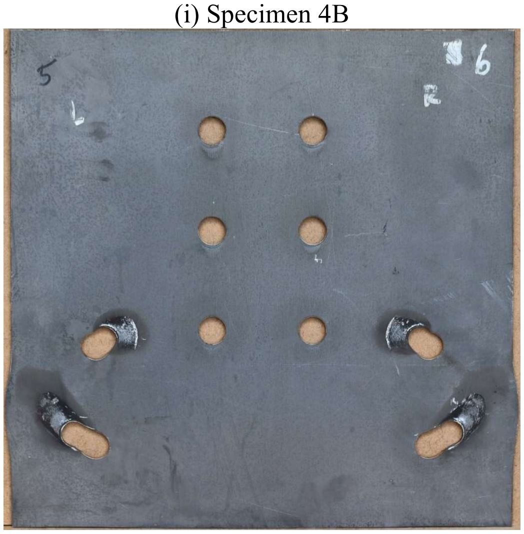

(k) Specimen 6

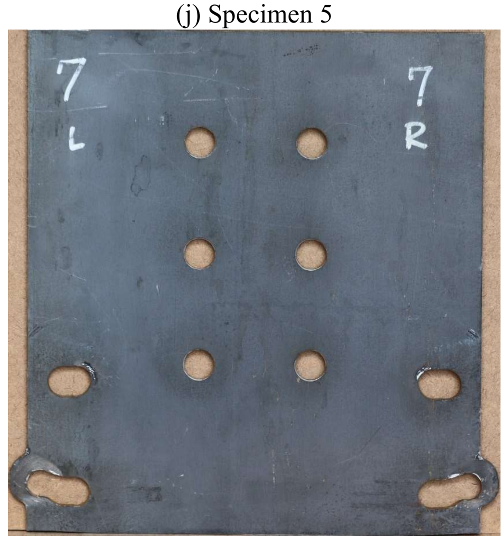

(l) Specimen 7

Figure 42: Photos of all specimens after testing. (continued)

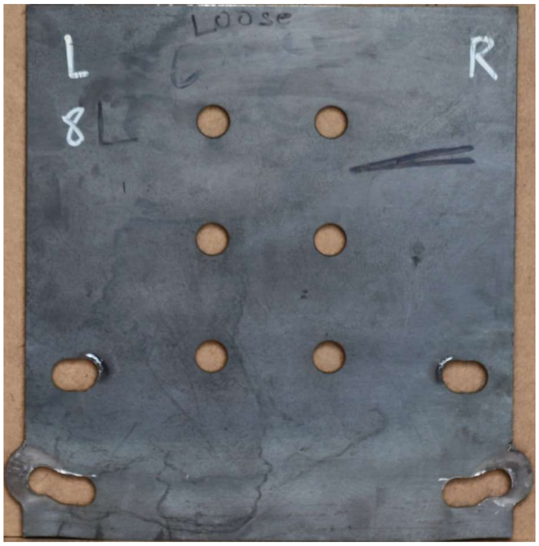

(m) Specimen 8

(n) Specimen 8L

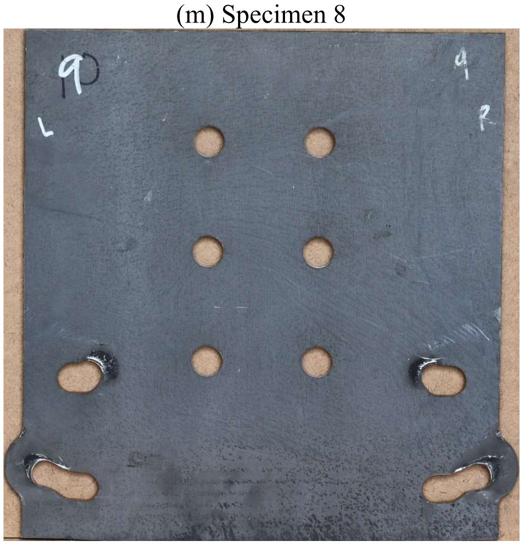

(o) Specimen 9

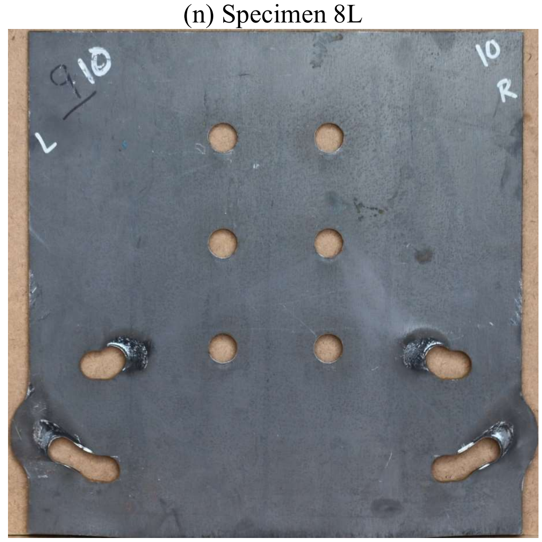

(p) Specimen 10

Figure 42: Photos of all specimens after testing. (continued)

Discussion

Specimens 2A and 2B (with 1 in. edge distance) and specimens 4A and 4B (with 1.5 in. edge distance) were tested as replicates to evaluate the repeatability of the experiment. As expected, the pairs of specimens behaved in the same manner, and failed at nearly the same load, indicating a high degree of repeatability among the samples. $R_{exp,u}$ of specimens 2A and 2B varied by 0.4%, and $R_{exp,d}$ varied by 1.6%. Similarly, for specimens 4A and 4B, $R_{exp,u}$ varied by 0.3% and $R_{exp,d}$ varied by 1.1%.

The ultimate strength ($R_{exp,u}$) and the strength at deformation limit ($R_{exp,d}$) of the connections increased with increasing edge distance as shown in Figure 43 and Figure 44. This trend is expected as strength for the limit state of tearout increases with increasing edge distance. The trend in ultimate strength is roughly linear with edge distance. This is unexpected since for 3/4 in. diameter bolts in standard holes, the controlling limit state according to the AISC *Specification* (AISC 2022) transitions from tearout to bearing at an edge distance of 1.9 in. Specimens 5 and 6 have edge distances of 2 in. and 2.5 in., respectively, and were expected to exhibit a bearing failure not affected by edge distance. In contrast, the plot of $R_{exp,d}$ vs edge distance does show the expected plateau.

The ratio $R_{exp,u}/R_{exp,d}$ also increases with increasing edge distance as shown in Figure 45. This effect was seen for the concentrically loaded specimens in Chapter 2 as well as in previous experiments (Franceschetti and Denavit 2021). This behavior is also seen in the load-deformation response (Figure 25 to Figure 40) where the post yielding stiffness of specimens with greater edge distances was notably steeper than those with smaller edge distance. This could potentially be attributed to the presence of more plate material around bolt holes in specimens with greater edge distance. With more material, the load can spread over a larger area and even though the material near the bolt hole yields, the extra material is available to bear additional load. The angle of deformation (α) of the lower bolts also generally increased with increasing edge-distance as shown in Figure 46, however specimen 6 with the largest edge distance has a lower angle than specimen 5.

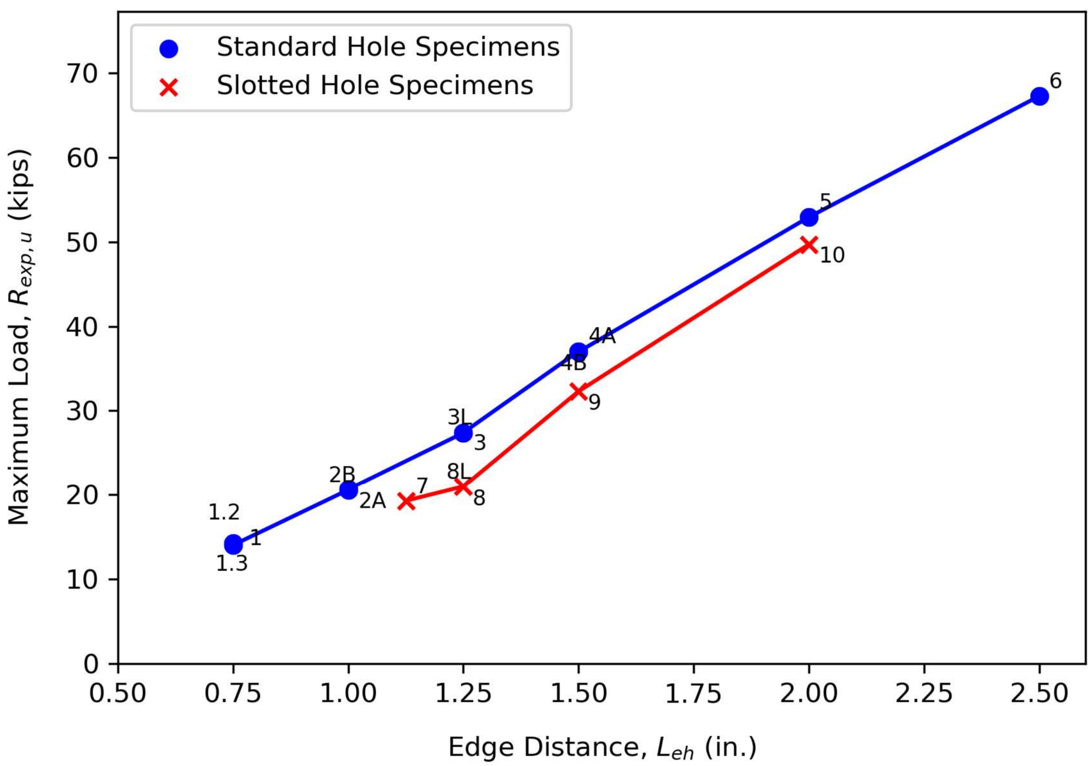

Figure 43:Increasing Trend of Ultimate Capacity of the Specimens with Edge Distance.

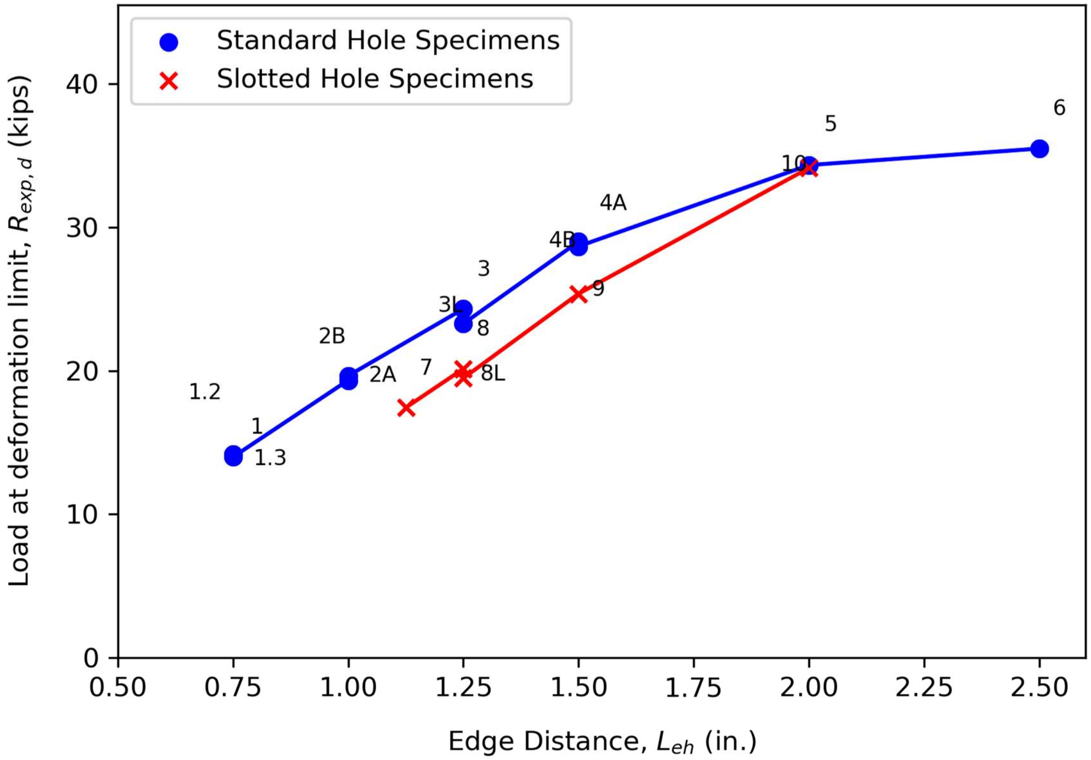

Figure 44: Increasing trend of load at deformation limit of the specimens with edge distance.

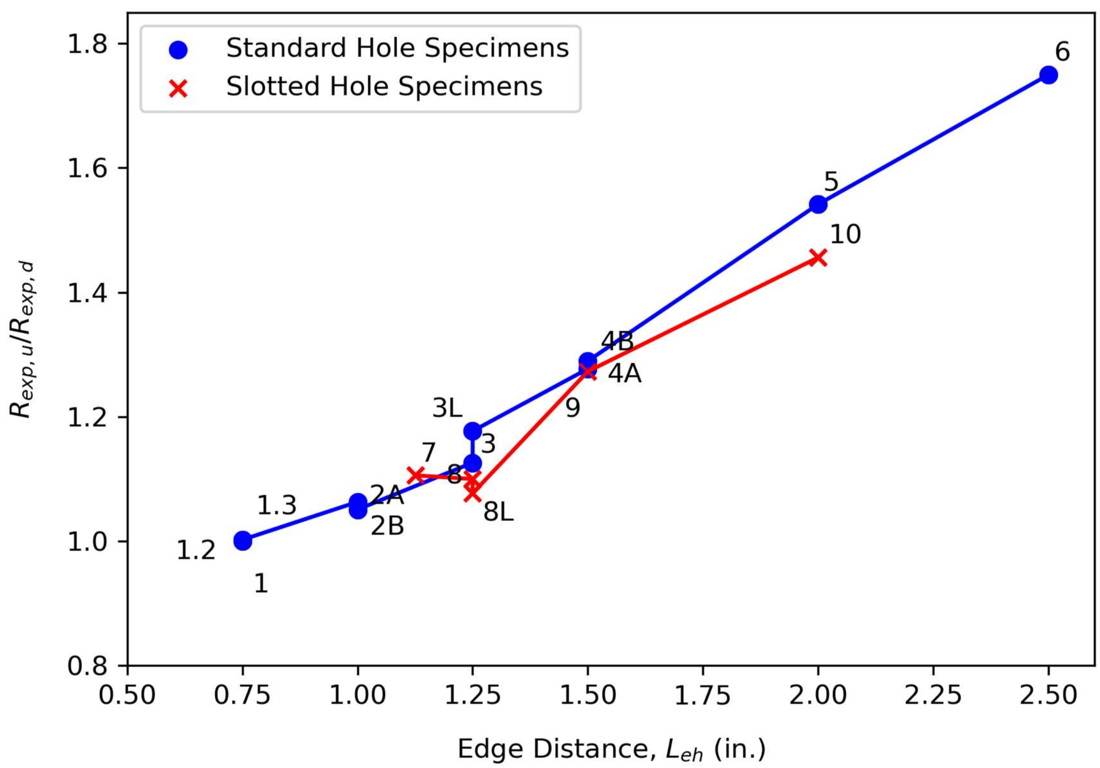

Figure 45: Ratio of Ultimate Capacity and Capacity at Deformation Limit of the Specimen vs Edge Distance.

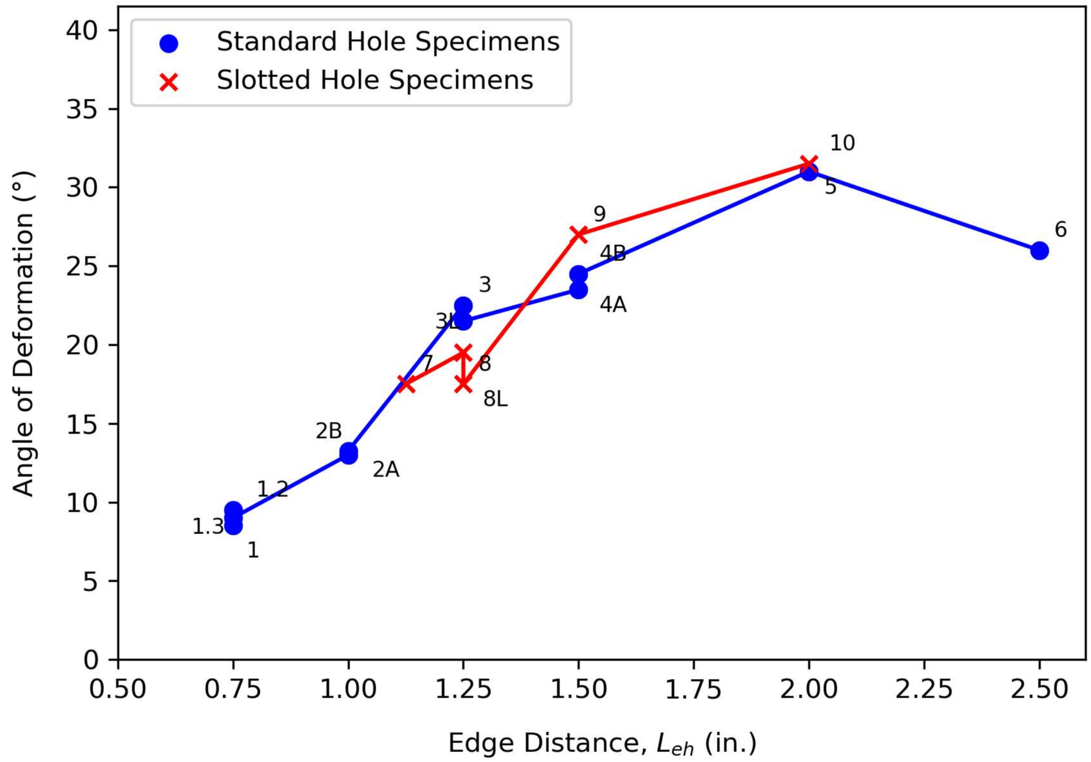

Figure 46: Angle of Resultant Force vs Edge Distance.

Specimens 1.1, 1.2, and 1.3 had the same horizontal edge distance but different vertical edge distances. The motivation for these tests came from a trial experiment (not described in this report) that showed yielding in the region between the bottom bolt hole and the edge below. Thus, it was hypothesized that a larger vertical edge distance may increase strength even though the direction of load was towards the vertical edge and the horizontal edge distance governed the calculation of the ultimate load. However, the three specimens behaved in a similar manner and failed at nearly the same load, not supporting the hypothesis.

At a given edge distance, specimens with slotted holes failed at a lower load than specimens with standard holes. The edge distance is defined in this work as the distance from the center of hole to the edge of material. The lower strength for slotted holes is expected because they have a smaller clear distance (i.e., distance from the edge of bolt hole to the edge of material) since the slotted holes were wider than the standard holes.

Specimens 3 and 3L and specimens 8 and 8L were nominally identical except specimens 3L and 8L were tested with loose bolts rather than finger-tight bolts. The motivation for these tests came from a trial experiment (not described in this report) that replicated the test of specimen 1 but where the bolts were tightened with a few impacts of an impact wrench. The trial specimen was significantly stronger than specimen 1. This unexpected behavior was likely due to the friction that developed among the plates in the trial specimen. Thus, tests were run with finger tight bolts and some specimens having bolts looser than finger tight were tested to determine if friction had any significant impact. The pairs of specimens failed at a comparable load (with <1% difference in strength values), and with mostly similar behavior and resulting wear on the test plate. The plastic region of the finger-tight bolts specimens was observed to be slightly steeper than the loose bolts specimens.

The nominal strength of the connections was calculated using three different methods: 1) the poison bolt method, 2) the modified IC method, and 3) the IC method neglecting tearout. Strengths were calculated using measured properties of the plate (i.e., t = 0.2481 in. and F_u = 75.48 ksi) and measured dimensions as shown in Table 23. Neither resistance factors nor safety factors were applied.

The poison bolt method is commonly used in practice and establishes a conservative lower bound of the nominal strength. Using this method, the least strength for any bolt subject to force in any direction is calculated based on the limit states of bolt shear rupture, bearing, and tearout. Since the shear rupture strength of the bolt was sufficiently large, the individual bolt strength was computed as the minimum of Equations 2 and 4 when comparing to $R_{exp,u}$ and as the minimum of Equations 1 and 3 when comparing to $R_{exp,d}$. The individual bolt strength is multiplied by the factor C determined using the IC method. For connections described in this chapter, C = 0.88, a value obtained from AISC *Manual* Table 7-6 (AISC 2023).

This value of C was also used in the IC method, neglecting tearout. Neglecting tearout establishes an upper bound of the nominal strength. Given that the shear rupture strength of the bolt was sufficiently large, this strength is computed based on the limit state of bearing and the strength is computed as the same for all specimens. When comparing to the maximum load, Equation 4 is used which results in a nominal bolt strength of $r_n = 3.0dtF_u$ = 3.0(0.75 in.)(0.2481 in.)(75.48 ksi) = 42.13 kips, and a nominal connection strength of $R_n = Cr_n$ = (0.88)(42.13 kips) = 37.08 kips. When comparing to the deformation limit load, Equation 3 is used which result in a nominal bolt strength of $r_n = 2.4dtF_u$ = 2.4(0.75 in.)(0.2481 in.)(75.48 ksi) = 33.71 kips, and a nominal connection strength of $R_n = Cr_n$ = (0.88)(33.71 kips) = 29.66 kips.

The modified IC method, developed by Denavit et al. (2021), was also used to compute the capacity of the specimens. The strength according to the modified IC method was computed using a MATLAB program developed by Denavit et al. (2021). The strength from the modified IC method is bounded on the low end by the strength from the poison bolt method and the high end by the strength from the IC method, neglecting tearout. The MATLAB program only considers round holes. The strength according to the modified IC method for the slotted hole specimens was computed assuming that the holes were circular with a diameter equal to the width of the slot. This simplification increases the calculated strength since it neglects additional material removed.

Nominal strengths and test-to-predicted ratios are presented in Table 25 for comparison to the maximum load, $R_{exp,u}$, and Table 26 for comparison to the deformation limit load $R_{exp,d}$.

Table 25. Nominal Strengths and Test-To-Predicted Ratios for Comparison to $R_{exp,u}$.

Specimen	Poison Bolt Method		Modified ICR Method		Neglecting Tearout	
	R_n (kips)	$R_{exp,u}/R_n$	R_n (kips)	$R_{exp,u}/R_n$	R_n (kips)	$R_{exp,u}/R_n$
1	8.41	1.684	9.62	1.472	37.08	0.382
1.2	8.35	1.705	9.63	1.478	37.08	0.384
1.3	8.43	1.666	9.61	1.461	37.08	0.379
2A	14.36	1.433	16.48	1.248	37.08	0.555
2B	14.47	1.428	16.59	1.245	37.08	0.557
3	20.16	1.359	23.19	1.181	37.08	0.739
3L	20.12	1.363	23.16	1.184	37.08	0.739
4A	26.56	1.395	30.86	1.200	37.08	0.999
4B	26.46	1.397	30.76	1.202	37.08	0.997
5	37.08	1.428	36.99	1.431	37.08	1.427
6	37.08	1.675	36.99	1.679	37.08	1.674
7	20.11	0.960	19.70	0.979	37.08	0.520
8	17.10	1.296	23.11	0.959	37.08	0.598
8L	19.97	1.052	23.11	0.909	37.08	0.566
9	26.48	1.220	30.77	1.050	37.08	0.871
10	37.08	1.340	36.99	1.344	37.08	1.340
Average		1.400		1.251		0.796
St. Dev.		0.214		0.216		0.397

Table 26. Nominal Strengths and Test-To-Predicted Ratios for Comparison to $R_{exp,d}$.

Specimen	Poison Bolt Method		Modified ICR Method		Neglecting Tearout	
	R_n (kips)	$R_{exp,d}/R_n$	R_n (kips)	$R_{exp,d}/R_n$	R_n (kips)	$R_{exp,d}/R_n$
1	6.73	2.104	7.70	1.839	29.66	0.477
1.2	6.68	2.127	7.66	1.854	29.66	0.479
1.3	6.74	2.078	7.72	1.814	29.66	0.472
2A	11.49	1.684	13.18	1.469	29.66	0.652
2B	11.58	1.699	13.27	1.482	29.66	0.663
3	16.12	1.509	18.55	1.311	29.66	0.820
3L	16.09	1.448	18.53	1.257	29.66	0.785
4A	21.25	1.365	24.69	1.175	29.66	0.978
4B	21.17	1.355	24.61	1.165	29.66	0.967
5	29.66	1.158	29.59	1.161	29.66	1.158
6	29.66	1.196	29.59	1.199	29.66	1.196
7	16.09	1.085	15.76	1.107	29.66	0.588
8	13.68	1.473	18.48	1.091	29.66	0.679
8L	15.97	1.221	18.38	1.061	29.66	0.658
9	21.19	1.198	24.62	1.031	29.66	0.856
10	29.66	1.151	29.59	1.154	29.66	1.151
Average		1.491		1.323		0.786
St. Dev.		0.354		0.284		0.245

For specimens with small edge distances, the poison bolt method was conservative and neglecting tearout was unconservative. Strengths calculated using the modified IC method were in between the two other methods, yielding conservative results on average. At the deformation limit load, the strength computed using the modified IC method was lower than the experimental strength for all specimens. At the ultimate load, the strength computed using the modified IC method was lower than the experimental strength for all specimens except for specimens 7, 8, and 8L. These specimens had slotted holes and as noted previously, when computing the strength by the modified IC method, slotted holes were treated as round holes because the program used in this work does not consider slotted holes.

The modified IC method results use the tearout strength equation in the AISC *Specification* (2022) based on the clear distance, l_c. As shown in Chapter 2 and previous research (Franceschetti and Denavit 2021), other strength equations using l_{v1} or l_{v2} can provide more accurate results. The modified IC method could potentially be improved by implementing these alternative strength equations.

Chapter 4: Eccentrically Loaded Bolt Group Experiments (Higher Eccentricity)

The experimental evaluation of eccentrically loaded bolt groups is divided into two configurations. This chapter describes testing of five- and eight-bolt connections with higher eccentricity.

Materials and Methods

Six specimens were tested with higher eccentricity. The connection investigated for each specimen was a bolted connection between the web of a W21×55 and 3/4 in. thick connector plates as shown in Figure 47. Two different bolt group configurations were used: one row with five bolts and two rows with four bolts in each row, each was subjected to an initial eccentricity of 9 in., defined with respect to the centroid of the bolt group. 3/4 in. diameter A490 bolts were used and the spacing between bolts within a row and between rows was maintained at 3 in. Test bolts were symmetrically arranged about the centerline of the W21. The edge distance from the center of the bolt holes to the edge of the W21 web (L_{ev}) was varied between 1 and 2 in. as listed in Table 27. The connections were designed to fail in the web of the W21. The minimum edge distance used in the connector plates was 2 in. Furthermore, the W21 was stiffened with full-depth 3/8 in. thick plate stiffeners at the point where force was applied by the actuator.

Table 27: Test Matrix for Higher Eccentricity Bolt Group.

Specimen	Number of Bolts	L_{ev} (in.)
H1	5	1.0
H2	5	1.5
H3	5	2.0
H4	8	1.0
H5	8	1.5
H6	8	2.0

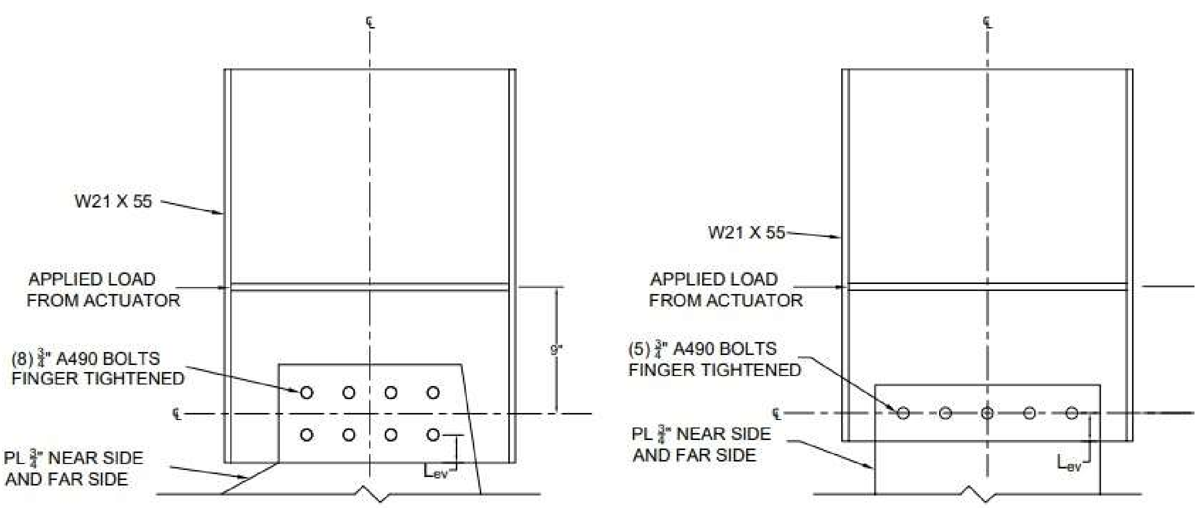

Figure 47: Configuration of test specimens.

The W21 wide flange shapes used in the tests conformed to ASTM A992 and had a nominal web thickness of 0.375 inches. Three tensile coupon tests were conducted on samples cut from the web of an extra length of W21 cut from the same piece as used for the experiments. Table 28 summarizes the results of the coupon tests. The average measured thickness was 0.3626 in., and the average yield and ultimate stress were 57.74 ksi and 71.39 ksi, respectively. These coupon tests were conducted with two strain measurement devices, an extensometer and an Optotrak optical positioning sensor. The extensometer measured the strain with a gage of 2 in. but was removed after yield occurred. The Optotrak sensor measured the strain with a gage of 8 in. through fracture. The stress-strain response of the three coupons with strain measured using the Optotrak sensor is shown in Figure 48. Before installing the markers for Optotrak, the mill scale at the point of installation was ground off to enhance the adhesion of the markers. Fracture due to tensile rupture consistently occurred between the marker attachment points across all coupons, unaffected by the removal of mill scale.

Table 28: Measured Stress of Test Material

Sample Number	Thickness (in.)	F_y (ksi)	F_u (ksi)	Elongation [a]
1	0.3652	57.54	70.91	25.78%
2	0.3608	58.00	71.74	27.34%
3	0.3618	57.69	71.51	24.22%
Average	0.3626	57.74	71.39	25.78%

[a] Gage length = 8in.

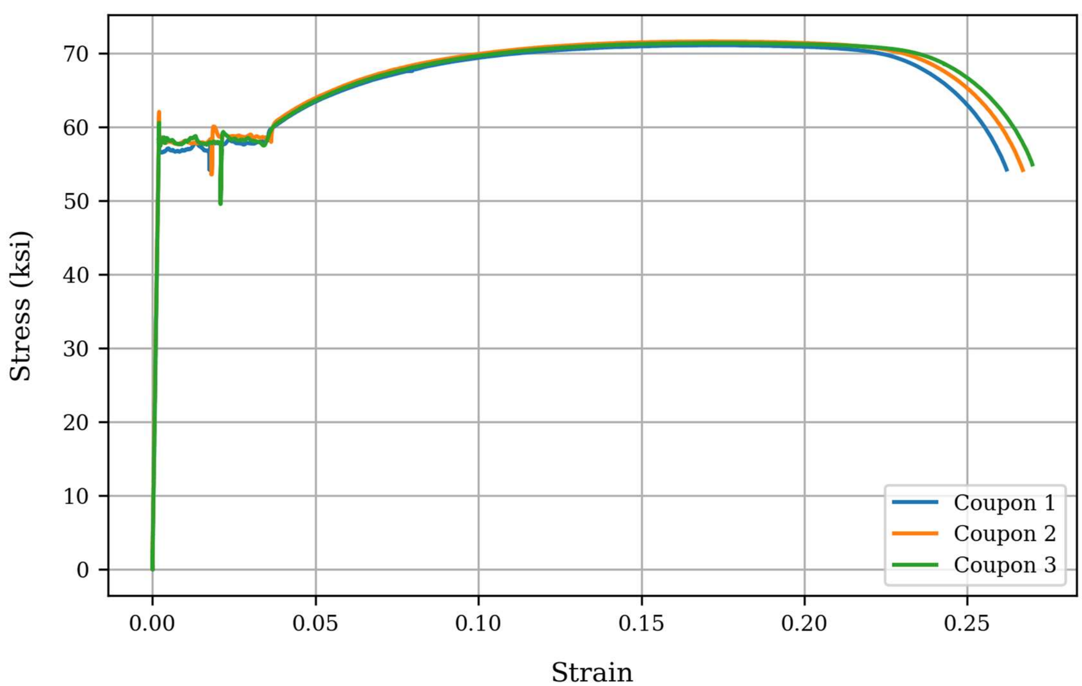

Figure 48: Material stress-strain response from tensile coupons.

The edges of the specimens were sawn, and the bolt holes were drilled. The diameter of the bolt holes, the bolt spacing, and the edge distances were measured for all specimens except H3 and are shown in Figure 49. The dimensions presented in Figure 49 for specimen H3 are nominal dimensions. The measured edge distance was taken as the measured distance from the edge of the bolt hole to the bottom edge plus half the measured bolt hole diameter. The measured spacing between bolt holes was taken as the measured distance between the edges of bolt holes plus half of the measured bolt hole diameters for both bolt holes.

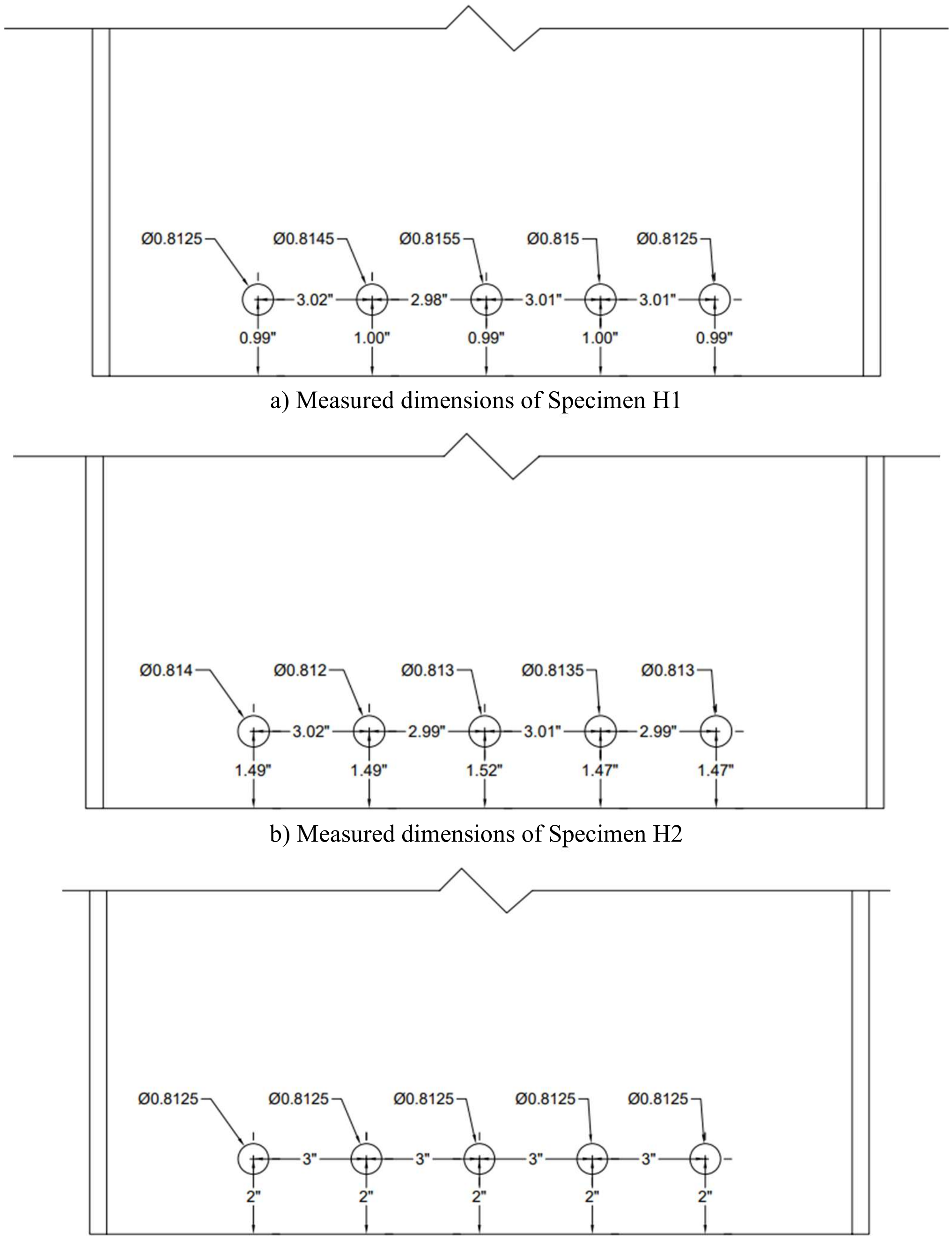

a) Measured dimensions of Specimen H1

b) Measured dimensions of Specimen H2

c) Nominal dimensions of Specimen H3

Figure 49. Dimensions of specimens.

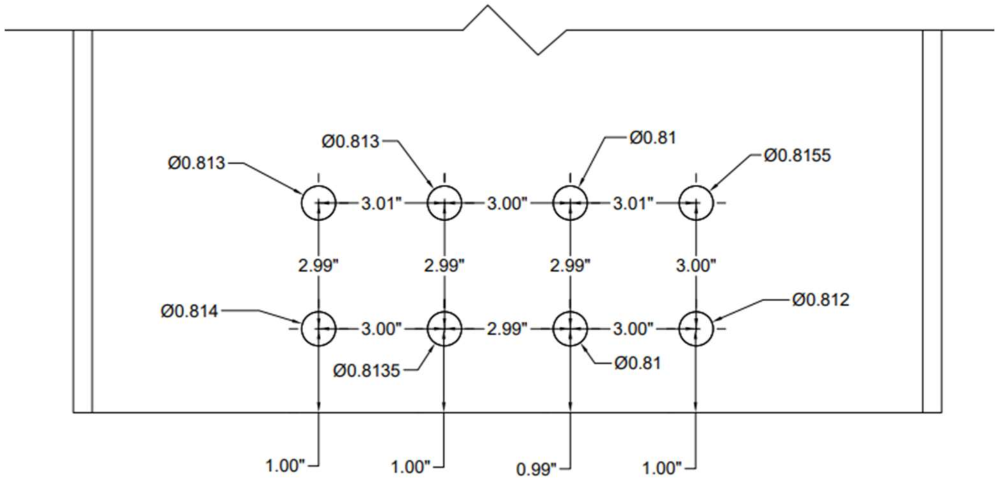

d) Measured dimensions of Specimen H4

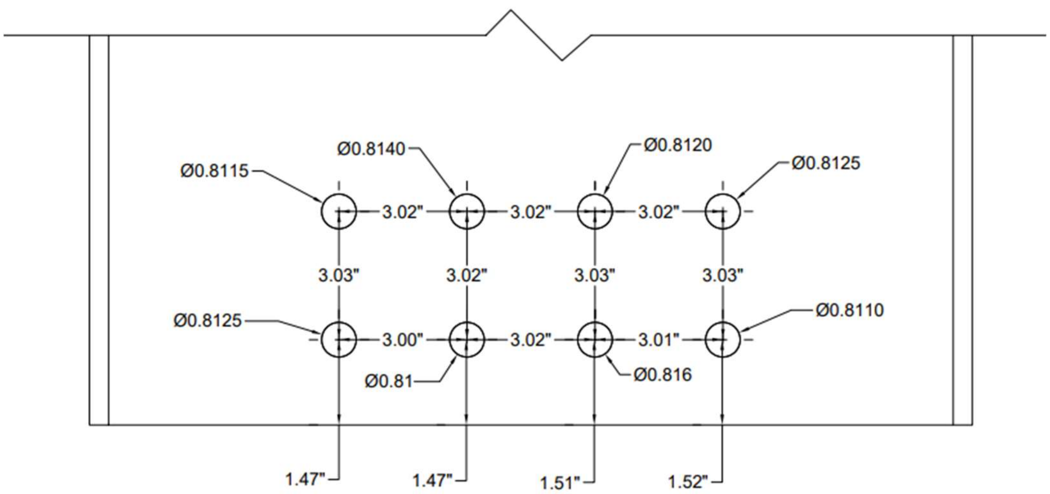

e) Measured dimensions of Specimen H5

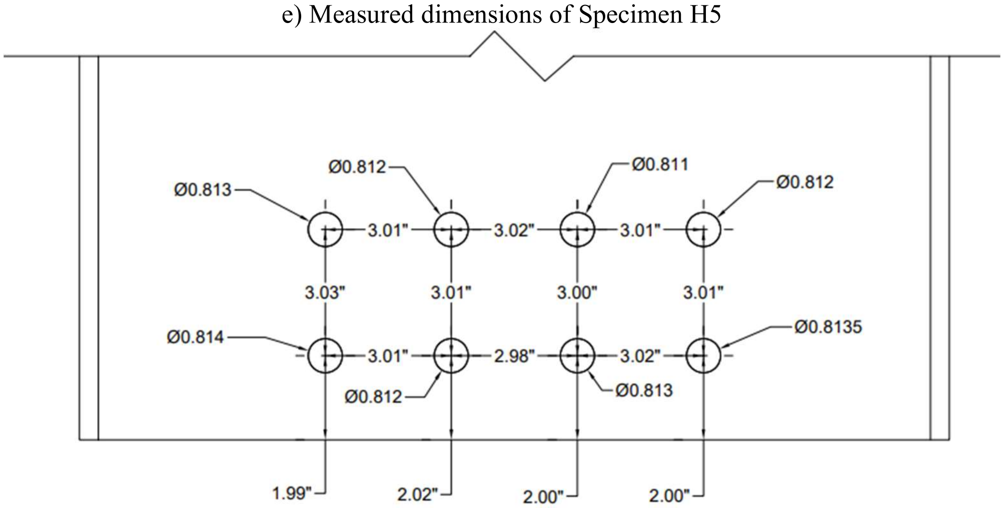

f) Measured dimensions of Specimen H6

Figure 49. Dimensions of specimens. (continued)

The test setup was placed atop a support beam connected to a strong floor as shown in Figure 50. Three sets of connector plates were used to hold the specimens while ensuring a firm connection with the support beam. These sets included two vertical plates welded to the support beam, two elongated horizontal plates linked to the vertical plates, and a pair of sandwiching plates designed to accommodate the W21 test specimen. An MTS 201.6 actuator was attached to a wall mount on one end and connected to the test specimen through an adapter plate on the other end. The actuator was oriented such that it was initially horizontal and provided an initial eccentricity of 9 in. with respect to the centroid of the bolt group. An adapter plate with four tapped holes was affixed to the loading side of the actuator. This plate facilitated the connection to the W21 using (4) 3/4 in. diameter bolts through the W21 flange and into the tapped holes. For each test, a new pair of sandwiching plates was utilized to mitigate any effects stemming from bearing deformation from prior testing. As a safety measure against support beam overturning, a hold-down beam was installed and anchored to the floor. Lateral bracing, not shown in Figure 50, prevented twisting of the test specimens. All bolts within the test connection and test set-up were finger-tightened before testing to reduce confounding variables such as friction effects that could obscure the assessment of tearout or bearing behavior in the connection.

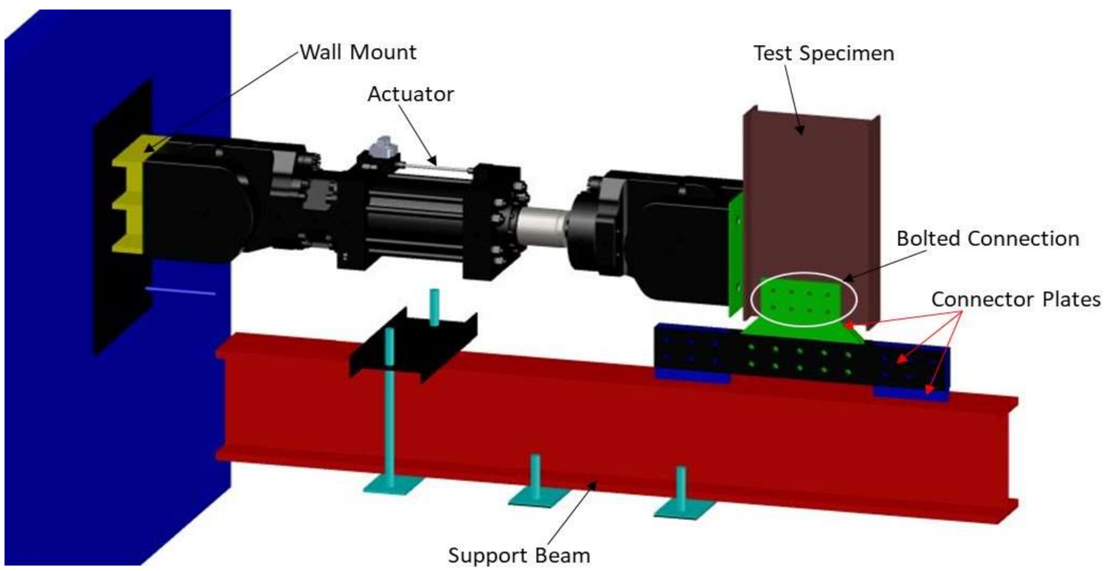

Figure 50: Test setup for higher eccentricity specimens.

A displacement-controlled compressive load was applied at a rate of 0.1 in. per minute until a displacement of 0.2 in. was reached. Subsequently, the specimen was unloaded to its initial position. This initial loading and unloading cycle served as a clear point for synchronization of data in post-processing and applied little load (less than 5 kips) to the specimen. After the initial synchronization cycle, the specimens were loaded at a rate of 0.1 in. per minute. The specimens with five bolts exhibited a sharp drop in load and testing was halted shortly after the drop in load. The specimens with eight bolts sustained a high level of load after yielding, without significant drop in load, and testing was halted after significant deformation was achieved.

The applied load was measured using the load cell in line with the actuator. Deformation of the specimens and the connector plates were measured with the Optotrak optical position measurement device. To measure deformation, sets of four LED markers were placed on both the web of the

W21 test specimen and the connector plates as shown in Figure 51. Through the Optotrak system the 3D coordinates of the markers were determined. The coordinate measurements were used to compute rotation of the test specimens and the connector plates.

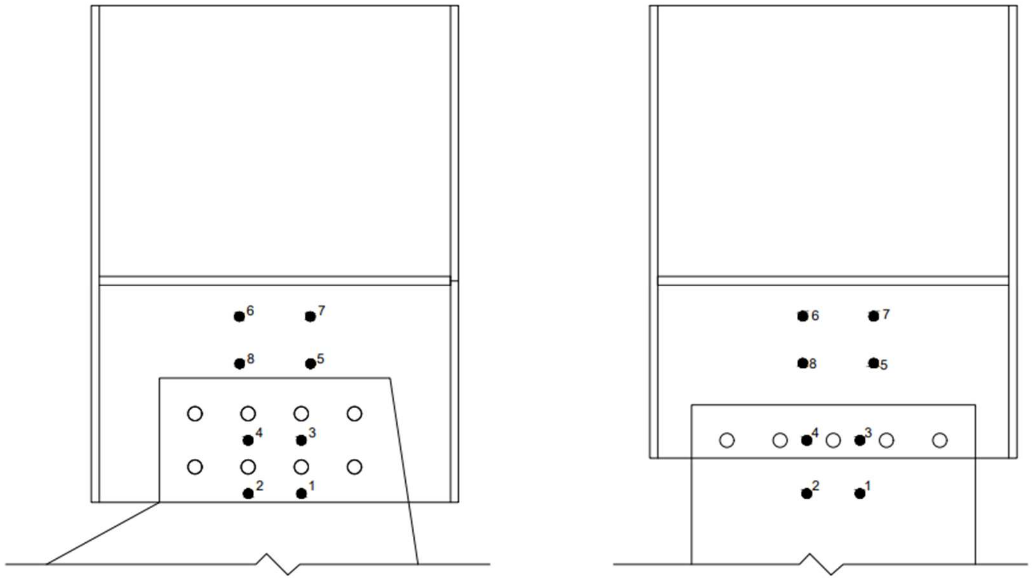

Figure 51: Placement of markers in test specimen.

Data from the MTS system and the Optotrak system were synchronized in post-processing using the synchronization cycle as a guide, as shown in Figure 52. The data from the Optotrak system was resampled at the sampling rate of the MTS system.

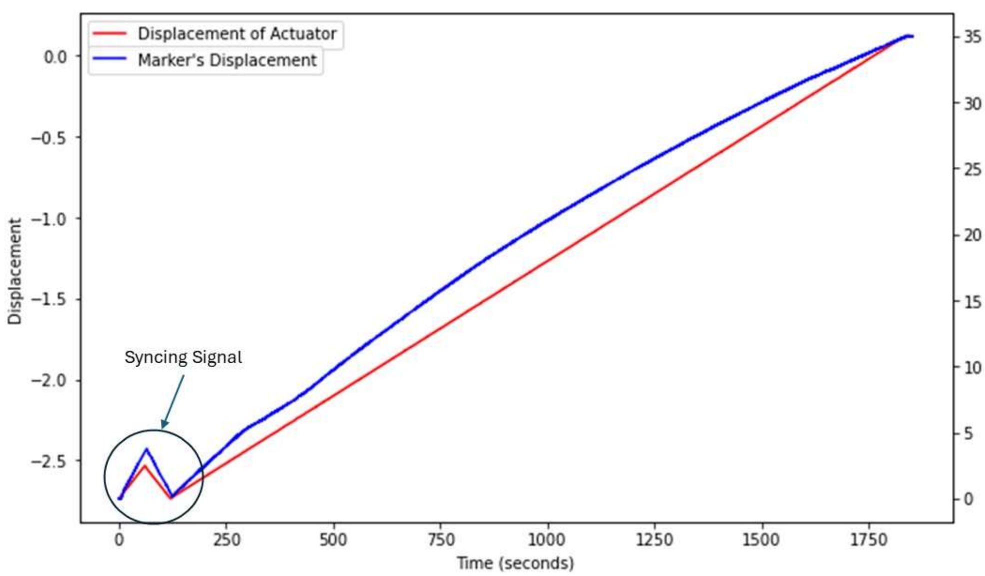

Figure 52: Measured data showing synchronization cycle.

After synchronizing the data, applied moment and rotations were calculated. The eccentricity of the connection was initially 9 in., but the eccentricity increased as the specimens rotated. For precise moment calculation, the displaced geometry of the test setup was considered, as shown in Figure 53. For the moment calculation, the test beam and the actuator swivel attached to the test beam were assumed to rotate about the center of gravity of the bolt group as a rigid body. With this assumption, the applied moment, *M*, was calculated using Equation 22.

$$M = Pd\cos\left(90^{\circ} - \Phi - \theta\right) \tag{22}$$

where, *P* is the measured force in the actuator, *d* is the distance from the center of the bolt group to the center of the loading end pin, Φ is the load angle (i.e., the angle of inclination of the actuator with respect to horizontal) and θ is the pin angle (i.e., the angle between a line from the center of the bolt group to the center of the loading end pin and the horizontal).

The pin distance, *d*, remained constant and was based on measurements prior to testing. The pin angle, θ, was taken as its initial value (based on measurements prior to testing) plus the measured rotation of the specimen. The load angle, Φ, was computed assuming the mounting end pin and the center of gravity of the bolt group were fixed in space.

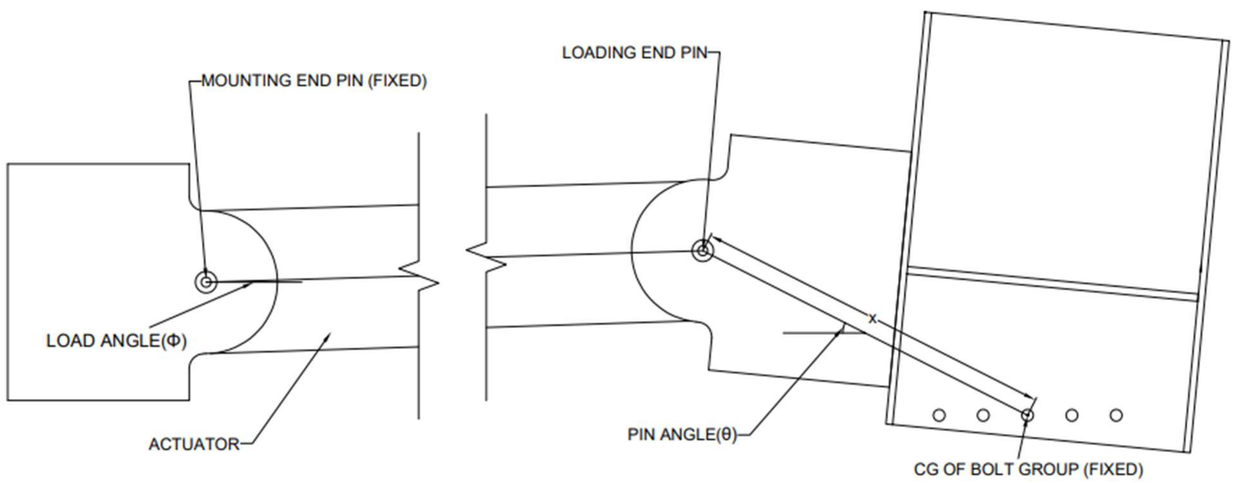

Figure 53: Displaced geometry of test setup.

Results

Plots of moment versus rotation for each specimen are shown in Figure 54 and Figure 55. All specimens exhibited similar patterns of behavior prior to reaching the peak moment. Significant deformation was observed at low loads as the bolts came into bearing with the web and connection plates. Once in bearing, the stiffness increased, with a linear-elastic response that was followed by reduction in stiffness as yielding occurred in the web. Specimens with one row of bolts (i.e., H1, H2, and H3) show a peak moment followed by a gradual decline and subsequent sharp drop in moment followed by a relatively constant residual moment. Specimens with two rows of bolts (i.e., H4, H5, and H6) maintained their peak moment for a longer period and the tests were stopped before any significant drop in moment.

Plots of force versus rotation for each specimen are shown in Figure 56 and Figure 57. The trends are generally consistent with those seen in the moment versus rotation plots. However, a peak load is seen for the specimens with two rows of bolts. This is in contrast with the moment versus rotation which generally showed increasing moment up to the maximum rotation. The reason for this discrepancy is that the eccentricity was also rising as the actuator tilted up, leading to an increasing moment despite the peak in the force. Plots of force versus eccentricity for each specimen are shown in Figure 58 and Figure 59.

The peak moment from the experiment ($M_{exp,u}$), the moment at the deformation limit ($M_{exp,d}$), and the ratio of the two are presented for each specimen in Table 29. The moment at the deformation limit is the moment attained at a rotation of 0.04167 radians for the specimens with one row of bolts, and 0.0527 radians for the specimens with two rows of bolts. These rotations were determined as 1/4 in. divided by the distance between the center of the bolt group to the most extreme bolt. The movement of the specimens as the connections were coming into bearing was excluded when determining $M_{exp,d}$. This was done by shifting the rotations such that a secant line connecting two points on the moment-rotation curve at 15% and 30% of maximum load intersected the origin.

Table 29: Experimental Moment Strength, and Moment at Deformation Limit.

Specimen	$M_{exp,u}$ (kips)	$M_{exp,d}$ (kips)	$M_{exp,u}/M_{exp,d}$
H1	651	571	1.141
H2	957	765	1.251
H3	1,208	904	1.336
H4	1,252	959	1.305
H5	1,434	1,053	1.362
H6	1,466	1,006	1.458

Photographs of the test specimens after testing are presented in Figure 60 through Figure 65. Notable differences in deformation are evident between specimens with one row of bolts and those with two rows of bolts. For the specimens with one row of bolts, the test plate deformed at all bolt hole locations, in various directions corresponding to the applied forces. These specimens also displayed tearout, characterized by distinct fractures, particularly at the edge bolt hole on the loading side. In contrast, for the specimens with two rows of bolts, in addition to localized deformations at the bolt holes, rotation of the web encompassing all bolt holes was evident.

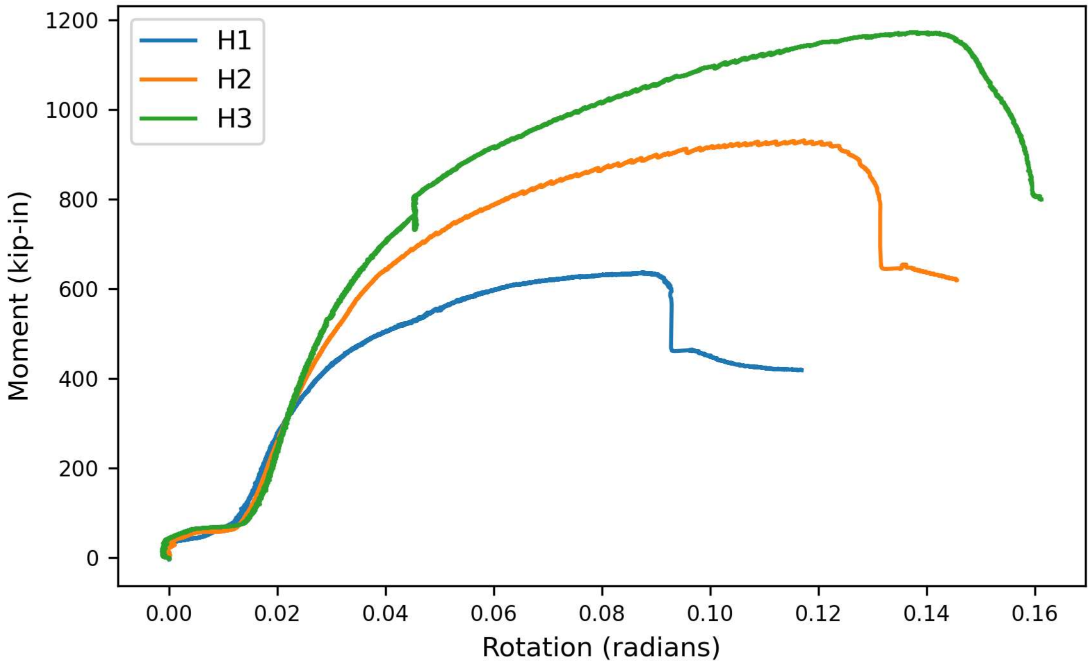

Figure 54: Moment vs Rotation Plots of Specimens H1, H2 and H3.

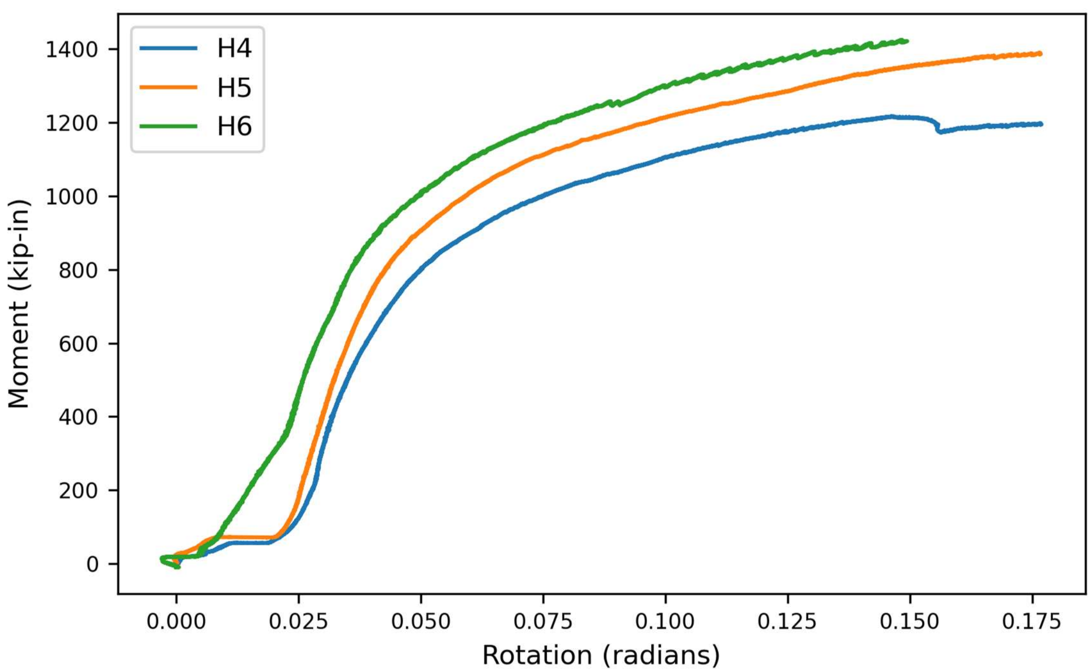

Figure 55: Moment vs Rotation Plot of Specimens H4, H5, and H6.

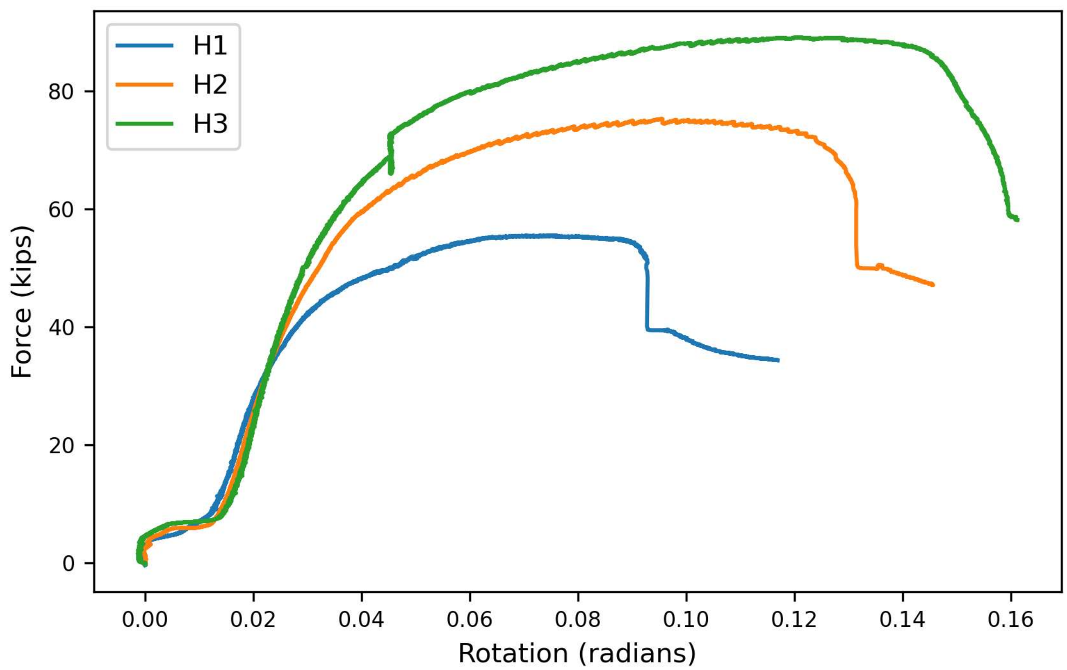

Figure 56: Force vs Rotation Plots of Specimens H1, H2 and H3.

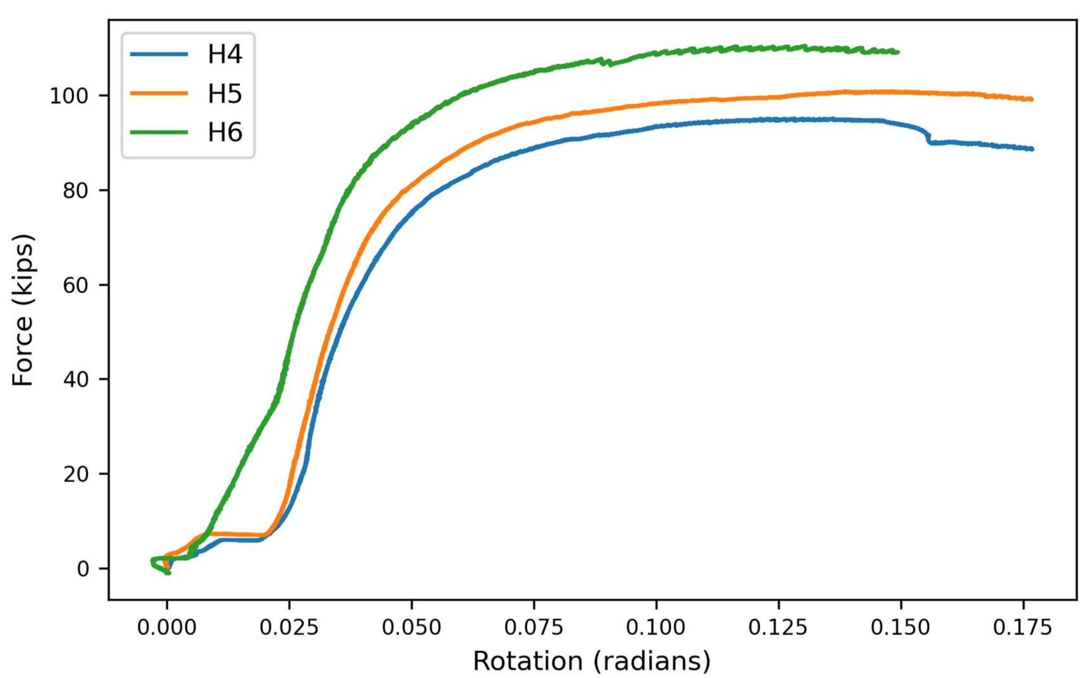

Figure 57: Force vs Rotation Plots of Specimens H4, H5, and H6.

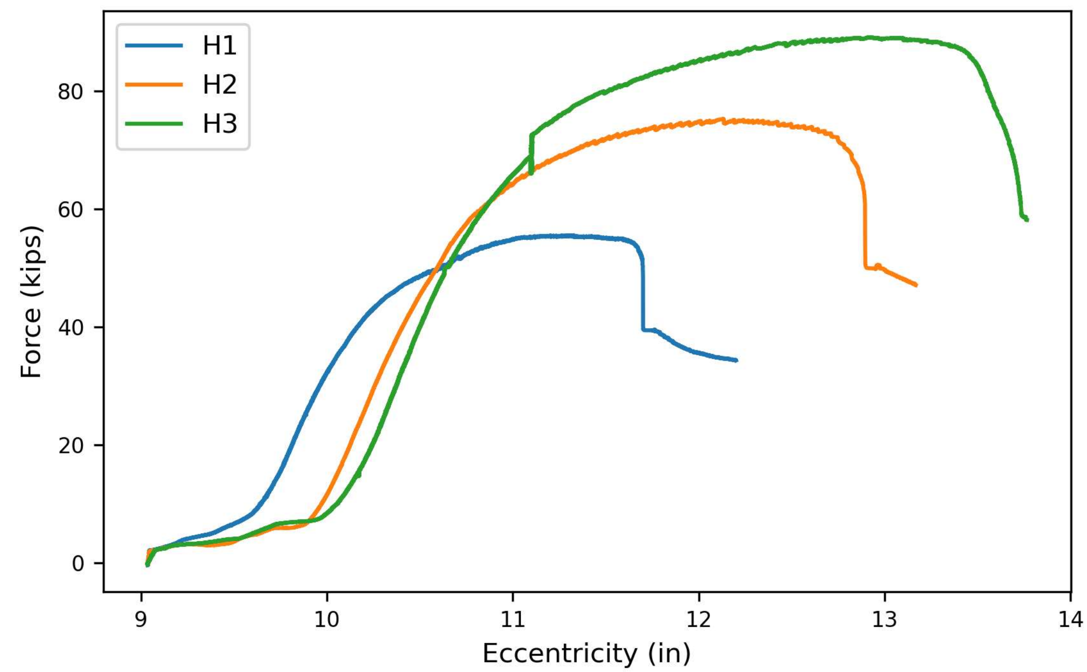

Figure 58: Force vs Eccentricity Plots of Specimens H1, H2 and H3.

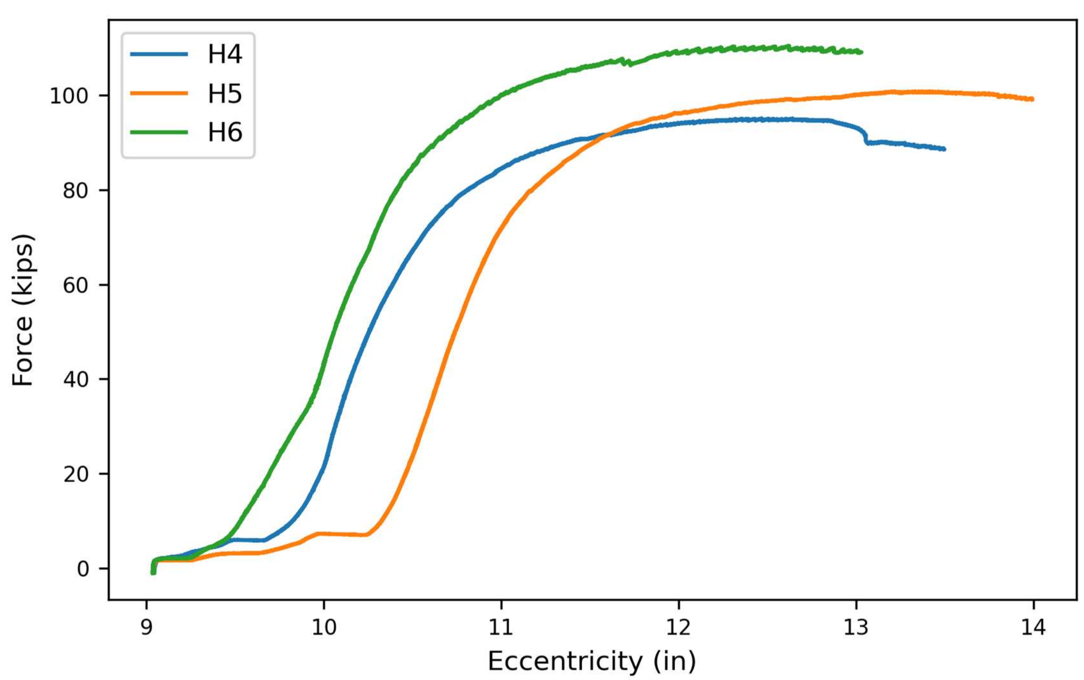

Figure 59: Force vs Eccentricity Plots of Specimens H4, H5, and H6.


Figure 60: Specimen H1 after testing.


Figure 61:Specimen H2 after testing.

Figure 62: Specimen H3 after testing.

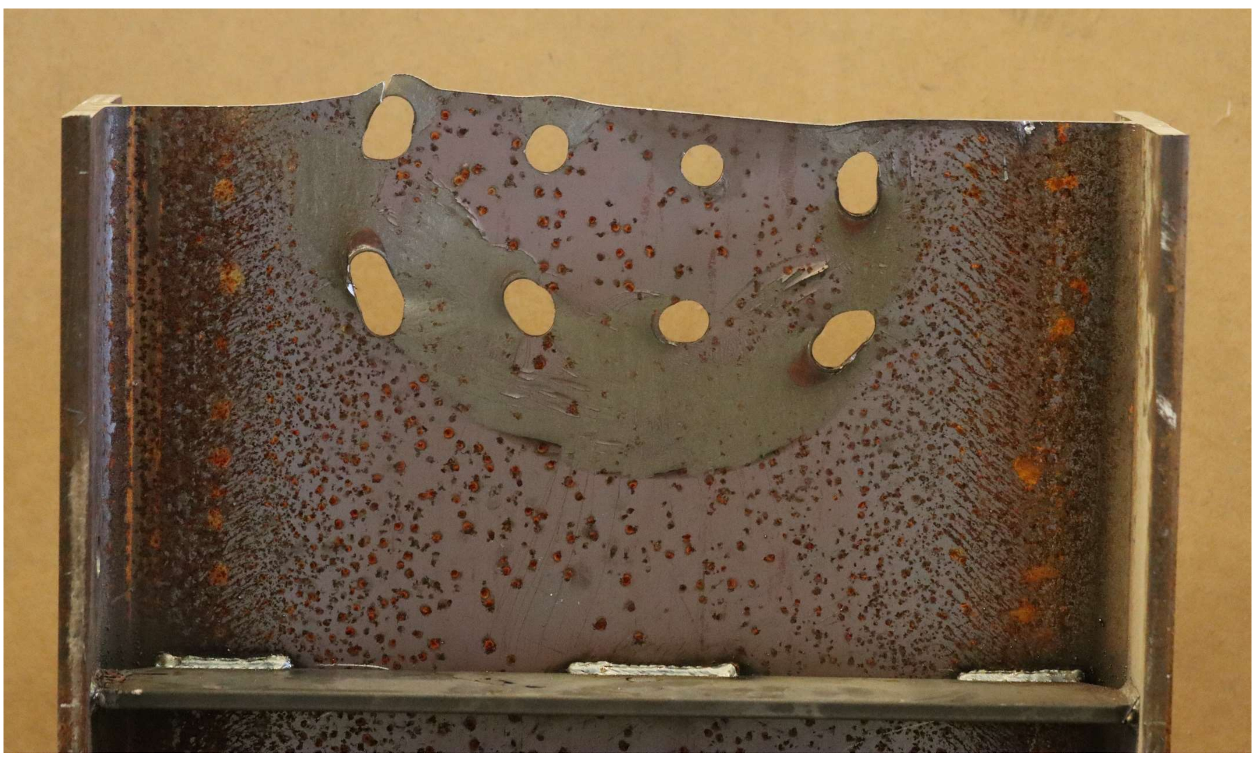

Figure 63: Specimen H4 after testing.

Figure 64: Specimen H5 after testing.

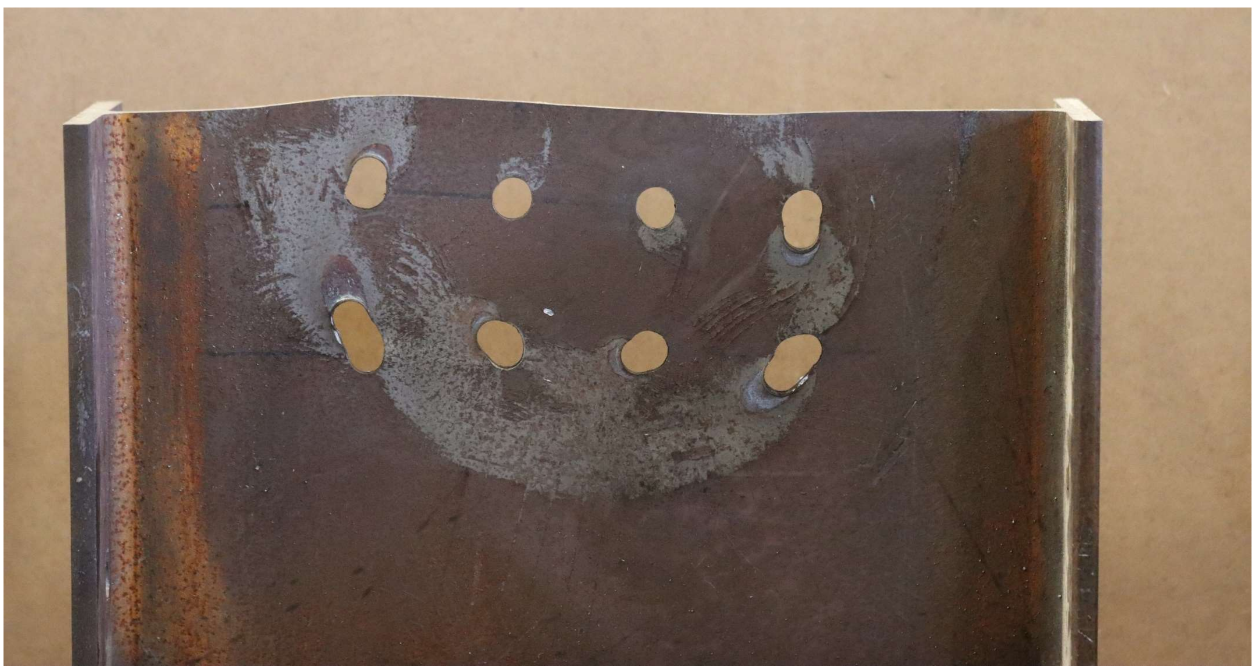

Figure 65: Specimen H6 after testing.

Discussion

The strength of the connections generally increased with edge distance. Figure 66 shows the trend of the ultimate moment, $M_{exp,u}$, with edge distance, L_{ev}, and Figure 67 shows the trend of the moment at the deformation limit, $M_{exp,d}$, with edge distance, L_{ev}. Specimens H1, H2 and H3 exhibited a greater increase in strength with edge distance than specimens H4, H5 and H6. The reason for this is the different failure modes of these two different groups of specimens. The strength of specimens H1, H2, and H3 was limited by bolt tearout and the strength of bolts in tearout is directly related to the edge distance. Specimens H4, H5 and H6 experienced a generalized block shear failure. Increased edge distance lengthened the failure path, but only marginally. An exception to the trend of increasing moment strength with increasing edge distance was the moment at the deformation limit for specimens H4, H5 and H6. $M_{exp,d}$ was roughly consistent for these specimens with specimen H5 showing the greatest strength. These differences are impacted somewhat by the adjustment for initial deformations as the bolts came into bearing. As seen in Figure 55, specimen H6 experienced an earlier increase in stiffness, potentially due to imperfect alignment of bolt holes.

The ratio of ultimate moment to moment at the deformation limit, $M_{exp,u}/M_{exp,d}$, also increases with edge distance as shown in Figure 68. This phenomenon was observed in the specimens with lower eccentricity (Figure 18) as well as in concentrically loaded specimens tested in this work and other work (Franceschetti and Denavit 2021). The increase in $M_{exp,u}/M_{exp,d}$ with L_{ev} for the specimens that failed in tearout is similar to that for the specimens that failed in generalized block shear.

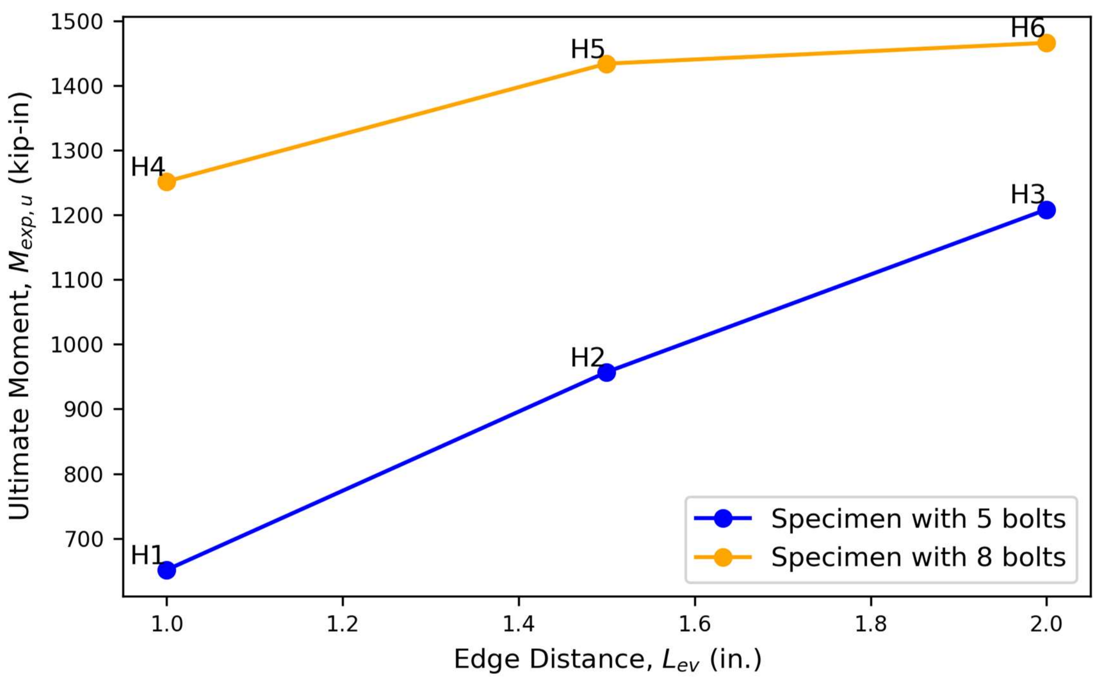

Figure 66: Ultimate Moment vs Edge Distance Plot for all Specimens.

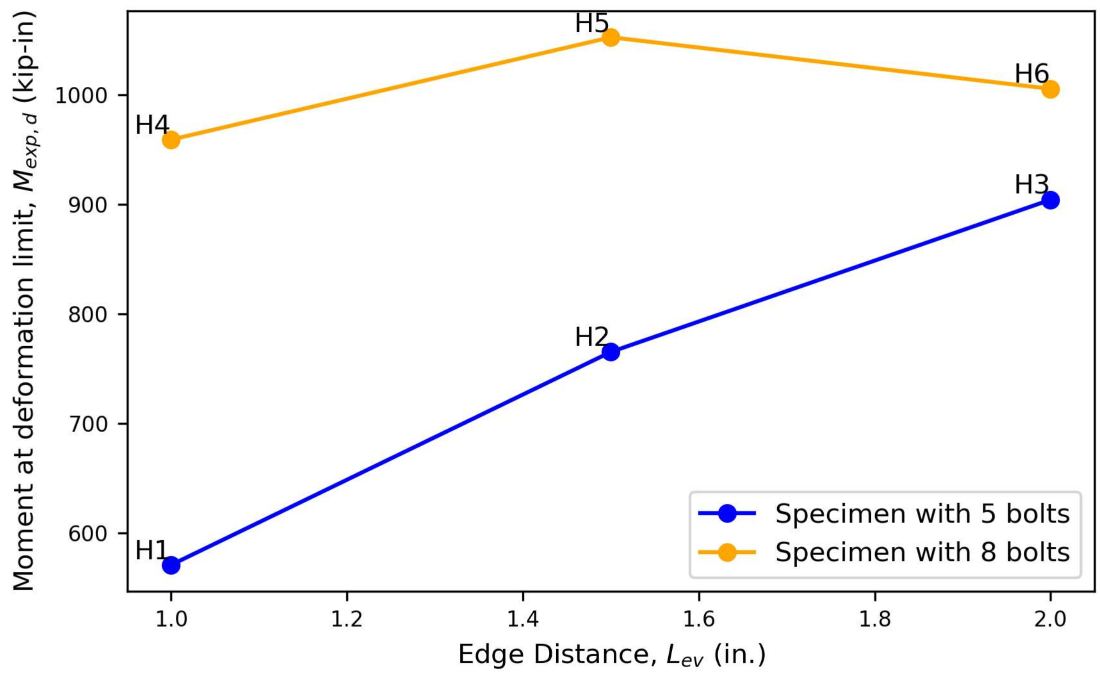

Figure 67: Moment at Deformation Dimit vs Edge Distance Plot for all Specimens.

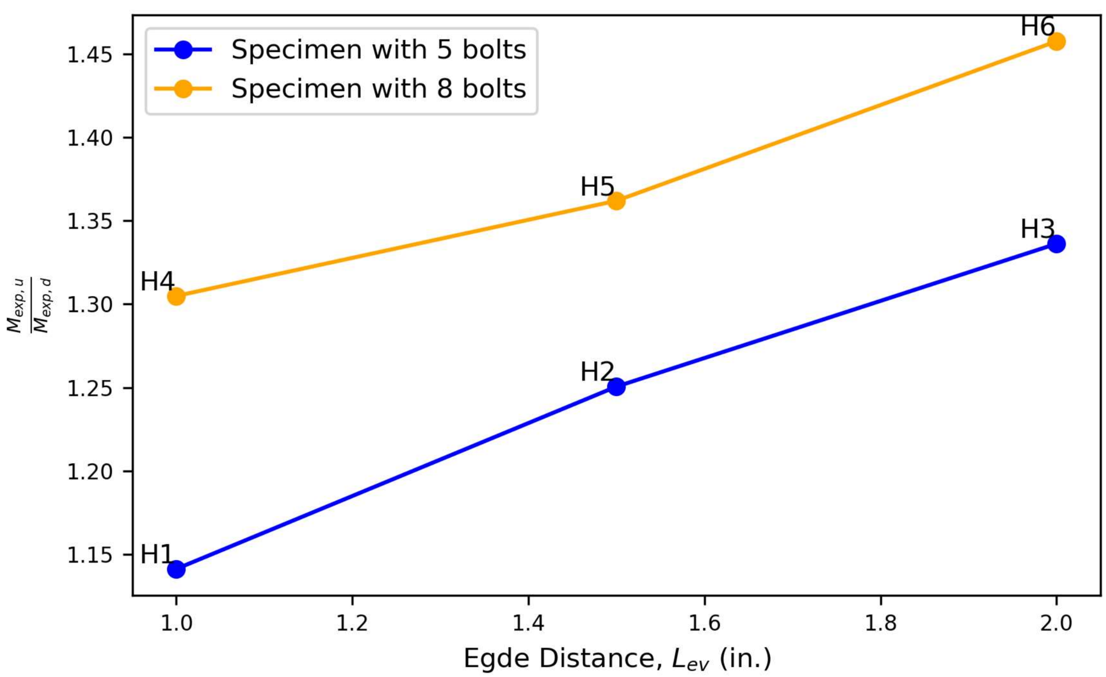

Figure 68: $M_{exp,u}/M_{exp,d}$ vs Edge Distance Plot of all Specimens.

The experimental results are compared to strengths computed using three different methods for the strength of the bolt group: 1) the poison bolt method, 2) the modified IC method, and 3) the IC method, neglecting tearout. Additionally, the results are compared to a strength computed using equations developed by Jönsson (2014) for generalized block shear failure. The strengths were calculated using the measured properties of the W21 web (i.e., t = 0.3626 in., F_y = 57.74 ksi, and F_u = 71.39 ksi), and measured dimensions of all test specimens Figure 49.

The methods for the strength of the bolt group are described in Chapter 3. The calculations of bolt group strength were based on loading applied at the displaced position of the loading end pin (Figure 53) and the displaced angle of the actuator. The displaced positions used were those concurrent with $M_{exp,d}$ for comparison to $M_{exp,d}$ and those concurrent with $M_{exp,u}$ for comparison to $M_{exp,u}$.

For eccentrically loaded connections, Jönsson (2014) suggests the use of Equation 23 to assess generalized block shear strength. For the specimens tested in this work, the required strengths are computed using Equations 24 to 26 and the available strengths are computed using Equations 27 to 29. Values of e and θ for each specimen are listed in Table 30 and Table 31 based on the measured values at the peak moment and moment at deformation limit from the experiments. Values of V_R, N_R, and M_R are based on stress distributions shown in Figure 69 and are listed for each specimen in Table 32. To determine the generalized block shear rupture strength, the value of P was back calculated such that the interaction equation (i.e., Equation 23) results in a value of 1.

$$\left(\frac{N}{N_R}+\frac{M}{M_R}\right)^2+\left(\frac{V}{V_R}\right)^2\leq 1 \tag{23}$$

$$N=P\sin\theta \tag{24}$$

$$V=P\cos\theta \tag{25}$$

$$M=Pe \tag{26}$$

$$N_R=tf_m\left(2\frac{b_g}{\sqrt{3}}+h_n\right) \tag{27}$$

$$V_R=tf_m\left(2b_n+\frac{h_g}{\sqrt{3}}\right) \tag{28}$$

$$M_R=th_g f_m\left(\frac{b_g}{\sqrt{3}}+\frac{h_n}{4}\right) \tag{29}$$

In the equations of N_R, V_R, and M_R, t is the thickness of the plate material in connection, f_m is the "formal yield stress" defined as $f_m = (F_y + F_u)/2$ corresponding to mean value of the yield and ultimate stress of materials, b_g and h_g are the gross width and depth of the block, and b_n and h_n are the net width and depth of the block after deducting the width of the hole from the gross dimension.

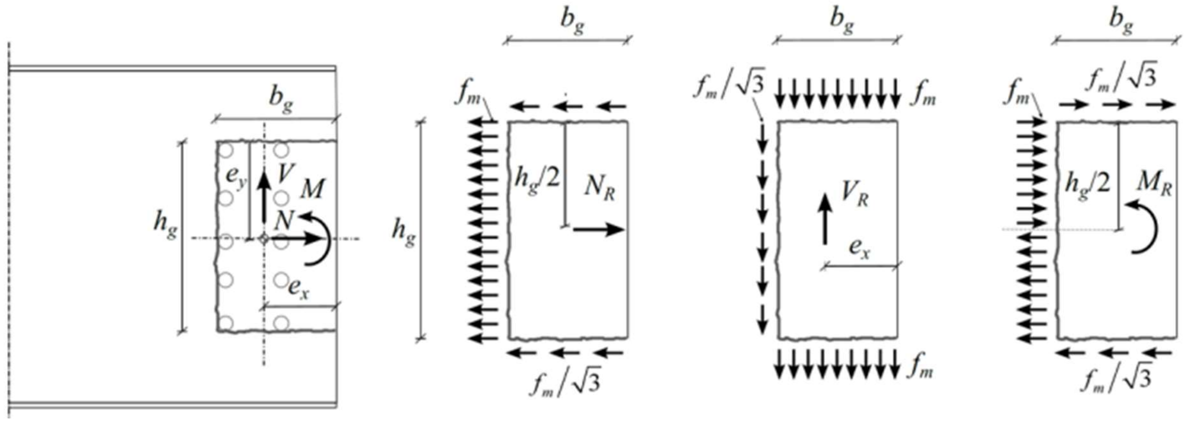

Figure 69: Block tearing forces and stress distribution (Jönsson 2014).

Table 30: Load Angle and Eccentricity at Peak Moment.

Specimen	*e* (in.)	θ (degrees.)
H1	11.85	1.59
H2	12.96	2.21
H3	13.71	1.66
H4	13.22	2.37
H5	14.44	3.09
H6	13.38	2.47

Table 31: Load Angle and Eccentricity at Deformation Limit Moment.

Specimen	*e* (in.)	θ (degrees.)
H1	10.91	1.06
H2	11.37	1.33
H3	11.62	1.47
H4	11.25	1.26
H5	11.76	1.56
H6	10.82	1.01

Table 32: Block Tearing Capacities.

Specimen	N_R (kips)	V_R (kips)	M_R (kip-in.)
H1	243	201	899
H2	256	224	986
H3	270	248	1,073
H4	273	263	962
H5	298	293	1,111
H6	323	323	1,269

A comparison of experimental strength results to computed strength results at the deformation limit load is presented in Table 33 and at the ultimate limit load in Table 34.

Table 33: Ultimate Limit Strength Comparison

Specimen	Poison Bolt Method		Modified IC Method		IC Method, Neglecting Tearout		Generalized Block Shear Failure	
	M_n (kip-in.)	$M_{exp,u}/M_n$	M_n (kip-in.)	$M_{exp,u}/M_n$	M_n (kip-in.)	$M_{exp,u}/M_n$	M_n (kip-in.)	$M_{exp,u}/M_n$
H1	387	1.684	551	1.183	1,062	0.614	835	0.780
H2	710	1.348	873	1.096	1,066	0.898	924	1.035
H3	1,052	1.149	1,071	1.129	1,074	1.125	1,011	1.196
H4	579	2.163	1,308	0.957	1,584	0.790	918	1.364
H5	1,059	1.354	1,462	0.981	1,587	0.903	1,061	1.352
H6	1,568	0.935	1,565	0.937	1,568	0.935	1,204	1.218
Average		1.439		1.047		0.877		1.157
St. Dev.		0.395		0.093		0.154		0.201

Table 34: Deformation Limit Strength Comparison

Specimen	Poison Bolt Method		Modified IC Method		IC Method, Neglecting Tearout		Generalized Block Shear Failure	
	M_n (kip-in.)	$M_{exp,d}/M_n$	M_n (kip-in.)	$M_{exp,d}/M_n$	M_n (kip-in.)	$M_{exp,d}/M_n$	M_n (kip-in.)	$M_{exp,d}/M_n$
H1	307	1.859	432	1.321	780	0.732	827	0.690
H2	563	1.360	669	1.145	781	0.980	913	0.838
H3	782	1.156	782	1.156	782	1.156	998	0.907
H4	450	2.132	952	1.008	1,141	0.841	909	1.055
H5	829	1.270	1,069	0.985	1,145	0.920	1,049	1.004
H6	1,136	0.885	1,136	0.885	1,136	0.885	1,186	0.848
Average		1.444		1.083		0.919		0.890
St. Dev.		0.424		0.142		0.131		0.119

Specimens H1, H2, and H3 experienced bolt tearout failure. The poison bolt method is generally conservative for these specimens and neglecting tearout is generally unconservative for these specimens. The differences are greater for specimens H1 and H2 as these specimens had smaller edge distance. The differences are less for specimen H3 which has a larger edge distance and the tearout strength was close to the bearing strength.

The modified IC method was the most accurate for the specimens that failed in tearout but still somewhat conservative. This accuracy is also evident in the force versus moment plots for specimens H1, H2, and H3 shown in Figure 70. Force-moment interaction diagrams constructed using the modified IC method are also included in Figure 70. The interaction diagram shows the relationship between force and moment strength at different eccentricities. The force-moment interaction diagram intersected the force-moment curve of the respective specimens close to their peaks, indicating that the modified IC method provides a good estimate of the strength of these specimens.

The test-to-predicted ratio for generalized block shear failure for specimens H2 and H3 was greater than 1. These specimens failed by tearout and not generalized block shear. This result indicates that the equations for generalized block shear failure are conservative for these specimens.

Specimens H4, H5, and H6 experienced generalized block shear failure. The average test-to-predicted ratio for these specimens is 1.157, further indicating that the equations for generalized block shear failure are conservative. Even though these specimens experienced generalized block shear failure, they show that the poison bolt method is conservative because the test-to-predicted ratio is greater than 1 for specimens H4 and H5. The test-to-predicted ratio is near 1 for the modified IC method, indicating that the specimens were close to tearout failure. This can also be seen in the force versus moment plot of these specimens as shown in Figure 71. The peak of the measured force-moment response for each specimen neared, but did not reach, their force-moment strength interaction diagram.

These observations suggest that eccentrically loaded bolted groups with two rows of bolts are more susceptible to generalized block shear tearout failure than bolt tearout. While this failure mode should be more extensively researched to establish code provisions, the equations developed by Jönsson (2014) provide a good estimate.

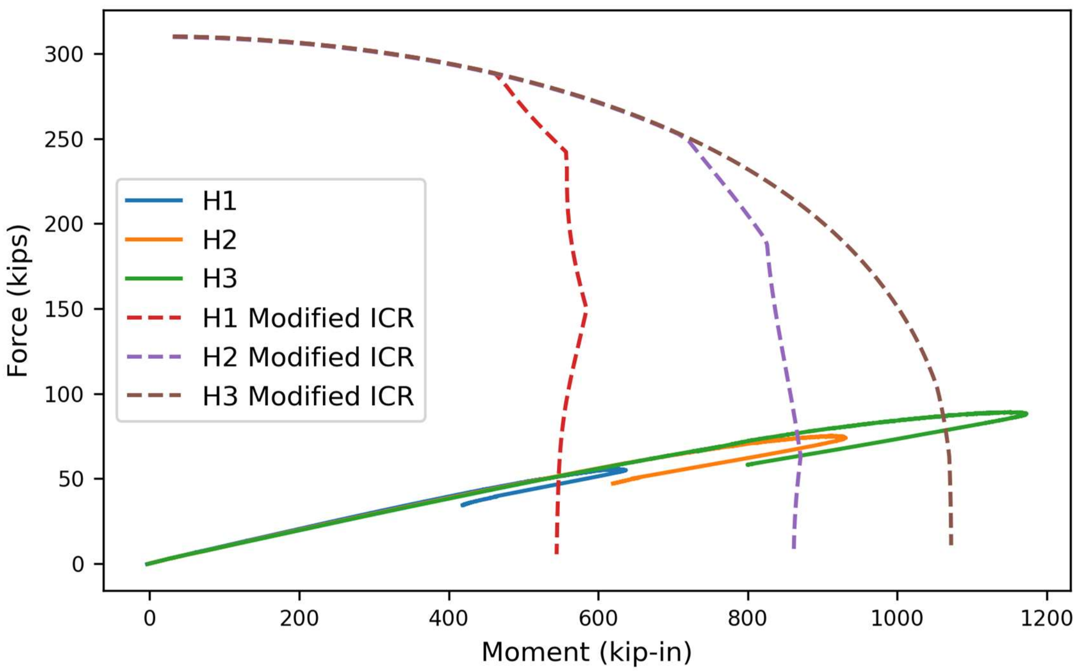

Figure 70: Force vs Moment Plots of Specimens H1, H2 and H3.

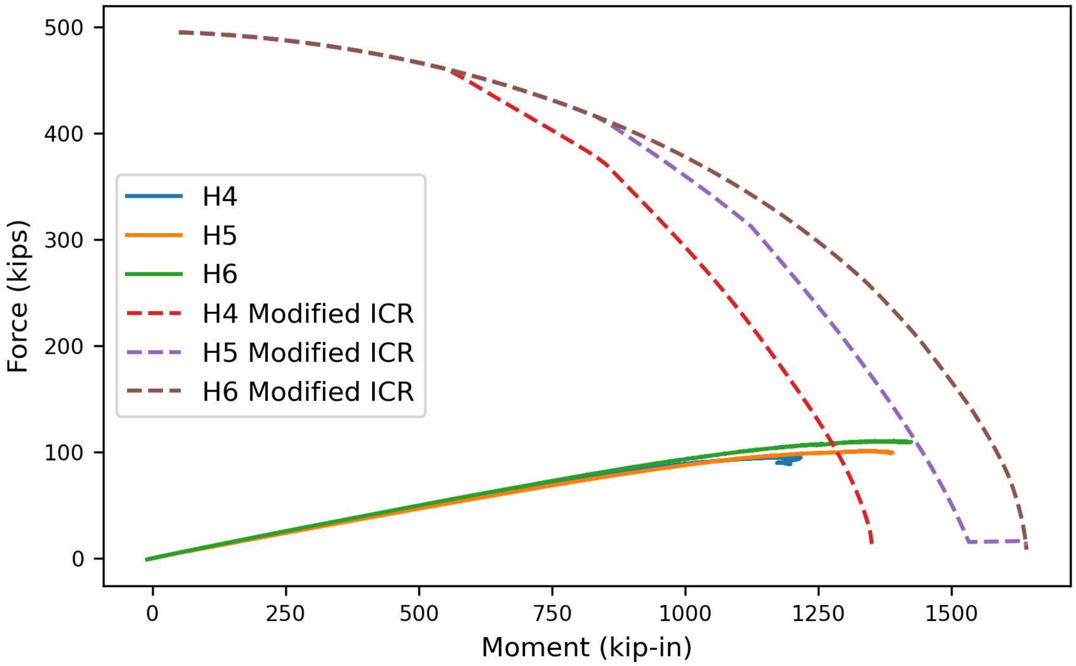

Figure 71: Force vs Moment Plots of Specimens H4, H5, and H6.

Chapter 5: Conclusions and Recommendations

The limit state of tearout is an important consideration in structural steel connection design. Tearout can control the strength of connections with small edge distances. However, current provisions are based on a limited range of physical experiments, leading to uncertainty in scenarios that differ from those tested.

Several design scenarios for the limit state of tearout where the applicability of current design requirements is uncertain were investigated in this research. These scenarios include bolts and bolt groups that were loaded concentrically, where skewed edges, corners beyond the bolt, interior bolts, and deformation compatibility were examined. Eccentrically loaded bolt groups were also examined.

Fifty-one concentrically loaded connections were tested. The following observations and conclusions were made from these experiments:

- For bolts with a skewed edge beyond the hole, tearout strength can be overestimated by current design provisions based on the clear distance, l_c. Improved estimates are provided by a tearout strength equation using the distance, l_{v1}, proposed by Kamtekar (2012) and modified in this work to be defined as the minimum distance between the edge of the bolt hole and the edge of the adjacent hole or edge of the material, measured in the direction of the applied force, along lines that are tangent to the bolt.

- For bolts with a corner beyond the hole, tearout strength can be overestimated by current design provisions based on the clear distance, l_c, and alternative design equations based on l_{v1}. Improved estimates are provided by a new equation, Equation 19, derived in this work.

- Spacing affects the strength of interior bolts. Both existing and proposed equations underestimate the strength observed in the experiments; however, the experimental strength evaluated for an interior bolt alone may be greater than the strength contribution of an interior bolt in a group.

- When controlled by tearout, bolts achieve their peak strength at relatively low deformations. When controlled by bearing, bolts achieve their peak strength at relatively high deformations. This behavior did not result in major unconservative errors for the specimens examined even though it is not explicitly addressed in the AISC *Specification* (which permits the strength of a bolt group to be taken as the sum of the strengths of the individual bolts). However, modest unconservative errors were noted in specimens with relatively small bolt spacing.

Twenty-two eccentrically loaded connections in two different configurations were tested. The following observations and conclusions were made from these experiments:

- The poison bolt method provides a conservative estimate of bolt group strength, which while accurate in some cases is overly conservative in others.

- Neglecting tearout results in an unconservative estimate of bolt group strength.

- The modified IC method developed by Denavit et al. (2021) is slightly conservative and more accurate than the other methods for the prediction of the strength of bolt groups when tearout controls.

- The eccentrically loaded bolt groups with two rows of bolt failed due to the yielding of the web material around the bolt group, rather than bolt tearout. Although this failure mode, referred to as generalized block shear, is not thoroughly studied and is not addressed in the AISC *Specification*, the equations developed by Jönsson (2014), which were utilized in this study, offer a promising starting point for further research and development.

In conclusion, this study highlights the need to revise current design guidelines to better predict tearout strength in bolted connections. The proposed alternative provisions and findings from this research offer valuable insights for enhancing the accuracy and reliability of design methods for structural steel bolted connections.

This study also highlights several areas where further research would be beneficial. Finite element simulations would be beneficial to further the range of investigation and better understand the causes of trends in the data, including 1) quantifying the potential effect of lateral restraint on skewed edge specimens; 2) identifying why low spacing results in low test-to-predicted ratios; and 3) further validating the modified IC method. Having shown promise as a means of estimating the strength of eccentrically loaded bolt groups, the modified IC method should be expanded to use the distance l_{v1} and to consider the geometry of slotted holes. Further development of design guidance for generalized block shear is recommended. This work could include further validation of the design equations as well as a study to determine under what conditions generalized block shear controls over bolt group strength. Simple guidance that identifies when connection strength is controlled by generalized block shear strength and not bolt group strength, would be beneficial to engineers.

Acknowledgements

This work was funded by the American Institute of Steel Construction (AISC). In-kind support was provided by the Siskin Steel & Supply Company. The authors thank the following individuals for their assistance with fabrication and performing the physical experiments: Alex Moore, Larry Roberts, and Andy Baker.

References

AISC. (2022). *Specification for Structural Steel Buildings*. American Institute of Steel Construction, Chicago, Illinois.

AISC. (2023). *Steel Construction Manual, 16th Edition*. American Institute of Steel Construction, Chicago, Illinois.

Al-Amery, F. (2022). "Experimental and Analytical Analysis of Eccentrically Loaded Bolded Steel Connections." Ph.D. Dissertation, Lawrence Technological University, Southfield, Michigan.

ASTM. (2022). *Standard Test Methods for Tension Testing of Metallic Materials*. ASTM E8/E8M-22, ASTM International, West Conshohocken, Pennsylvania.

Badawi, H. E.-D. S. (1983). "Behavior of Eccentric Bolted Shear Connections." Master's Thesis, McGill University, Montreal, Quebec.

Clements, D. D. A., and Teh, L. H. (2013). "Active Shear Planes of Bolted Connections Failing in Block Shear." *Journal of Structural Engineering*, ASCE, 139(3), 320–327.

Crawford, S. F., and Kulak, G. L. (1971). "Eccentrically Loaded Bolted Connections." *Journal of the Structural Division*, ASCE, 97(3), 765–783.

Denavit, M. D., Franceschetti, N., and Shahan, A. (2021). *Investigation of Bearing and Tearout of Steel Bolted Connections*. Final Report to the American Institute of Steel Construction, University of Tennessee, Knoxville, Knoxville, Tennessee.

Franceschetti, N., and Denavit, M. D. (2021). "Tearout Strength of Concentrically Loaded Bolted Connections." *Engineering Journal*, AISC, 58(3), 165–183.

Frank, K. H., and Yura, J. A. (1981). *An Experimental Study of Bolted Shear Connections*. Report No. FHWA/RD-81/148, FHWA, Washington, D.C.

Jönsson, J. (2014). "Block Failure in Connections Including Effects of Eccentric Loads." *Proceedings of the 7th European Conference on Steel and Composite Structures (EUROSTEEL 2014)*, Naples, Italy.

Kamtekar, A. G. (2012). "On the bearing strength of bolts in clearance holes." *Journal of Constructional Steel Research*, 79, 48–55.

Kim, H. J., and Yura, J. A. (1999). "The effect of ultimate-to-yield ratio on the bearing strength of bolted connections." *Journal of Constructional Steel Research*, 49(3), 255–269.

Kulak, G. L. (1975). "Eccentrically Loaded Slip-Resistant Connections." *Engineering Journal*, AISC, 12(2), 52–55.

Soliman, M., Russell, B., Waite, C., Shen, L., and Stringer, E. (2021). *Understanding the Behavior of Steel Connections with Bolts and Welds in Combination*. Final Report to the American Institute of Steel Construction, Oklahoma State University, Stillwater, Oklahoma.

Wing, P. C., and Harris, P. J. (1983). "Eccentrically loaded bolted beam connections." *Canadian Journal of Civil Engineering*, NRC Research Press, 10(2), 295–305.

130 E Randolph St, Ste 2000
Chicago, IL 60601
312.670.2400
www.aisc.org

Research Report No. 044